Functional characterization of *Arabidopsis thaliana* CC-type glutaredoxin ROXY9

Dissertation
for the award of the degree
"*Doctor rerum naturalium*"
of the Georg-August-Universität Göttingen

within the doctoral program
"Microbiology and Biochemistry"
of the Georg-August-University School of Science (GAUSS)

Submitted by
Pascal Mrozek
from Düsseldorf, Germany

Göttingen, July 21, 2022

Thesis Committee

Prof. Dr. Christiane Gatz, Department of Plant Molecular Biology and Physiology, Albrecht-von-Haller-Institute for Plant Sciences, University of Göttingen

Prof. Dr. Ivo Feussner, Department for Plant Biochemistry, Albrecht-von-Haller-Institute for Plant Sciences, University of Göttingen

Prof. Dr. Kai Tittmann, Department of Molecular Enzymology, Göttingen Center of Molecular Biosciences, University of Göttingen

Members of the Examination Board

Referee: Prof. Dr. Christiane Gatz, Department of Plant Molecular Biology and Physiology, Albrecht-von-Haller-Institute for Plant Sciences, University of Göttingen

2^{nd} Referee: Prof. Dr. Ivo Feussner, Department for Plant Biochemistry, Albrecht-von-Haller-Institute for Plant Sciences, University of Göttingen

Further members of the Examination Board

Prof. Dr. Kai Tittmann, Department of Molecular Enzymology, Göttingen Center of Molecular Biosciences, University of Göttingen

Prof. Dr. Volker Lipka, Department of Plant Cell Biology, Albrecht-von-Haller-Institute for Plant Sciences, University of Göttingen

PD Dr. Thomas Teichmann, Department of Plant Cell Biology, Albrecht-von-Haller-Institute for Plant Sciences, University of Göttingen

Prof. Dr. Jörg Stülke , Department of General Microbiology, Institute for Microbiology and Genetics, University of Göttingen

Date of oral examination: 07.09.2022

Contents

Abbreviations

Abbreviation	Description
°C	Degree Celsius
AMS	4-Acetamido-4'-maleimidylstilbene-2,2'-disulfonic acid
A. thaliana	*Arabidopsis thaliana*
APS	Ammoniumpersulfat
ATP	Adenosine triphosphate
ATOX1	Antioxidant protein 1
BAK1	BRI1-associated receptor kinase 1
BEVS	Baculovirus expression vector system
BSA	Bovine Serum Albumin
bZIP	Basic region/leucine zipper
βME	β-Mercaptoethanol
CaMV	Cauliflower mosaic virus
CD	Circular dichroism
CE	Crude extract
CHP	Cumene hydroperoxide
Col-0	Arabidopsis ecotype Columbia-0
Cys	Cysteine
DEP	Dishevelled, Egl-10 and Pleckstrin domain
DLO1	DMR6-Like Oxygenase 1
DMPD	*N*,*N*'-Dimethyl-p-phenylenediamine
DMSO	Dimethyl sulfoxide
DNA	Deoxyribonucleic acid
dNTP	Desoxyribonucleoside triphosphate (DNA building block)
Dsb	Bacterial disulphide bond family enzyme
DTT	Dithiothreitol
DUF	Domain of unknown function
dYT	Double yeast extract and tryptone
E^{0}'	Biological standard potential
EDTA	Ethylenediaminetetraacetic acid
EGTA	Ethylene glycol-bis(β-aminoethyl ether)-*N*,*N*,*N*',*N*'-tetraacetic acid
E. coli	*Escherichia coli*
ER	Endoplasmic reticulum
ET	Ethylene

EtOH	Ethanol
F	Faraday
FBPase	Fructose 1,6-bisphosphatase
FEA4	Fasciated Ear4
Ferene	3-(2-Pyridyl)-5,6-di(2-furyl)-1,2,4-triazine-5',5"-disulfonic acid disodium salt
FTR	Ferredoxin-thioredoxin reductase
g	g-force
GAPDH	Glyceraldehyde 3-phosphate dehydrogenase
GAPDH-SG	Glutathionylated glyceraldehyde 3-phosphate dehydrogenase
GFP	Green fluorescent protein
GR	Glutathione reductase
GRX	Glutaredoxin
GST	Glutathione *S*-transferase
GSH	Glutathione (reduced)
GSNO	*S*-Nitrosoglutathione
GSSG	Glutathione (oxidized)
h	Hours
HA	Hemagglutinin
HEDS	2-Hydroxyethyl disulphide
HEPES	4-(2-Hydroxyethyl)-1-piperazineethanesulfonic acid
His	6xHistidine tag
Hi5	*T. ni* High Five cell line
HPLC	High-performance liquid chromatography
HRP	Horseradish peroxidase
kDa	Kilodaltons
IAM	Iodoacetamide
IDCR	Ionic detergent compatibility reagent
IgG	Immunoglobulin G
IPTG	Isopropyl β-D-1-thiogalactopyranoside
ISCA	Iron-sulfur cluster assembly protein
JA	Jasmonic acid
LB	lysogeny broth
LIC	Ligation independent cloning
M	Molar/mole per litre
MBP	Maltose binding protein
MG-132	26S proteasome inhibitor
min	Minutes
mM	Millimolar

mmPEG	Methoxy maleimide polyethylene glycol
mRNA	Messenger RNA
MSCA1	Male Sterile Converted Anther1
MW	Molecular weight
MWCO	Molecular weight cut-off
NADH	Nicotinamide adenine dinucleotide
NADPH	Nicotinamide adenine dinucleotide phosphate
NASC	Nottingham Arabidopsis Stock Centre
NEM	*N*-ethylmaleimide
NLS	Nuclear localization sequence
NMR	Nuclear magnetic resonance
NPR1	Nonexpressor of PR-1 genes
NRT2.1	High-affinity nitrate transporter 2.1
ON	Over night
Page	Polyacrylamide gel electrophoresis
PAMP	Pathogen-associated molecular pattern
PAN	PERIANTHIA TGA transcription factor
PCR	Polymerase chain reaction
pH	Negative decadic logarithm of the H^+-ion concentration
pKa	Negative decadic logarithm of the acid dissociation constant
PR-1	Arabidopsis *Pathogenesis Related-1*
PVDF	Polyvinylidene difluoride
qRT-PCR	Quantitative reverse transcriptase PCR
RNA	Ribonucleic acid
roGFP	Reduction-oxidation sensitive green fluorescent protein
ROS	Reactive oxygen species
ROXY	*A. thaliana* class III glutaredoxin
RPB	Rapid purification buffer
rpm	Rotations per minute
RT	Room temperature
S. cerevisiae	Baker's yeast *Saccharomyces cerevisiae*
SA	Salicylic acid
SDS	Sodium laurylsulfate
s, sec	Seconds
S. frugiperda	Fall armyworm *Spodoptera frugiperda*
strep	Peptide sequence with affinity to Streptactin
TAE	Tris acetat EDTA buffer

TBS	Tris buffered saline
TBST	Tris buffered saline with 0.1% (v/v) Tween
TCA	Trichloroacetic acid
TCEP	Tris(2-carboxyethyl)phosphine
TEMED	Tetramethylethylenediamine
TEV	Tobacco Etch Virus protease
TGA	TGA-transcription factor
TIBA	2,3,5-Triiodobenzoic acid
T. ni	Cabbage looper *Trichoplusia ni*
TRIS	Tris(hydroxymethyl)aminomethane
TRX	Thioredoxin
UBQ	Ubiquitin
UPLC	Ultrahigh-performance liquid chromatography
UV	Ultraviolet
UV/Vis	Ultraviolet-visible spectroscopy
V	Volt
V0	Initial baculovirus infection to generate a new virus
V1	Baculovirus Infection aimed at propagating the virus in *S. frugiperda*
V2	Baculovirus Infection aimed at protein expression in *T. ni*
W	Watt
WT	Wild-type
X-Gal	5-Bromo-4-chloro-3-indolyl-$beta$-D-galactopyranoside
YFP	Yellow fluorescent protein
µL	Microliter
µm	Micrometer
µmol	Micromole
µM	Micromolar
35S	Promoter required for formation of the 35S-mRNA from cauliflower mosaic virus

1 Summary

Glutaredoxins are small proteins with a conserved thioredoxin fold. This fold allows for two functions, depending on the sequence of the active site. Class I glutaredoxins, which are characterized by a CPYC motif, show oxidoreductase activity and serve to control the redox status of reactive thiols in proteins under conditions of oxidative stress. The tripeptide glutathione serves as a co-factor for the underlying redox reactions. Class II glutaredoxins, which encode a highly conserved CGFS motif, are instrumental for the assembly and transfer of Fe-S-clusters. Here, the co-factor glutathione provides two of the four thiols that coordinate the cluster, while two cysteines of two glutaredoxins provide the other two thiols. Based on the two different functions, members of both classes do not only differ in the active site but also in their binding mode for glutathione. Because of the essential functions of glutaredoxins in the anti-oxidative system and in Fe-S-cluster biogenesis, class I and class II glutaredoxins are widely distributed from archaea to eukaryotes.

Class III glutaredoxins encode a CCM/LC/S motif and are only found in land plants. Their gene family has expanded during evolution and the genome of the model plant *Arabidopsis thaliana* contains 21 members, which contribute to different functions in e.g. development, stress responses and adaptation to nutrient supply. Up to now, their molecular mechanism of action is unknown, but based on a number of indirect evidences, it has been speculated that they control the redox status of transcription factors of the TGA family. In this thesis, the question was addressed, whether class III glutaredoxin ROXY9 can function as an oxidoreductase or as an Fe-S-cluster binding protein.

To this aim, an insect cell expression system was established which allowed to obtain mg amounts of soluble ROXY9. Class I glutaredoxin GRXC2 was used as a control in all *in vitro* assays. Comparison of the CD spectra of both proteins showed that ROXY9 adopts a thermostable thioredoxin fold, which is influenced by glutathione, with this influence leading to less pronounced minima as compared to GRXC2. ROXY9 did not function as a reductase in the standard HEDS assay and not as an oxidase with roGFP2 or TGA1 as substrates. A weak deglutathionylation activity was observed with the enzyme GAPDH. GRXC2 was active in these assays, with the exception of TGA1 as a substrate. In conclusion, ROXY9 rather resembles class II glutaredoxins with respect to oxidoreductase activity. Similar to class II glutaredoxins, ROXY9 was found to form dimers during *in vitro* reconstitution experiments with Fe and S. Dimers and monomers were separated by gel filtration and Fe and S was only detectable in the fractions containing the dimer.

An interesting difference between ROXY9 and GRXC2 was observed when

comparing their midpoint redox potentials. In the presence of the redox pair DTT/dithiane, both proteins were identified to have a midpoint redox potential of approximately −240 mV, with the oxidized species containing a disulphide bridge between the cysteines of the active center predominantly formed at lower redox potentials. The same midpoint redox potential was observed for ROXY9 when the redox potential was adjusted by reduced and oxidized glutathione (GSH/GSSG). Again only the reduced and oxidized species with the disulphide bridge were detected for ROXY9. In contrast, GRXC2 was already oxidized at a very low redox potential, with a glutathionylated species and the species with the disulphide bond being formed in roughly equimolar amounts. Based on these results, we postulate that the high tendency of a class I glutaredoxins to bind a glutathione moiety of GSSG or of other substrates might determine their ability to efficiently (de-)glutathionylate target molecules. We further speculate that due to a different glutathione binding mode, ROXY9 does not efficiently accept and transfer a glutathione. The highly unfavourable glutathionylation of the active site cysteine is resolved either by GSH or by the second cysteine of the active site. Thus, ROXY9 might not function as a promiscuous oxidoreductase, but could have the potential to redox modulate specific proteins.

2 Introduction

2.1 Redox homeostasis and signalling in plants

Protein cysteines can undergo a great variety of oxidative modifications, including the formation of sulfenic, sulfinic or sulfonic acids, S-nitrosylation or disulphide bridges with an additional cysteine originating either from within the protein (intramolecular), from other proteins (intermolecular) or from the low molecular weight antioxidant glutathione (S-glutathionylation) (Zaffagnini et al., 2012b). Many cysteine modifications are caused by reactive molecular species, especially reactive oxygen species (ROS). In plant cells, ROS are mainly generated as a by-product of photosynthetic electron transport in the chloroplasts or mitochondrial respiration. ROS are also formed in peroxisomes or by NADPH oxidases at the plasma membrane (Moller et al., 2007).

To prevent oxidative damage, excess levels of ROS are degraded by scavenging systems involving enzymes like superoxide dismutases, catalases, and peroxidases and low molecular weight antioxidants like ascorbate and glutathione (Foyer and Noctor, 2009, 2013; Noctor et al., 2018; Dumanović et al., 2021). The low molecular weight antioxidants, especially the cytosolic glutathione pool maintained at a redox potential of around –320 mV (Schwarzländer et al., 2008), keep the vast majority of cellular thiols in a reduced state (Foyer and Noctor, 2005).

The tight control of ROS levels and cysteine redox state allows for important signalling functions of ROS molecules in, among others, plant defence, development and cell death (Foyer and Noctor, 2005, 2009; Frederickson Matika and Loake, 2014; Considine and Foyer, 2014; Noctor et al., 2018; Bleau and Spoel, 2021).

One of the first discovered examples of redox-based regulators process in plants was the regulation of enzymes as function of the photoperiod (Buchanan, 2016; Zaffagnini et al., 2019; Cejudo et al., 2019). Enzymes like glyceraldehyde 3-phosphate dehydrogenase (GAPDH) (Anderson and Lim, 1972) and fructose 1,6-bisphosphatase (FBPase) (Baier and Latzko, 1975) were found to be light activated, which could be linked to the electrons provided by the photosynthetic electron transport at the onset of light, that lead to a reduction of the enzymes (Wolosiuk and Buchanan, 1977; Buchanan, 2016). Over the past decades, the field of thiol based redox regulation in plants has greatly expanded (Zaffagnini et al., 2019).

2.2 The thioredoxin protein superfamily

A large number of proteins involved in redox processes belong to the thioredoxin superfamily, which includes among others thioredoxins, glutaredoxins, glutathione *S*-transferases, glutathione peroxidases, protein disulfide isomerases and bacterial Dsb proteins (Martin, 1995; Carvalho et al., 2006; Meyer et al., 2008). Superfamily members share the common thioredoxin fold detailed in figure 1 which conveys a relatively high stability, for instance at high temperatures (Laurent et al., 1964; Pan and Bardwell, 2006).

The core fold consists of four beta strands and three alpha helices as dis-

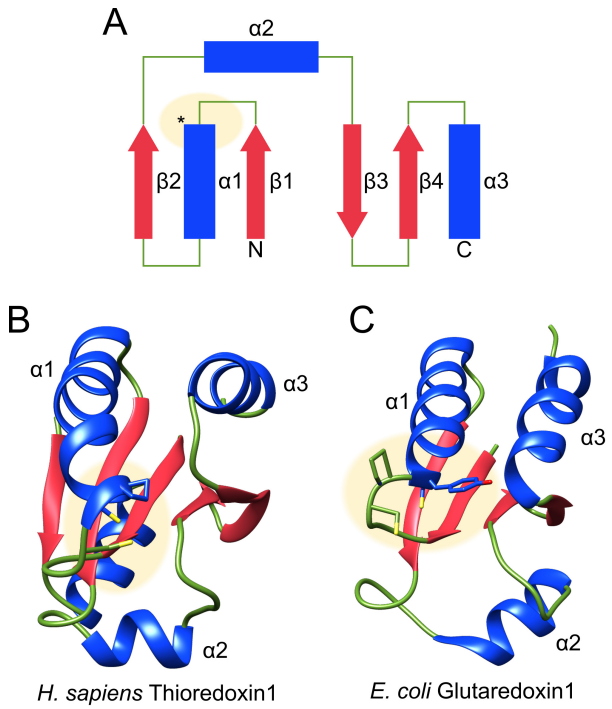

Figure 1: **The thioredoxin fold.** (A) schematic 2D representation of the core thioredoxin fold. Secondary structure elements are labelled with β strands represented as red arrows, α helices as blue boxes and loops as green lines. N- and C-termini are labelled. The active site location is marked with a star and highlighted in yellow. This figure was adapted from Martin (1995). (B) crystal structure of *H. sapiens* Thioredoxin1 (pdb: 1ERT, Weichsel et al. (1996)). β strands are shown in red, loops in green and α helices are coloured in blue and labelled. The active site residues are shown and highlighted by yellow background. (C) structure of *E. coli* Glutaredoxin1 solved by NMR (pdb: 1EGR, Sodano et al. (1991)). β strands are shown in red, loops in green and α helices are coloured in blue and labelled. The active site residues are shown and highlighted by yellow background.

played in figure 1 (A). In the three dimensional structure, a single beta sheet is formed, which is sandwiched by the three alpha helices as shown in figure 1 (C) for *E. coli* Glutaredoxin1, which is nicely representing this most basic form of the thioredoxin fold (Lillig et al., 2008). Thioredoxins like *H. sapiens* Thioredoxin1 shown in figure 1 (B) have an extended N-terminus expanding the fold by additional secondary structure elements (Martin, 1995).

The active site is located at the beginning of the first alpha helix $\alpha 1$. It comprises four amino acids and is usually a variation of CXXC or CXXS in oxidoreductases (Atkinson and Babbitt, 2009a). Within the active site, the N-terminal cysteine is regarded as the catalytic cysteine due to its surface exposure and relatively low pKa (Lillig et al., 2008). For enzymatic functioning as a whole, also other parts of the protein play a role (Ren et al., 2009; Mavridou et al., 2014).

For thioredoxins, the active site motif often consists of the consensus sequence CGPC (Ren et al., 2009) as exhibited by *H. sapiens* Thioredoxin1 displayed in figure 1 (B). Thioredoxins were originally identified in the 1960s as components of the enzymatic synthesis of L-methionine and deoxyribonucleotides, providing electrons to the respective reductase enzyme (Black et al., 1960; Laurent et al., 1964). In these reactions, the thioredoxin reduces a disulphide within the target enzyme and in turn becomes oxidized itself, forming an intramolecular disulphide between the two cysteines of the active site. This disulphide can be reduced by thioredoxin reductases in an NADPH-dependent manner (Holmgren, 1995). Reducing protein disulphides constitutes the main function of thioredoxins and a large number of target proteins have since been identified (Lee et al., 2013; Holmgren, 1985) which broadens the role of thioredoxins from metabolic pathways to, among others, detoxification and signalling (Netto and Antunes, 2016; Nakamura et al., 2001; Serrato et al., 2013). One prime example for a signalling function is the activation of chloroplast enzymes at the beginning of the light period (Buchanan, 2016). Specificity is likely controlled by the electrostatic properties of the thioredoxins around the active site (Begas et al., 2015; Hossain et al., 2021).

Typical protein disulphide isomerases contain four thioredoxin domains, two of which are inactive while the outer two carry the active site consensus motive CGHC (Tian et al., 2006) although other domain structures are also possible (Appenzeller-Herzog and Ellgaard, 2008). They are mainly present in the ER, where they catalyse disulphide formation and reduction, but especially the rearrangement of non-native disulphides (Laboissiere et al., 1995; Okumura et al., 2015). This is particularly relevant for the correct folding of secretory proteins (Anelli and Sitia, 2008).

In bacteria, this function is carried out by Dsb proteins in the periplasm.

It is divided between DsbA and DsbB, which are responsible for the oxidation of target proteins, and DsbC, DsbG and DsbD, which catalyse isomerisation and reduction (Łasica and Jagusztyn-Krynicka, 2007; Messens and Collet, 2006). DsbA has a single thioredoxin domain with a CPHC active site motif, but comparable reactivity in the oxidation of substrates than protein disulphide isomerases (Zapun et al., 1993). In a second step, non-native disulphides can be rearranged by DsbC (Rietsch et al., 1996).

Peroxiredoxins are another noteworthy class of thioredoxin fold proteins, usually carrying a CPTE or CTTE active site motif (Schröder and Ponting, 1998). The lack of a second cysteine within the active site leads to the requirement for a resolving cysteine located outside the active site motif or provided by an interaction partner (Copley et al., 2004; Perkins et al., 2015). In *A. thaliana* 10 different peroxiredoxins are known (Umate, 2010) with varying resolving mechanisms. Oxidized peroxiredoxins are reduced by thioredoxins (Telman et al., 2020). With a rather low catalytic activity, peroxiredoxins are often regarded as signalling components (Perkins et al., 2015). For instance, the yeast peroxiredoxin Tsa1 is involved in the regulation of the transcription factor Yap1 (Tachibana et al., 2009) while in *A. thaliana* peroxiredoxins are involved in the deactivation of chloroplast enzymes at the onset of the dark period (Ojeda et al., 2018).

A number of thioredoxin fold proteins interact with glutathione as a cofactor (Deponte, 2013). Some glutathione peroxidases from mammals utilize the cellular glutathione pool as reductants and can contain selenocystein within their active site (Toppo et al., 2008). Similarly folded proteins in plants are not using glutathione as reductants and rather rely on thioredoxins (San Koh et al., 2007). Glutathione peroxidases are involved in both antioxidant defence and cellular signalling (Toppo et al., 2008), similar to peroxiredoxins. A well-studied example is the yeast glutathione peroxidase Gpx3, which is required for the oxidation of Yap1 under condition of enhanced oxidative stress. (Delaunay et al., 2002; Paulsen and Carroll, 2009).

Glutathione *S*-transferases contain a thioredoxin fold domain as well as an additional C-terminal domain (Pan and Bardwell, 2006). The active site motif of the thioredoxin fold domain deviates strongly from the CXXC motif, in some cases lacking cysteines all together (Atkinson and Babbitt, 2009b). Instead, the thioredoxin fold domain is utilized to bind glutathione, while the C-terminal domain provides a hydrophobic binding site for substrates, onto which the glutathione can be transferred (Nishida et al., 1998; Armstrong, 1991). With this activity, glutathione *S*-transferases play a role in the conjugation of xenobiotics for detoxification, as well as in endogenous metabolic processes (Vuilleumier, 1997; Edwards et al., 2000).

2.3 The glutaredoxin family

Other important members of the thioredoxin superfamily are glutaredoxins. Glutaredoxins bind glutathione as cofactor with a binding site between the active site motif and the $\alpha 2$ helix. The thiol of glutathione is directed towards the active site (Deponte, 2013). Dependent on the active site motif, glutaredoxins are usually subdivided into two major classes. Class I or dithiol glutaredoxins carry a CXXC active site, usually with the CPYC consensus sequence while class II or monothiol glutaredoxins exhibit a CXXS active site with a highly conserved CGFS motif and an overall higher degree of homology of the thioredoxin fold domain(Lillig et al., 2008; Deponte, 2013).

Class I glutaredoxins are oxidoreductases that can catalyse the reduction of protein disulfides (Holmgren, 1976) and especially glutathionylation and deglutathionylation reactions (Gravina and Mieyal, 1993; Deponte, 2013; Lillig et al., 2008; Avval and Holmgren, 2009; Meyer and Dick, 2010). The activity can be investigated with small artificial substrates like bis(2-hydroxyethyl)disulfide (HEDS) (Holmgren and Aslund, 1995; Begas et al., 2015, 2017) or protein substrates like roGFP2 (Meyer et al., 2007; Meyer and Dick, 2010) that can even be employed *in vivo* (Schwarzländer et al., 2016). Catalysis on the molecular level requires a complex set of intermediate steps with glutathione bound and activated in different ways and positions (Lillig et al., 2008; Deponte, 2013; Begas et al., 2017; Ukuwela et al., 2018; Mashamaite et al., 2015). Some reaction pathways are independent of the second thiol within the consensus CPYC active site motif and directly utilize the thiol of glutathione as the resolving thiol. (Mesecke et al., 2008; Fernandes and Holmgren, 2004). Depending on whether or not the second thiol, which forms an intramolecular disulphide with the first thiol, is involved, reaction pathways are denoted as monothiol or dithiol mechanism (Ukuwela et al., 2018; Mashamaite et al., 2015).

Class II glutaredoxins can be subdivided into two subgroups, either containing a single glutaredoxin domain or an N-terminal thioredoxin-like domain as well as one or more glutaredoxin domains. The active site is the highly conserved CGFS motif (Li and Outten, 2012; Rouhier et al., 2010). They are known to bind 2Fe-2S-Cluster as dimers, coordinating the cluster with the active site thiols as well as the thiols of the glutathione bound within the binding site (Iwema et al., 2009; Picciocchi et al., 2007; Li and Outten, 2012). Functionally, class II glutaredoxins are involved in Fe-S-Cluster biogenesis by binding and transferring clusters in mitochondria and chloroplasts (Rodrıguez-Manzaneque et al., 2002; **?**; Bandyopadhyay et al., 2008; Rouhier et al., 2010; Couturier et al., 2015).

Some class I glutaredoxins have been shown to also bind 2Fe-2S-Clusters

as dimers (Rouhier et al., 2007; Mesecke et al., 2008; Lillig et al., 2005). These clusters are usually less likely to be transferred to target proteins as compared to class II glutaredoxin bound clusters and have been discussed as potential redox sensors that break apart under oxidative stress conditions, releasing the catalytically active monomers, which can in turn counteract the oxidative damage as reductases (Rouhier et al., 2010; Lillig et al., 2005). Until recently, this property was restricted to class I glutaredoxins that deviate from the CPYC consensus active site in the second position, usually replacing proline by a serine or glycine, and mutating this position to a proline would abolish the cluster binding (Rouhier et al., 2007) while mutating the proline in a CPYC glutaredoxin to serine or glycine would enable cluster binding (Berndt et al., 2007; Rouhier et al., 2007). But the discovery of a 2Fe-2S-Cluster bound by *Chlamydomonas reinhardtii* Glutaredoxin 2 with CPYC active site motif implies a more complex determination of cluster binding capabilities (Roret et al., 2021).

Moreover, some class II glutaredoxins have also been shown to exhibit residual oxidoreductase activity (Herrero and de la Torre-Ruiz, 2007). Protein substrates like GAPDH or carbonic anhydrase were deglutathionylated by class II glutaredoxins from *Chlamydomonas reinhardtii* (Zaffagnini et al., 2008; Gao et al., 2010) and *S. cerevisiae* (Tamarit et al., 2003) respectively, with a proposed mechanism including a resolving cysteine outside the active site. *A. thaliana* class II glutaredoxins show a low but detectable oxidase activity towards roGFP2 (Moseler et al., 2015; Zannini et al., 2019). In the later example, mutation of the potential resolving cysteine actually led to an increase of oxidase activity (Zannini et al., 2019).

With these recent results softening the boundaries between catalytically active class I glutaredoxins and Fe-S-cluster binding class II glutaredoxins, the question arises how the functionality of glutaredoxins is determined aside from the active site motif. One aspect appears to be the orientation of the glutathione within the binding site which differs between non-Fe-S-binding class I glutaredoxins, Fe-S-binding class I glutaredoxins and Fe-S-binding class II glutaredoxins (Berndt and Lillig, 2017). Especially the interaction mode between the lysine located in proximity to the N-terminus of the active site motif and glutathione varies between holo-proteins of class I and II. This is largely caused by the different loop length connecting the lysine with the active site motif, with class I glutaredoxins possessing only two amino acids while class II glutaredoxins having seven. Extending the loop of a class I glutaredoxin to resemble the class II loop decreases oxidoreductase activity but enables Fe-S-Cluster transfer. Shortening the loop of a class II glutaredoxin to a class I loop leads to higher oxidoreductase activity but limits Fe-S-Cluster transferase activity (Trnka et al., 2020; Liedgens et al., 2020). Besides the loop structure,

also other residues coordinating the glutathione within the binding site have an influence on the catalytic activity of glutaredoxins (Liedgens et al., 2020).

2.4 Glutaredoxins in *A. thaliana*

The genome of the model plant *A. thaliana* encodes at least 31 different glutaredoxins (Rouhier et al., 2004). The glutaredoxin domains are aligned in figure 2. Six and four proteins belong to the conventional classes I and II, respectively, with GRXS17 being a multidomain protein containing three glutaredoxin domains with CGFS active sites. While the CGFS active site is strictly conserved for members of the class II, the active site motif deviates from the CPYC consensus for three members of the class I. The remaining 21 glutaredoxins have a different active site composition with a CCMC or CCMS consensus sequence. These CC-type or class III glutaredoxins are specific to land plants (Lemaire, 2004; Rouhier et al., 2004) and have been termed ROXY proteins after one of the first characterized members, ROXY1 (Xing et al., 2005).

It is noteworthy that the position C-terminally adjacent to the active site indicated by a purple star in figure 2 is highly conserved among class III glutaredoxins compared to class I and II. Most ROXYs contain a histidine in this position while only ROXY6,7,8 and 9 have a tyrosine. This subclass highlighted by a red background in figure 2 also deviates from the other ROXYs regarding the C-terminus marked with green stars, where the otherwise highly conserved ALWL motif is altered or even truncated. ROXY9 contains two additional cysteins outside the active site indicated by yellow stars in figure 2. The C-terminal cystein, Cys61, is conserved among most ROXYs while the other is only present in the closely related ROXY6,7 and 8. The lysine prior to the active site that is involved in glutathione binding and orientation (Berndt and Lillig, 2017; Trnka et al., 2020) is denoted in figure 2 by a dark blue star. Concerning the sequence between this lysine and the active site, ROXYs rather resemble class I glutaredoxins in having only two amino acids rather than seven as in class II glutaredoxins. However, a closer inspection reveals that the lysine is altered in some ROXYs to a similarly-charged arginine, uncharged but polar asparagine or even an apolar valine, which could alter the binding mode of glutathione. ROXY20 employs a unique three amino acids linker between the arginine and the active site. Additional residues, that are involved in the binding of glutathione (Berndt and Lillig, 2017), are marked with light blue stars in figure 2. Similarly, some degree of deviation in these motifs can be observed for the different classes.

Predictions of the cellular localization indicate that most plant glutaredoxins have a nuclear-cytoplasmic location, including all ROXYs. This localization was

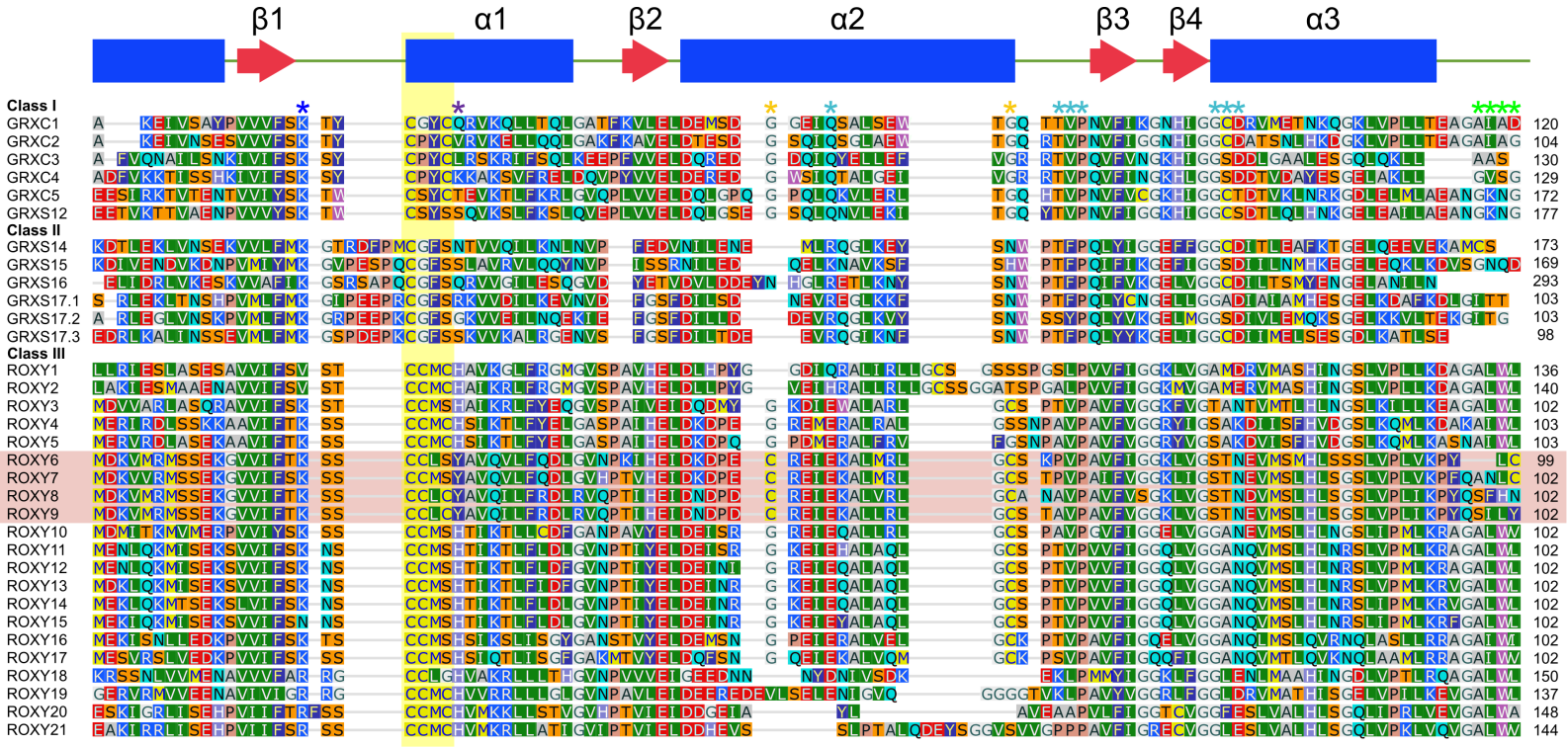

Figure 2: **Alignment of *A. thaliana* glutaredoxins**. Protein sequences of the 31 glutaredoxins from *A. thaliana* were ordered according to established conventions (Rouhier et al., 2004; Xing et al., 2006) and aligned by COBALT (Papadopoulos and Agarwala, 2007). All three glutaredoxin domains of GrxS17 were included. The alignment was trimmed to show the glutaredoxin domain and secondary structure elements are assigned based on the available crystal structure of GRXC5 (pdb: 3RHB, Couturier et al. (2011)). Different amino acids are coloured, the active site position is highlighted by yellow background. ROXY9 and the closely related ROXY6,7 and 8 are highlighted by red background. Important residues are indicated by stars; dark blue for conserved lysine prior to active site, light blue for additional residues involved in glutathione binding for GRXC5 (Berndt and Lillig, 2017), purple for position adjacent to the active site conserved in ROXYs, yellow for additional cysteines in ROXY9 and green for the conserved ALWL C-terminus in most ROXYs.

experimentally confirmed for class III glutaredoxins from poplar Xu et al. (2022). The class I members GRXC5, GRXS12 and the class II members GRXS14 and S16 locate to the plastids (Müller-Schüssele et al., 2021) while GRXS15 locates to the mitochondria. GRXC3 and C4 are potentially secreted (Moseler et al., 2015).

2.4.1 Class I

The six class I glutaredoxins can be subdivided into three subgroups in *A. thaliana*, with each group containing two members; GRXC1 and C2, GRXC3 and C4 and GRXC5 and S12 (Zaffagnini et al., 2019; Müller-Schüssele et al., 2021). For dithiol class I glutaredoxins from poplar, a disulphide within the active site could be observed under oxidizing conditions which could be reduced by DTT or GSH in combination with glutathione reductase and NADPH. The redox potential was determined to be around –250 mV and the pKa of the catalytic cysteine is around 5 (Couturier et al., 2013a).

GRXC1 and GRXC2 are the two cytosolic class I glutaredoxins. They are essential as the double mutant is not viable. Both proteins show enzymatic activity in classical assays. While GRXC1 with the CGYC active site motif is able to bind a 2Fe-2S-cluster in recombinant protein and is present as dimers *in planta*, GRXC2 with the CPYC active site is not able to bind a cluster. The cluster is sensitive to oxidation and GRXC1 is not able to complement the Δ*grx5* mutant phenotype in *S. cerevisiae*, which is deficient in Fe-S-cluster metabolism. However, both GRXC1 and C2 can complement the Δ*grx1* mutant phenotype in *S. cerevisiae*, which is more sensitive to oxidative stress (Riondet et al., 2012).

GRXC1 was recently found to interact with a Glucose-6-phosphate transporter at the ER with a yet to be fully unravelled function (Baune et al., 2020). GRXC2 is potentially involved in pathogen response as an interaction partner of the BAK1, a co-receptor of multiple PAMP receptors. GRXC2 glutathionylates BAK1, which inhibits kinase activity (Bender et al., 2015).

GRXC3 and C4 contain a CPYC active site motif and have an N-terminal extension that might target the proteins to the secratory pathway or potentially function as a membrane anchor (Moseler et al., 2015; Couturier et al., 2013a; Zaffagnini et al., 2019), but the exact localization is still unknown for GRXC3. GRXC4 has been shown to interact with vacuolar sorting receptors and is transported to the vacuole (Shen et al., 2013). While the poplar homologues exhibited a rather enzymatic activity in assays (Couturier et al., 2013a), the biochemical properties of *A. thaliana* GRXC3 and C4 have not been investigated to this date. On the physiological level, GRXC3 has been associated

with floral morphology (Xie et al., 2015), but the exact functions of GRXC3 and C4 are not known.

The two plastidial class I glutaredoxins deviate in their active site motif from the CPYC consensus with GRXC5 containing a CSYC motif and GRXS12 a CSYS motif. With the serine in the second postion, GRXC5 was shown to bind a 2Fe-2S-cluster. Mutating any of the two active site cysteines abolished cluster binding (Couturier et al., 2011), which is in line with GRXS12 beeing not able to bind a cluster with the wild-type active site motif (Couturier et al., 2009b). Reductase activity of GRXC5 in classical assays is increased when mutating the second cysteine within the active site to a serine, similarly, the reverse exchange in GRXS12 reduces reductase activity(Couturier et al., 2011). Also another cysteine outside the active site plays a role in the reactivity of GRXC5 and S12 towards protein substrates, but in general the proteins are able to operate via a monothiol mechanism (Couturier et al., 2009b, 2011). Analysis of the poplar homologue of GRXS12 showed a relatively low pKa of 3.9 for the active site thiol and a sensitivity to glutathionylation, which lead to a decrease in activity. This could argue for a role as stress-related redox sensor (Zaffagnini et al., 2012a).

2.4.2 Class II

The class II glutaredoxins have been intensively studied in recent years, revealing their role in Fe-S-cluster metabolism and beyond.

GRXS14 is one of the two plastidial class II glutaredoxins. It consists of a single glutaredoxin domain, the structure of which has been solved by X-ray crystallography (PDB: 3IPZ, (Li et al., 2010)). It was shown to bind an 2Fe-2S-cluster after expression in *E. coli* (Picciocchi et al., 2007) and both GRXS14 from *A. thaliana* as well as the poplar homologue are able to complement the $\triangle$*grx5* mutant phenotype in *S. cerevisiae* (Liu et al., 2013; Bandyopadhyay et al., 2008), but the exact role in the plastidial Fe-S metabolism is still unknown (Couturier et al., 2015).

Physiologically, GRXS14 is involved in the regulation of calcium channels (Cheng and Hirschi, 2003), overall tolerance to oxidative stress (Cheng et al., 2006) and chlorophyll content (Rey et al., 2017) and interacts with selenium binding protein 1, which has implications in selenium and metal detoxification (Valassakis et al., 2019).

GRXS15 is the second class II glutaredoxin consisting just of a single glutaredoxin domain. Even though GRXS15 is essential and the only glutaredoxin reported to be located within the mitochondria (Moseler et al., 2015), the main site of Fe-S-cluster biogenesis, the GRXS15 homologue from poplar initially

failed to complement the Δ*grx5* mutant phenotype in *S. cerevisiae* (Bandyopadhyay et al., 2008), potentially due to the use of rare codons (Ströher et al., 2016). Further investigation revealed, that it indeed can complement Δ*grx5* mutant phenotypes (Cheng, 2008; Moseler et al., 2015), bind a 2Fe-2S-cluster and transfer this cluster onto aconitase (Moseler et al., 2015) and ISCA proteins (Azam et al., 2020). The protein also exhibits a minor oxidase activity towards roGFP2 (Moseler et al., 2015), which is surprising as it is to this date the only glutaredoxin identified in mitochondria, a compartment with a high GSH-dependent metabolism (Zaffagnini et al., 2019).

GRXS15 protects root growth against oxidative stress (Cheng, 2008) and arsenic treatment (Ströher et al., 2016). Alteration in the glutathione binding site lead to changes in carbohydrate and amino acid metabolism (Moseler et al., 2021).

The second plastidial class II glutaredoxin is GRXS16. Aside from the glutaredoxin domain with the CGFS active site motif, it also contains an N-terminal endonuclease domain that is catalytically active (Liu et al., 2013). While the poplar homologue is able to complement the Δ*grx5* mutant phenotype in *S. cerevisiae* (Bandyopadhyay et al., 2008), the *A. thaliana* protein was only able to do so in the absence of the N-terminal domain or when a cysteine within the endonuclease domain is mutated that otherwise forms a disulphide with the active site thiol of the glutaredoxin domain. Purified protein from *E. coli* contains brownish dimer fraction indicating Fe-S cluster binding (Liu et al., 2013; Bandyopadhyay et al., 2008). Similar to GRXS14, the exact role in the plastidial Fe-S metabolism is yet to be identified (Couturier et al., 2015). GRXS16 shows an oxidase activity towards roGFP that could be enhanced by mutating a potential resolving cysteine. The disulphide between this resolving cysteine and the active site thiol could not be reduced by GSH and requires the FTR TRX system, which links GRXS16 to a potential control by light (Zannini et al., 2019). GRXS16 interacts with several selenium binding proteins, which potentially links it to metal detoxification (Valassakis et al., 2019).

GRXS17 is the only cytosolic class II glutaredoxin. It is a multidomain protein that contains a thioredoxin-like domain as well as three glutaredoxin domains all with the CGFS active site motif. This domain structure is specific to higher plants (Couturier et al., 2009a). The protein is found in dimeric form *in planta* and recombinant protein can bind an 2Fe-2S-cluster with all three domains (Knuesting et al., 2015). It is able to complement the Δ*grx5* mutant phenotype in *S. cerevisiae* (Bandyopadhyay et al., 2008), with the second glutaredoxin being the main player (Knuesting et al., 2015). GRXS17 associates with other components of the cytosolic Fe-S-cluster assembly pathway

and the *grxs17* mutant shows similar phenotypes as mutants in these other components (Iñigo et al., 2016). However, cytosolic aconitase activity is not strongly affected in the *grxs17* mutant (Knuesting et al., 2015).

On a broader scale, the *grxs17* mutant shows growth defects under high temperature (Cheng et al., 2011; Knuesting et al., 2015; Martins et al., 2020) and long light periods which is related to interaction with Nuclear Factor Y Subunit C11/Negative Cofactor 2α, a known regulator of developmental processes (Knuesting et al., 2015). The tolerance against heat stress has recently been correlated to a holdase function which requires oligomerization (Martins et al., 2020). GRXS17 is also important for the overall growth under iron deficiency (Yu et al., 2017).

2.4.3 Class III

Although the land-plant specific class III glutaredoxins or ROXYs comprise the biggest class with 21 members in *A. thaliana* (Rouhier et al., 2004; Xing et al., 2006), they have not been extensively studied on a biochemical level, mainly due to difficulties obtaining recombinant protein (Couturier et al., 2010; Zannini et al., 2019). Poplar class I GRXC1 with a CCMC active site motif was able to bind an Fe-S-cluster, both poplar GRXC1 and GRXC4 with CCMC active site motif showed a low reductase activity in classical assays while a hybrid version of the poplar class III GRXS7.2 with the C-terminus of GRXC4 showed next to no activity (Couturier et al., 2010). In a recent publication, several poplar class III glutaredoxins could be recombinantly expressed in *E. coli* with an MBP tag and investigated regarding reductase activity. No activity could be detected with the classical HEDS substrate, but a low activity towards cummene hydroperoxide could be detected with some of the proteins (Xu et al., 2022).

The ROXY proteins are thought to have a nucleo-cytoplasmic localization, which has been demonstrated for instance for ROXY1 (Li et al., 2009) as well as ROXY18 and ROXY20 (Couturier et al., 2011). The most detailed functional studies have been conducted mainly with ROXY1, ROXY9 and ROXY19.

ROXY1 was identified as a regulator of floral development, where it controls petal number (Xing et al., 2005) and acts redundantly with ROXY2 when controlling anther development (Xing and Zachgo, 2008). ROXY1 is reported to locate to the nucleus and to interact with TGA transcription factors, mainly PAN for petal development (Li et al., 2009) and TGA9 and 10 for anther development (Murmu et al., 2010), via the C-terminal LXXLL motif (Li et al., 2011). Epistasis analysis has shown that ROXY1 is a negative regulator of PAN (Li et al., 2009). The C-terminal ALWL motif, which is important for ROXY1 activity, interacts with the transcriptional co-repressor TOPLESS, which might explain the

repressive effect on the transcriptional activity of PAN. Site specific mutation of individual cysteines connected to complementation studies showed that C341 of PAN is important for its function. While oxidizing treatment impedes DNA binding of PAN (Gutsche and Zachgo, 2016), a direct connection to a potential redox regulation via ROXY1 has not been proven. In a recent study ROXY1 was found to co-localize with RNA Polymerase II throughout transcription, this co-localization decreased after H_2O_2 treatment (Maß et al., 2020).

Due to the potential redundancy of ROXYs loss of function evidence for their *in vivo* significance is scarce. Still, ROXYs 6,7,8, and 9, are important for the activation of nitrate uptake genes under conditions of low nitrate availability (Ohkubo et al., 2017; Ota et al., 2020, Pelizeus, unpublished). One feature of the ROXY9 subclass is the missing ALWL motif (see figure 2) which explains why they cannot directly interact with TOPLESS (Uhrig et al., 2017).

ROXY6,*8* and *9* together with *ROXY19*,*20* and *21* are induced under nitrogen starvation, whereas *ROXY7* and *ROXY10-18* are repressed (Jung et al., 2018). While *ROXY9* over-expressors showed an increased root hair length, *ROXY15* over-expressors had shorter root hairs (Jung et al., 2018). This points into the direction of an antagonistic role of the ROXY6,8 and 9 subclass and the ROXY10,11,12,13,14 and 15 subclass in regulating root growth under different nitrogen levels (Patterson et al., 2016; Jung et al., 2018; Ehrary et al., 2020).

ROXY19 was isolated in a screen for proteins interacting with TGA transcripton factors, which are important for the activation of the jasmonic acid/ethylene-activated defense pathway and the salicylic acid-activated pathway. *ROXY19* expression is induced by salicylic acid and jasmonic acid (Ndamukong et al., 2007). Since ectopically expressed protein interferes with the activation of the JA/ET pathway, it has been suggested that ROXY19 and other redundant SA-inducible ROXYs mediate the antagonistic effect of SA on the JA/ET pathway (Zander et al., 2012). The repressive function is connected to the C-terminal ALWL motif, which is recognized by the transcriptional co-repressor TOPLESS (Zander et al., 2012; Uhrig et al., 2017). However, the postulated function SA-inducible repressors of the JA/ET pathway cannot be confirmed by loss of function analysis. Ectopically expressed ROXY19 also represses the TGA-controlled detoxification pathway, but no hyperactivation is observed in loss of function plants (Huang et al., 2016). ROXY18 has a role in pathogen defence signalling, it is required for successful infection by the necrotrophic fungus *Botritis cinerea* (La Camera et al., 2011).

Aside from *A. thaliana*, class III glutaredoxins have been connected to the drought response (Ruan et al., 2018) and osmotic stress (Ruan et al., 2022) in manioc, with manioc class III glutaredoxins exhibiting an autonomous transactivation capacity in yeast, which is somewhat in contrast to the mainly repressory

role in *A. thaliana* (Uhrig et al., 2017). In maize, they are also associated with drought stress (Ding et al., 2019). Class III glutaredoxins form rice have been linked to salt stress (Verma et al., 2021), iron (Kobayashi et al., 2022) and nitrogen metabolism (El-Kereamy et al., 2015). In cucumber, class III glutaredoxins were differentially expressed after a variety of different stress treatments (Yang et al., 2021b).

A very detailed analysis was performed with the maize class III glutaredoxin MSCA1, which was reported to redox modulate the TGA transcription factor FEA4 to regulate inflorescence meristem development (Yang et al., 2021a).

2.4.4 Glutaredoxin-like proteins

In addition to the three conventional classes of glutaredoxins, *A. thaliana* also contains two glutaredoxin-like proteins, AT3G12540 and AT4G08550, that are sometimes described as class IV glutaredoxins (Couturier et al., 2009a; Zaffagnini et al., 2019). They consist of an N-terminal glutaredoxin domain with a strongly deviating CRDS or CEEC active site motif followed by a DEP domain and a DUF457 domain, but have not been further investigated.

2.5 ROXY9 and TGA1

The TGA transcription factors which were identified as ROXY interaction partners in multiple studies (Li et al., 2009; Murmu et al., 2010; Uhrig et al., 2017; Li et al., 2019; Yang et al., 2021a), are basic leucine zipper transcription factors that bind to the palindromic TGACGTCA consensus sequence and are involved in the regulation of different stress responses. The TGA family contains ten members in *A. thaliana* and can be subdivided into five different clades (Gatz, 2013). The physical and genetic interactions between the 21 ROXYs and the 10 TGA factors might yield complex signalling networks for developmental processes or stress responses (Gutsche et al., 2015). Ectopically expressed ROXY9 represses the positive function of TGA1 and TGA4 in the hyponastic growth response, while it does not repress the TGA2-regulated response to xenobiotic stress. Therefore, it has been speculated that it regulates the function of TGA1 and TGA4 (Li et al., 2019).

An important function of TGA1 and 4 is the regulation of plant defence, conveying resistance against *Pseudomonas* infection (Kesarwani et al., 2007) and regulating a subset of defence genes (Shearer et al., 2012; Budimir et al., 2021), which involves the regulation of defence hormone biosynthesis genes (Sun et al., 2018). Although gene regulation is to some extend independent of the important regulator of plant defence NPR1 (Shearer et al., 2012), TGA1 and

NPR1 have been shown to interact *in planta* after treatment with the defence hormone salicylic acid. This observation was attributed to the reduction of an intramolecular disulphide within TGA1, namely between Cys260 and Cys266, under these conditions, which enables the interaction of the reduced protein with NPR1 (Després et al., 2003). This interaction also enhances the binding of TGA1 to DNA (Després et al., 2003; Lindermayr et al., 2010), though the latter study identified the two other cysteines, Cys172 and Cys287, as targets of redox modulation after GSNO treatment (Lindermayr et al., 2010). TGA1 and 4-dependent target genes like *DLO1* were not pre-induced in complementation lines with all four cysteines exchanged for serines, which disqualifies the role of a potential redox modulation of TGA1 *in vivo* (Budimir et al., 2021).

Another function of TGA1 and 4 is the regulation of hyponastic growth, the tilting of the leaves upwards, away from unfavourable conditions like shade, which is reduced in the *tga1,4* double mutant. In this context, ROXY9 was identified as a negative regulator with over-expression of ROXY9, as well as ROXY8, leading to constitutive repression of hyponastic growth under low light conditions. ROXY9 physically interacts with TGA1 in yeast and in protoplasts, and this interaction in yeast is independent of the ROXY9 active site (Li et al., 2019). However, the active site motif does play a role in the supression of hyponastic growth as it was shown to be lifted in over-expressors with a SCLC or CSLC active site (Li et al., 2019; Li, 2017), as well as over-expressors with the class I active site CPYC or a mutation in the conserved tyrosine right after the active site (CCLCA) (Treffon, 2019), as shown in figure 3. For this, three plants of the respective line were grown in a single pot, which lead to an activation of hyponastic response due to mutual shading.

ROXY9 is also reportedly involved in the regulation of nitrogen uptake where

Figure 3: **Supression of hyponastic growth depends on ROXY9 active site.** Col-0 wild-type plants as well as ROXY9 over-expressor variants with different active sites as indicated were grown with three plants in one pot for 4 weeks under long-day conditions. Plant lines are described by Li et al. (2019) and Treffon (2019).

it induces the expression of *NRT2.1* in roots. In this context, ROXY9 is likely transported from the shoot to the root under condition that require more nitrogen uptake (Ohkubo et al., 2017). While also ROXY6 and ROXY8 are involved in this signalling (Ohkubo et al., 2017; Ota et al., 2020), a potential involvement of TGA1 has not yet been reported.

2.6 Aim of this thesis

While class I and II glutaredoxins have been extensively studied on a biochemical level in the last twenty years, knowledge concerning the plant-specific class III glutaredoxins has been scarce. However, on a physiological level, class III glutaredoxins have been identified as important components of different signalling networks. For ROXY9 especially, different cellular functions as well as interaction partners are known, but the actions of ROXY9 on a molecular level have remained elusive.

The aim of this thesis is thus to fill this gap and provide a detailed biochemical and biophysical characterization of the class III glutaredoxin ROXY9. One of the most important prerequisites for such an analysis was the identification of a proper expression system for the production of recombinant protein, which had been found in the bacculovirus expression vector system shortly before the start of the thesis (Treffon, 2019). In a first step, the properties of these recombinant ROXY9 proteins should be examined with regard to protein folding and a potential redox modulation.

Class I glutaredoxins are conventionally known for their oxidoreductase function while class II glutaredoxins are involved in the binding and transfer of Fe-S-clusters. Recent results have softened the distinctions between the classes with the identification of Fe-S-cluster binding class I glutaredoxins and catalytically active class II glutaredoxins. In a second step, it should be investigated which of the known functions of class I and II glutaredoxins can be performed by the class III glutaredoxin ROXY9.

With interaction partners like TGA1 in mind, additional steps should be taken to relate the properties and potential biochemical activities of ROXY9 to its *in vivo* function.

3 Materials

3.1 Devices

Device	Model	Manufacturer
ÄKTA chromatography system	prime plus	GE Healthcare
Autoclave	VX-95	Systec
	VX-150	Systec
Blot apparatus	Self-made	Workshop Albrecht-von-Haller institute
Casy cell counter		OLS OMNI Life Science
CCD Camera	ChemoCam	Intas
Centrifuge	Rotina 380R	Hettich
	Mikro 200R	Hettich
Cooling chamber		Johnson Control
Climate chamber		Johnson Control
Desiccator		Glaswerkstatt Wertheim
Desk centrifuge	Pico17	Thermo Scientific
Desk centrifuge (small)		Sprout
Electroporation device	Gene Pulser II	BioRAD
Fridge	MEDline	Liebherr
Freezer	L542-85	New Brunswick Scientific
Gel electrophoresis apparatus	Self-made	Workshop Albrecht-von-Haller institute
Heating block	TH26	HLC
Incubator		Memmert
Ice machine		Ziegra
Magnetic stirrer	RH basic 2	IKA Labortechnik
Micro pipette	pipetman	Gilson
Mixer mill	MM301	Retsch
Nanodrop	Nanodrop One	PeqLab
pH-Meter	pH211	HANNA instruments
Plate reader	Synergy HT	BioTek
Power supply	E323	Consert
	EV243	Consert
	EV231	Consert
	PowerPac	BioRAD
Precision scale	ED124S	Sartorius
Rotor	1798	Hettich

	SLA-3000	Dupont
	SS-34	Dupont
Scale	SPO 51	SCALTEC
SDS-Page running chamber	Mini-PROTEAN	BioRAD
Shaker	mini gyro rocker SSM3	Stuart
	VX7	IKA-Werke
Sterile bench	Safe 2020	Thermo Scientific
	HERAguard	Thermo Scientific
Thermocycler	MyCycler	Bio-RAD
	MyiQ	Bio-RAD
Vortex	Vortex Genie 2	Scientific Industries
Water treatment unit	Arium pro DI	Sartorius

3.2 Chemicals

Chemical	Supplier
Acetic acid	Roth
Acrylamide/Bisacrylamide (37.5:1)	Sigma
Ampicillin	Roth
AMS	Setareh Biotech
APS	Roth
ATP	Roche
$B(OH)_3$	Roth
Bromophenol blue	Roth
BSA	Roth
$Ca(NO_3)_2$	Sigma-Aldrich
CHP	Sigma
Citric acid	Roth
Coomassie Briliant Blue	KMF
cOmplete Protease Inhibitor	bimake
$CuSO_4$	Roth
Diamid	Sigma
Dithiane	Sigma
DMSO	Roth
dNTPs	Roth
DTT	Roth
EDTA	SIGMA

EGTA	Roth
Ethanol	Hilmer Brauer
Ethidium bromide	Roth
$FeCl_3$	AppliChem
Fluorescein	Sigma
Formaldehyde	Roth
Gene Ruler DNA Ladder	Thermo Fischer Scientific
Glucose	Roth
Glycerol	Roth
Glycine	Roth
GSH	Sigma
GSSG	Sigma
H_3BO_3	Roth
HCl	Roth
HEDS	Sigma
HEPES	Roth
H_2O_2	Roth
H_3PO_4	Roth
IAM	Sigma
Imidazole	Roth
IPTG	Roth
KCl	Roth
KH_2PO_4	Roth
KNO_3	Roth
KOH	Roth
Lactose	Merck
Mannitol	Roth
Maltose	Roth & Merck
Methanol	Merck
$MgCl_2$	Thermo Scientific
$MgSO_4$	Roth
mmPEG 5k	Fluka
mmPEG 2k	Sigma
$MnSO_4$	Merck
$Na_2B_4O_7$	Roth
NaCl	Roth
NADH	Sigma
NADPH	Roth
NaF	Sigma
Na_2MoO_4	Sigma

NaOH	Roth
NaH_2PO_4	Roth
Na_2HPO_4	Roth
$NaSiO_3$	Roth
NEM	Sigma
Orange G	Sigma
PageRuler protein ladder	MBI Fermentas
Potassium ferricyanide	Sigma
Potassium ferrocyanide	Sigma
Proteasome inhibitor MG132	Sigma
Saccharose	Roth
SDS	Roth
Skim milk powder	Sucofin
Sodium acetate	Roth
Sodium citrate	Roth
Sodium hypochlorite	Roth
Sodium salicylate	Merck
TCEP	Aldrich
TEMED	Roth
TRIS	Roth
Triton-X	Roth
Trypton	Roth
Tween	Roth
Urea	Sigma
X-Gal	Fermentas
Yeast extract	Roth
$ZnSO_4$	Sigma
β-Mercaptoethanol	Roth
2-propanol	Roth
3-phosphoglycerate	Sigma

3.2.1 Consumables and other supplies

Product	Supplier
ÄKTA tubes	Greiner bio-one
MiniTrap desalting column	GE/Cytiva
PD10 desalting column	GE/Cytiva
MBPTrap column	GE/Cytiva
HISTrap column	GE/Cytiva

VivaSpin concentrators	GE Healthcare
Corning concentrators	Sigma
Steel grinding balls 5 mm	Martin Balls
Sterile filter	Sartorius
Superloop	GE Healthcare
Western blot membrane PVDF 0.45 µm	Roth
Whatman paper	GE Healthcare

3.3 Organisms

3.3.1 Plants

Genotype	Description	Reference
Col-0	wild type	NASC stock number N1092
Col-0 + HA-ROXY9 #7-18	Over-expressor of HA-ROXY9 in Col-0 background	Li (2017)
Col-0 + HA-ROXY9 SCLC #20-5	Over-expressor of HA-ROXY9 SCLC in Col-0 background under the control of the CaMV 35S promoter	Li (2017)
Col-0 + HA-ROXY9 CSLC #26-1	Over-expressor of HA-ROXY9 CSLC in Col-0 background under the control of the CaMV 35S promoter	Li (2017)
Col-0 + HA-ROXY9 CCLS #15-1	Over-expressor of HA-ROXY9 CCLS in Col-0 background under the control of the CaMV 35S promoter	Li (2017)
Col-0 + HA-ROXY9 CPYC #18-1	Over-expressor of HA-ROXY9 CPYC in Col-0 background under the control of the CaMV 35S promoter	Treffon (2019)
Col-0 + HA-ROXY9 CCLCA #1-13	Over-expressor of HA-ROXY9 CCLCA in Col-0 background under the control of the CaMV 35S promoter	Treffon (2019)

3.3.2 Insect Cell Culture

Organism	Cell line	Reference
T. ni	High Five (Hi5)	Thermo Fisher Scientific
S. frugiperda	Sf9	Thermo Fisher Scientific

3.3.3 Bacteria

Species	Properties	Reference
E. coli DH5α	*F-, gyrA 96 (Nalr), recA1, endA1, thi-1, hsdR17 (rkmk+), glnV44, deoR, D (lacZYA-argF) U169 [p80dD(lacZ)M15]*	Thermo Fisher Scientific
E. coli BL21	*F– ompT gal dcm lon hsdS$_B$(rB$_B$–m$_B$–) λ(DE3 [lacI lacUV5-T7p07 ind1 sam7 nin5]) [malB+]$_{K-12}$(λS)*	NEB, USA
DH10αBac	Transformed with AcMNPV-Bacmid	Thermo Fisher Scientific

3.4 Primer

Primer	Sequence (5'→3')	Reference
ROXY9 Lic v1 For	1 TACTTCCAAT CCAATGCAAT 21 GGACAAAGTG ATGAGAATGT 41 CTTC	Treffon (2019)
ROXY9 Lic v1 Rev	1 TTATCCACTT CCAATGTTAT 21 TACTAGTAAA GGATGGACTG 41 ATAGG	Treffon (2019)
GRXC2 Lic v1 For	1 TACTTCCAAT CCAATGCAAT 21 GGCGATGCAG AAAGCTAAG	This work
GRXC2 Lic v1 Rev	1 TTATCCACTT CCAATGTTAT 21 TATTAAGCAG AAGTTGTTGC 41 AGTCTTTC	This work

TGA1 Lic Fwd	1 TACTTCCAAT CCAATGCAAT 21 GAATTCGACA TCGACACATT 41 TTG	This work
TGA1 Lic Rev	1 TTATCCACTT CCAATGTTAT 21 TACTACGTTG GTTCACGATG 41 TCGAG	This work
roGFP Lic Fwd	1 TACTTCCAAT CCAATGCAAT 21 GGTGAGCAAG GGCGAG	This work
roGFP Lic Rev	1 TTATCCACTT CCAATGTTAT 21 TACTTGTACA GCTCGTCCAT 41 GCC	This work
roGFP GW Fwd	1 GGGGACAAGT TTGTACAAAA 21 AAGCAGGCTC CATGGTGAGC 41 AAGGGCGAG	This work
roGFP GW Rev	1 GGGGACCACT TTGTACAAGA 21 AAGCTGGGTT TATTACTTGT 41 ACAGCTCGTC CATGCC	This work
Link ROXY9 fwd	1 GTGGTGGTGG ATCCGGAGGA 21 GGTGGTTCAA ATGCAATGGA 41 CAAAGTGATG AGAATGTCTT 61 C	This work
Link ATTB rev	1 CCGGATCCAC CACCACCTGA 21 ACCTCCTCCT CCGGAGCCTG 41 CTTTTTTGTA CAAACTTG	This work
Link DIS fwd	1 GTGGTGGTGG ATCCGGAGGA 21 GGTGGTTCAA ATGCAGATAT 41 CTCTAGGCAG ATCACAAGTT 61 TG	This work
Link HA rev	1 CCGGATCCAC CACCACCTGA 21 ACCTCCTCCT CCTGCATAGT 41 CCGGGACGTC	This work
JFU1383 LIC pUBQHA-fw	1 TACTTCCAAT CCAATGCATC 21 GAGAACAATG GCATACC	J. Uhrig, unpublished

438 seq rev	1 TGTGGTATGG CTGATTATGA 21 TCC	Treffon (2019)
MBP-752-for	1 CAAGGGTCAA CCATCCAAAC	Oberdiek (2018)
pB2GW7-rev	1 CATGAGCGAA ACCCTATAAG 21 AACC	C. Thurow, unpublished
T7	1 TAATACGACT CACTATAGGG	C. Thurow, unpublished
Seq-L1-pDONR	1 TCGCGTTAAC GCTAGCATGG 21 ATCTC	C. Thurow, unpublished
Seq-L2-pDONR	1 GTAACATCAG AGATTTTGAG 21 ACAC	C. Thurow, unpublished

3.5 Plasmids

Plasmid	Description	Resistance	Reference
438A	Expression vector for bacmid generation harboring an open reading frame	amp^R	Department for Molecular Biology, Prof. Dr. Patrick Cramer, MPI for Biophysical Chemistry, Göttingen
438B	Expression vector for bacmid generation harboring the coding sequence of a His tag for N-terminal fusion	amp^R	Department for Molecular Biology, Prof. Dr. Patrick Cramer, MPI for Biophysical Chemistry, Göttingen

438C	Expression vector for bacmid generation harboring the coding sequence of a His-MBP tag for N-terminal fusion	amp^R	Department for Molecular Biology, Prof. Dr. Patrick Cramer, MPI for Biophysical Chemistry, Göttingen
438SC	Expression vector for bacmid generation harboring the coding sequence of a strep-MBP tag for N-terminal fusion	amp^R	Treffon (2019)
438SC ROXY9	Expression vector for bacmid generation harboring strep-MBP-ROXY9 Wild-type	amp^R	Treffon (2019)
438SC ROXY9 SCLC	Expression vector for bacmid generation harboring strep-MBP-ROXY9 SCLC	amp^R	K. Treffon, unpublished
438SC ROXY9 CSLC	Expression vector for bacmid generation harboring strep-MBP-ROXY9 CSLC	amp^R	K. Treffon, unpublished
438SC ROXY9 CCLS	Expression vector for bacmid generation harboring strep-MBP-ROXY9 CCLS	amp^R	K. Treffon, unpublished
438SC ROXY9 CPYC	Expression vector for bacmid generation harboring strep-MBP-ROXY9 CPYC	amp^R	K. Treffon, unpublished
438SC ROXY9 CCLCA	Expression vector for bacmid generation harboring strep-MBP-ROXY9 CCLCA	amp^R	K. Treffon, unpublished
pDONR207	pDONR207 vector for gateway cloning	$gent^R$	Life Technologies
pDONR207-ROXY9 C49S	pDONR207 harboring ROXY9 C49S coding sequence;	$gent^R$	This work
438SC ROXY9 C49S	Expression vector for bacmid generation harboring strep-MBP-ROXY9 C49S	amp^R	This work
pDONR207-ROXY9 C61S	pDONR207 harboring ROXY9 C61S coding sequence;	$gent^R$	This work

438SC ROXY9 C61S	Expression vector for bacmid generation harboring strep-MBP-ROXY9 C61S	amp^R	This work
pB2GW7-HA-ROXY9	Binary plasmid for expression of HA-ROXY9 in plants under the control of the CaMV 35S promoter	$gent^R$	M. Zander, unpublished
438SC HA-ROXY9	Expression vector for bacmid generation harboring strep-MBP-HA-ROXY9	amp^R	This work
438SC HA-A-L-ROXY9	Expression vector for bacmid generation harboring strep-MBP-HA-A-L-ROXY9	amp^R	This work
438SC HA-L-A-ROXY9	Expression vector for bacmid generation harboring strep-MBP-HA-L-A-ROXY9	amp^R	This work
438SC HA-L-ROXY9	Expression vector for bacmid generation harboring strep-MBP-HA-L-ROXY9	amp^R	This work
pDONR207-GRX370	pDONR207 harboring GRXC2 cDNA sequence;	$gent^R$	Oberdiek (2018)
438SC GRXC2	Expression vector for bacmid generation harboring strep-MBP-GRXC2	amp^R	This work
pDONR201-TGA1	pDONR201 harboring TGA1 cDNA sequence;	kan^R	M. Zander, unpublished
438SC TGA1	Expression vector for bacmid generation harboring strep-MBP-TGA1	amp^R	This work
438B TGA1	Expression vector for bacmid generation harboring His-TGA1	amp^R	This work
35S-GRX480-roGFP2	Binary plasmid for expression of GRX480-roGFP2 in plants under the control of the CaMV 35S promoter	$gent^R$	LJ. Huang, unpublished
438B roGFP2	Expression vector for bacmid generation harboring His-roGFP2	amp^R	This work

pDONR207-roGFP2	pDONR207 harboring roGFP2 coding sequence from 35S-GRX480-roGFP2;	$gent^R$	This work
pDEST17 roGFP2	Expression vector for *E. coli* expression His-roGFP2	amp^R	This work
pMA/CL-TEV-A	Expression of an MBP-His-tagged TEV protease under control of the T7 promoter, a TEV site is placed in between the MBP and the His tag	amp^R	Treffon (2019)

3.6 Enzymes

Enzyme	Supplier
AcTEV Protease (10 U/µL)	Invitrogen
GAPDH from rabbit muscle	Sigma-Aldrich
Glutathione reductase from *S. cerevisiae* (255 U/µL)	Sigma-Aldrich
Phusion High-Fidelity DNA Polymerase (2 U/µL)	Thermo Fisher Scientific
Lysozyme	AGS GmbH
SspI	Fermentas
T4 DNA Polymerase (5 U/µL)	Fermentas
3-phosphoglygceric acid phosphokinase 15 U/µL	Sigma-Aldrich

3.7 Kits and commercially available reagents

Kit/reagent	Supplier
Luminata Forte Western HRP substrate	EMD Millipore
SuperSignal West Femto Maximum Sensitivity substrate	Thermo Scientific
Ionic Detergent Compatibility Reagent	Thermo Scientific
Pierce 660nm Protein Assay	Thermo Scientific
RotiQuant (5x)	Roth
CasyTon	OLS OMNI Life Science
CasyClean	OLS OMNI Life Science

Xtreme Gene 9 transfection agent	Roche
5x HF-buffer	Thermo Fischer Scientific
5x T4 buffer	Fermentas
Buffer Green	Fermentas

3.8 Antibodies

Antibody	Source	Dilution	Reference / Supplier
αHA ChIP grade (ab91110)	from rabbit	1:4000	abcam
αTGA1	from rabbit	1:1000	Agisera
αRabbit IgG HRPlinked	from donkey	1:8000	Amersham NA934-100UL

3.9 Standard solutions, culture media and buffers

The composition of standard solutions and buffers are listed in the respective methods section were they are first used.

3.9.1 Media for bacteria

LB-Media

- 10 $\frac{g}{L}$ Trypton
- 5 $\frac{g}{L}$ Yeast extract
- 10 $\frac{g}{L}$ NaCl

pH 7.0 adjusted with NaOH and autoclaved.
For plates add 12 $\frac{g}{L}$ Select Agar prior to autoclaving, after autoclaving, cool down to 60 °C and add antibiotic before casting plates.

dYT (full media)

- 16 $\frac{g}{L}$ Trypton
- 10 $\frac{g}{L}$ Yeast extract
- 5 $\frac{g}{L}$ NaCl

pH 7.0 adjusted with NaOH and autoclaved.

Autoinducing media

- 6 $\frac{g}{L}$ Na_2HPO_4
- 3 $\frac{g}{L}$ KH_2PO_4
- 10 $\frac{g}{L}$ Trypton
- 5 $\frac{g}{L}$ Yeast extract
- 10 $\frac{g}{L}$ NaCl
- 40 $\frac{mL}{L}$ Sugar stock solution

All components except for the sugar stock solution added, pH 7.2 adjusted with NaOH, water added to a volume of 960 $\frac{mL}{L}$ and autoclaved. Prior to use, add 40 $\frac{mL}{L}$ Sugar stock solution under the sterile bench.

Sugar stock solution:

- 15% (v/v) Glycerol
- 1.25% (w/v) Glucose
- 5% (w/v) Lactose

Sterile filtrate solution through a 0.2 µm filter.

3.9.2 Insect cell culture media

Ready-made media for the cultivation of insect cells

Media	Supplier	Cell line
Sf-900 III SFM	gibco	*S. frugiperda* Sf9
Insect-Xpress	LONZA	*S. frugiperda* Sf9
ESF 921	Expression Systems	*T. ni* Hi5

4 Methods

4.1 Growth conditions and cultivation

4.1.1 Growth conditions and cultivation of plants

Surface sterilization of *A. thaliana* seeds

Seeds were filled into a 1.5 mL reaction tube up to a volume of approximately 100 µL. The tube was labeled with a self-adhesive label and pencil. Open tubes were positioned in a plastic rack, which was placed on a 250 mL glass beaker containing 50 mL sodium hypochlorite solution within a desiccator. With the desiccator lid almost closed, 2.5 mL hydrochloric acid were pipetted into the glass beaker and the desiccator was rapidly closed. A vacuum of 800 mbar was applied to the desiccator. The seeds were sterilized for at least 1 h for planting on pots and at least 4 h for planting on sterile plates. The desiccator was opened under a fume hood and after a 10 min evaporation period, the plastic rack was transferred to a sterile bench for a further 30 min evaporation period.

Growth of *A. thaliana* on soil

To grow *A. thaliana* plants on soil, sterile seeds were sown on pots. For propagation and analysis, three to five seeds were placed on round pots with a wetted, sterile toothpick. For transformation, a large number of seeds were spread on square pots. Afterwards, the pots were sprayed with tap water and stratified for one to two nights in the cold room. The pots were transferred to climate chambers and grown under long day conditions (16 h light/8 h dark, 100 $\frac{\text{mol}}{\text{m}}$) unless otherwise noted.

4.1.2 Growth conditions and cultivation of insect cells

Two different insect cell culture lines were routinely propagated, Sf9 from *S. frugiperda* and Hi5 from *T. ni*. Sf9 cells were typically kept in a volume of 25 mL Insect-Xpress medium in a 250 mL flask, maintaining a ratio of air to cell medium of 9:1. Hi5 were typically kept in a volume of 50 mL ESF 921 in a 1 L flask, but the volume was increased to 200 mL to generate suitable amounts for infection. This corresponds to a maximum ratio of air to cell medium of 4:1. The cell culture lines were grown at 27 °C shaking at 90 rpm.

Concentration of both cell culture lines was measured on Mondays, Wednesdays and Fridays by removing 500 µL of cell culture under the sterile bench,

mixing 50 µL of the sample with 10 mL CasyTon and measuring with the respective program of the Casy device. Concentration, share of viable cells as well as mean and peak diameter were documented. On Mondays, cell cultures were diluted under the sterile bench to a concentration of 0.7×10^6 cells/mL with fresh culture medium. On Wednesdays, cells were transferred to new flasks and diluted to a concentration of 0.7×10^6 cells/mL. On Fridays, cells were diluted to a concentration of 0.4×10^6 cells/mL over the weekend. For Hi5 cells, the volume was increased to 200 mL for infections scheduled on Monday.

4.1.3 Generation of baculovirus expression vectors

The generation of new baculoviruses as expression vectors was carried out in Sf9 cells in two steps referred to as V0 and V1. For the V0 generation, the additional incubator was switched on and heated to 27 °C. Two replicate samples of the bacmid obtained from DH10αBac *E. coli* cells were transferred under the sterile bench and the ethanol was removed. The pellet was dried for 10 min at the back of the sterile bench and dissolved by adding 20 µL dH_2O and incubation for 20 min. A mastermix of 10 µL Xtreme Gene 9 transfection agent and 100 µL Insect-Xpress medium per bacmid was prepared and 100 µL mastermix were added to each bacmid together with additional 200 µL Insect-Xpress medium.

During the following 60 min incubation time, the Sf9 cell culture line was measured and diluted in a fresh 250 mL flask to a final volume of 20 mL at 1.0×10^6 cells/mL with Insect-Xpress medium. A 6-well plate with lid was prepared by adding 3 mL of Insect-Xpress medium to one well as medium control while adding 3 mL of Sf9 cells at 1.0×10^6 cells/mL to the other wells. One well served as cell culture control. Each dissolved bacmid was transferred to two wells by carefully pipetting 150 µL dropwise into each well. The plate was covered by the lid, meaningfully labelled and incubated at 27 °C.

After 2 to 3 d, the plate was checked on the inverse fluorescence microscope at the AG Heinrich. Successful infection was indicated by the emergence of individual fluorescing cells due to the YFP expressed by the virus. V0 infections were ready for harvest when clusters of fluorescing cells became visible. Under the sterile bench, the supernatant was transferred into a 15 mL falcon tube and stored at 8 °C.

V1 infections were typically initiated on Mondays. The Sf9 cell culture line was measured and diluted in a fresh 500 mL flask to a final volume of 25 mL at 1.0×10^6 cells/mL. 100 to 300 µL of V0 supernatant were added dependent on the degree of fluorescence. On Tuesdays, typically a concentration of around 2.0×10^6 cells/mL was measured. The V1 was diluted back to

1.0×10^6 cells/mL, normally leading to a final volume of 50 mL that complies with the ratio of air to cell medium of 9:1. On Wednesdays, the V1 typically did not further divide and cells started to increase in size. Optionally, the progression of the infection can be tracked by checking samples under a fluorescence microscope.

The V1 infection was ready for harvest when the share of viable cells dropped below 88%, usually on Thursdays or Fridays. The cell suspension was transferred to a 50 mL falcon tube and centrifuged at 320g for 15 min at 4 °C. The V1 supernatant was transferred to a fresh 50 mL falcon tube under the sterile bench and stored at 8 °C. The pellet was frozen in N_2 (*l*) and stored at −70 °C to check the protein expression.

4.2 Biochemical standard methods

4.2.1 SDS Page and immuno blot

Proteins were separated by size via Sodium Dodecylsulfate (SDS) Polyacrylamid Gel Electrophoresis (PAGE). In this work, the BIO Rad system (He, 2011) was used with self-casted gels.

Discontinuous gels consisted of a running gel with a suitable PA concentration for the proteins of interest and a 4% stacking gel and were casted sequentially. First, the glas panels were cleaned successively with water, 70% EtOH and 100% EtOH and inserted into the BIO Rad casting mount. The running gel was prepared and casted up to a height of 5.5 cm. To remove air bubbles ontop of the gel and to prevent desiccation, 1 mL of isopropanol were added. After at least 30 min polimerization time, the isopropanol was poured out and the stacking gel was prepared, casted ontop the running gel and a suitable comb was inserted. After at least further 30 min of polimerization time, the gel was removed from the mount, wrapped with a paper towel, wetted with deionized water and stored in a plastic bag at 4 ℃ over night or up to two weeks.
SDS-running gel (10%, 15 mL):

- 5.9 mL dH_2O
- 3.8 mL 1.5 M Tris-HCl pH 8.8
- 5.0 mL 30% Acrylamide-/bisacrylamide solution (37.5:1)
- 150 µL SDS (10% (w/v))
- 150 µL APS (10% (w/v))
- 15 µL TEMED

SDS-running gel (12%, 15 mL):

- 4.9 mL dH_2O
- 3.8 mL 1.5 M Tris-HCl pH 8.8
- 6.0 mL 30% Acrylamide-/bisacrylamide solution (37.5:1)
- 150 µL SDS (10% (w/v))
- 150 µL APS (10% (w/v))
- 15 µL TEMED

SDS-running gel (15%, 15 mL):

- 3.5 mL dH_2O
- 3.8 mL 1.5 M Tris-HCl pH 8.8
- 7.5 mL 30% Acrylamide-/bisacrylamide solution (37.5:1)
- 150 µL SDS (10% (w/v))
- 150 µL APS (10% (w/v))
- 15 µL TEMED

SDS-stacking gel (4%, 10 mL):

- 7.2 mL dH_2O
- 1.25 mL 1 M Tris-HCl pH 6.8
- 1.34 mL 30% Acrylamide-/bisacrylamide solution (37.5:1)
- 100 µL SDS (10% (w/v))
- 100 µL APS (10% (w/v))
- 10 µL TEMED

For the SDS Page run, samples (15 µL for 1.5 mm gels with 15 pockets, 20 µL for gels with 10 pockets) were prepared by adding equal volumes of 2x rapid purification buffer (RPB). For the marker, 6 µL of Page Ruler Protein Standard were mixed with RPB up to the same total volume.
2x Rapid purification buffer (RPB):

- 2 mL dH_2O
- 1 mL 1 M Tris-HCl pH 6.8
- 2 mL SDS (20% (w/v))
- 2 mL glycerol
- Spade point bromophenol blue
- 200 mM DTT
  Add water up to 10 mL

For non-reducing RPB, the DTT was omitted

All samples were heated to 95 °C for 5 min followed by centrifugation at 13000 rpm for 5 min while assembling the gel casket, filling it with fresh SDS running buffer and placing it on the magnetic stirrer. The samples are loaded into the gel pockets and the gel electrophoresis is carried out at 120 V for up

to 2 h, checking the progress of the running front during the second hour. After completion, the gel casket is disassembled and the glass planes are seppa-rated with a plastic wedge. The stacking gel is removed and the running gel is either directly stained or utilized for immuno blot.
10x running buffer:

- 142.75 g Glycine ($\rightarrow$ 2 M)
- 30.29 g Tris ($\rightarrow$ 250 mM)
- 50 mL SDS (20% (w/v)) ($\rightarrow$ 1%)
  Add water up to 1 L

For staining, the gel is transferred into a plastic tray and incubated with fixing solution (10% acetic acid, 20% 2-propanol in water) for 10 min. Afterwards, the solution is exchanged for staining solution (10% acetic acid, 0.006% Coomassie Brilliant Blue in water) and incubated for 2 h up to overnight. After removing the staining solution, the gel is rinsed with deionized water and incubated multiple times with destaining solution (10% acetic acid in water) until bands are sufficiently visible. The gel is documented by scanning with Epson Perfection V700 Photo scanner.

For blotting, the gel is transferred into a plastic tray and incubated in transfer buffer for 10 min. Meanwhile, the self-made blotting apparatus is cleaned and three layers of whatman paper are wetted with transfer buffer and placed onto the bottom part. A PVDF filter membrane is first activated in Methanol for 15 s, briefly equilibrated in transfer buffer and carefully placed ontop of the whatman paper stack. The gel is transferred onto the filter membrane avoiding air bubbles between filter and gel. Additional three layers of whatman paper are wetted with transfer buffer and placed ontop the stack, the blotting apparatus is assembled by adding the top part and optionally weighted. The blotting is carried out at a constant current of 1 $\frac{\text{mA}}{\text{cm}^2}$ for 60 to 90 min, depending on the size range of interest.
Transfer buffer:

- 5.82 g Tris (48 mM)
- 2.93 g Glycine (40 mM)
- 500 µL SDS (20% (w/v)) ($\rightarrow$ 0.01%)
- 200 mL MeOH ($\rightarrow$ 20%)
  Add water up to 1 L

After blotting, the filter membrane is reactivated in Methanol and transferred into TBS +5% milk powder for blocking. Blocking is performed for at least 1 to

2 h, afterwards the blocking solution is exchanged for a solution containing the first antibody (for concentration see) in TBST +5%milk powder. For binding of the first antibody, the blot is incubated over night, afterwards the antibody solution is stored in a 15 mL Falcon at –20 °C and reused up to three times. The blot is washed three times with TBST for 10 min each, followed by incubation with a solution containing the corresponding second antibody (for concentration) in TBST +5% milk powder for 2 h. Prior to detection, the blot is washed four times with TBS and once with TBST for 5 min each. The blot membrane is transferred to a transparent sheet , 1 mL of Luminata Forte detection reagent are pipetted onto the blot and evenly distributed by adding a second transparent sheet. The marker position is quickly redrawn on the transparent sheet and the blot is detected with
10x TBS:

- 24.2 gTris
- 80 g NaCl
  Add water up to 1 L, pH 7.6 set with HCl
  for TBST: add 0.1% (v/v) Tween

After detection, the blot membrane is stained with Coomassie by 20 min incubation in Coomassie staining solution, brief washing with destaining solution and drying on a sheet of whatman paper.

4.2.2 Determination of protein concentration

Different methods for the determination of protein concentration have been employed based on the specific sample composition

For analysis of samples containing SDS, the Pierce 660 protein assay was utilized including 50 $\frac{mg}{mL}$ ionic detergent compatibility reagent (IDCR). 10 µL of a standard containing 0.0, 0.1, 0.3, 0.6 and 0.9 $\frac{mg}{mL}$ BSA in dH_2O was pipetted into a 96-wells microtiter plate. For each sample, 10 µL dH_2O were pipetted into each well and 1 to 2 µL of protein sample were added. Equal amounts of sample buffer were added to the standard. 150 µL of Pierce reagent + IDCR was pipetted to each well, incubated for 10 min and absorbance measured at 660 nm with the Synergy HT plate reader.

To analyse samples after protein purification, the Bradford assay was utilized with a Bradford solution obtained by diluting RotiQuant (5x) in dH_2O. 10 µL of a standard containing 0.0, 0.1, 0.2, 0.4 and 0.8 $\frac{mg}{mL}$ BSA in dH_2O was pipetted into a 96-wells microtiter plate. For each sample, 10 µL dH_2O were pipetted into each well and 1 to 2 µL of protein sample were added. Equal amounts of sample buffer were added to the standard. 200 µL of Bradford solution was

pipetted to each well, incubated for 5 min and absorbance measured at 595 nm with the Synergy HT plate reader.

A more precise determination of protein concentration was carried out when verifying protein concentrations for biochemical assays with the NanoDrop One at the AG Tittmann. The extinction coefficient was calculated using the ExPasy ProtParam tool (Gasteiger et al., 2005) and provided to the NanoDrop software. After calibration with sample buffer, 2 µL of sample were placed on the NanoDrop and the measurement started. Measurements were strictly carried out in triplicates.

4.3 Molecular biology standard methods

4.3.1 Polymerase chain reaction

The standard method to generate DNA fragments, e.g. for LIC cloning, is polymerase chain reaction (PCR). The Phusion polymerase was utilized in reaction mixtures composed as follows:
PCR reaction mix:

- 2.5 µL Primer fwd (10 $\frac{\text{pmol}}{\mu\text{L}}$)
- 2.5 µL Primer rev (10 $\frac{\text{pmol}}{\mu\text{L}}$)
- 1 µL Plasmid/Template (10 $\frac{\text{ng}}{\mu\text{L}}$)
- 1 µL dNTPs (10 mM)
- 10.0 µL 5x HF-buffer
- 0.5 µL Phusion-Polymerase (2 U/µL)
- 32.5 µL dH_2O

Standard PCR program for Thermocycler:

- Initial melting; 1 min at 98°C
- Cycling; 35 repeats
  - Melting; 15 sec at 98°C
  - Annealing; 30 sec at 60°C
  - Elongation at 72°C ; 30 sec/1kb
- Final elongation; 10 min at 72°C
- Cooling to 4°C

The annealing temperature was changed based on the melting temperature of the primers utilized.

4.3.2 Agarose gel electrophoresis

20x TAE buffer:

- 0.80 M Tris/HCl
- 0.83 M $B(OH)_3$
- 0.10 M EDTA in water

10x Loading Dye:

- 67% (w/v) Saccharose
- 50 mM EDTA
- 0.42% (w/v) Orange G
  pH adjusted to 8.3

To separate DNA fragments according to size, agarose gel electrophoresis was employed. Gels were casted from 1% agarose solutions (in 1x TAE buffer) stored at 60 °C, a comb was inserted and the gels were solidified by cooling for 10 min. Afterwards, the comb was removed and the gel inserted into the running chamber. DNA samples were mixed with loading dye and up to 18 µL were loaded per gel pocket alongside with one pocket containing 6 µL DNA size standard. Electrophoresis was conducted with 130 V for 45 min. The gel was subsequently transferred to the ethidium bromide bath containing 0.005% (v/v) ethidium bromid for 10 min. The gel was destained in water for 20 min and documented under UV light with the Intas documentation system.

For the extraction of DNA fragments, the respective bands were cut out prior to documentation with the help of an UV lamp at 366 nm. Extraction was performed with the NucleoSpin Gel and PCR clean up kit according to the manufacturers manual. In the final step, the fragment was eluted with dH_2O.

4.3.3 LIC cloning

For the generation of plasmids for bacmid generation and insect expression, the Ligation independent cloning (LIC) method was utilized. The DNA fragment coding for the desired protein was generated by PCR with specific primers containing the LIC extension and

Forward LIC sequence:

5’ TACTTCCAATCCAAT G CA XXXXXXXXXXXXXX 3’

Reverse LIC sequence:
5' TTATCCACTTCCAAT G TTA TTA XXXXXXXXXXXXXXX 3'

The desired target plasmid from the 438er vector series contains a complementary sequence and was prepared by cleavage for 2 h at 37 °C.

- 2 µg plasmid
  add dH_2O to 17.7 µL
- 2 µL buffer green (G)
- 0.3 µL SspI

Both PCR fragment as well as cleaved vector were purified by agarose gel electrophoresis. Subsequently, T4 DNA polymerase treatment was conducted to create complementary 5'-overhangs. The treatment utilizes the 3'-exonuclease activity of T4 DNA polymerase which leads to the removal of nucleotides when no correct dNTP is available for the polymerase activity.

- 50 ng PCR fragment or 150 ng cleaved vector
  add dH_2O to 12.6 µL
- 1 µL 10 mM DTT
- 4 µL 5x T4 buffer
- 2 µL 25 mM dNTP (C for PCR, G for cleavage)
- 0.4 µL T4 DNA polymerase

The samples were incubated for 30 min at 22 °C followed by heat inactivation for 20 min at 75 °C in a thermocycler. LIC annealing was carried out by mixing 2 µL of T4-treated PCR fragment with 2 µL of T4-treated vector and 6 µL dH_2O and incubating for 1 h at RT. This sample was subsequently transformed into DH5α and the plasmid was isolated.

4.3.4 Transformation of bacteria

Chemically competent *E. coli* strains like BL21 and DH5α were transformed by a heat shock. For this, a 200 µL aliquote of the desired cell line was thawed on ice. A small amount of the desired plasmid, typically 1 µL of purified plasmids of 5 µL of LIC annealing samples, was added, carefully stirring the cells with the pipette tip. The sample was incubated on ice for 30 min, followed by a heat shock treatment at 42 °C for 90 s. The sample was cooled on ice for 5 min and 800 µL dYT media were added. The sample was incubated for 45 min at 37 °C,

rolling the sample and afterwards plated on an LB plate containing the correct antibiotic. The plates were incubated at 37 °C over night.

The DH10αBac strain is electrocompetent. For transformation, a 100 µL aliquote was thawed on ice and 1 µg of the desired 438er plasmid was added. After 15 min incubation on ice, the suspension was transferred to a electroporation cuvette sterilized with 70% EtOH and pulsed with the BioRad Gene pulser (25 µF, 1.8 kV). 1 mL dYT was added to the cuvette and the suspension was transferred into a culture tube. After shaking at 220 rpm and 37 °C for 5 h to over night without antibiotic, the cells were plated onto LB plates containing gentamycin and pretreated by subsequently spreading 50 µL 20 $\frac{\text{mg}}{\text{mL}}$ X-Gal and 50 µL 100 mM IPTG.

The plates were incubated for up to two days and correct transformants were identified by a white colour. Four of these colonies were picked and transferred to 5 mL dYT after swiping along a fresh master LB plate containing gentamycin and pretreated by subsequently spreading 50 µL 20 $\frac{\text{mg}}{\text{mL}}$ X-Gal and 50 µL 100 mM IPTG. A blue control colony was also transferred onto the master plate, which was subsequently incubated for up to two days to check if the colonies remain white. In this case, the 5 mL culture was utilized for bacmid precipitation.

4.3.5 Plasmid isolation from *E. coli*

For the isolation of plasmids, individual clones were picked from a transformation plate incubated over night and mixed with 5 mL dYT. This culture was again incubated over night, shaking at 220 rpm and 37 °C. The plasmid DNA was isolated with the NucleoSpin Plasmid kit according to the manufacturers manual. In the final step, the plasmid was eluted with dH_2O. Subsequently, the concentration was determined and the identity checked by sequencing.

4.3.6 Bacmid precipitation

A 5 mL culture of a verified DH10αBac clone was incubated shaking at 220 rpm and 37 °C over night. The entire culture was harvested and resuspended in 250 µL buffer A1 from the NucleoSpin plasmid kit. 250 µL buffer A2 were added, the sample was mixed by inverting and incubated for 10 min at RT. 350 µL buffer A3 were added and the sample was mixed by inverting. After centrifugation at 13000 rpm for 10 min at RT, the supernatant was transferred to a fresh tube and again centrifuged at 13000 rpm for 10 min at RT. The supernatant was transferred to a fresh tube containing 700 µL 2-propanol. The sample was inverted and precipitated at –20 °C over night.

The sample was centrifuged at 13000 rpm for 30 min at 4 °C. The supernatant was discarded and the pellet was washed with 500 µL 70% EtOH followed by centrifugation at 13000 rpm for 10 min at 4 °C. The ethanol was exchanged with 200 µL fresh 70% EtOH and the bacmid pellet was utilized for the generation of a Baculovirus expression vector.

4.3.7 Determination of nucleic acid concentration

The concentration of nucleic acid samples was determined with the PeqLab NanoDrop One. After calibration with water, 2 µL of sample were placed on the NanoDrop and the measurement started. A conversion factor of 50 $\frac{\text{ng cm}}{\mu\text{L}}$ was used for DNA samples and the purity of the sample was monitored by checking the ratios of absorbance $\frac{260}{280}$ and $\frac{260}{230}$ for protein and salt contaminations respectively.

4.4 Protein expression and purification

4.4.1 Expression of proteins in insect cells

Following the V0 and V1 infections, the infection aimed at protein expression was referred to as V2. V2 infections were typically initiated on Mondays. The Hi5 cell culture line was measured and diluted in a fresh 3 L flask to a final volume of 600 mL at 1.0×10^6 cells/mL. 100 to 400 µL of V1 supernatant were added dependent on the quality and age of the V1. On Tuesdays, typically a concentration of around 2.0×10^6 cells/mL was measured. The V2 was divided to a second 3 L flask (”V2’”) and each flask was diluted back to 1.0×10^6 cells/mL, normally leading to a final volume of 600 mL that complies with the ratio of air to cell medium of 4:1. On Wednesdays, the V2 typically did not further divide and cells started to increase in size. Optionally, the progression of the infection can be tracked by checking samples under a fluorescence microscope.

The V2 infection was ready for harvest when the share of viable cells dropped below 88%, usually on Thursdays or Fridays. The cell suspension from each flask was transferred to two 450 mL ultracentrifuge bottles, tared and centrifuged at 240g for 30 min at 4 °C with an SLA-3000 rotor. The supernatant was discarded and the pellet was resuspended in 12 mL of the respective lysis buffer. The two suspensions stemming from one culture flask were combined in a fresh 50 mL falcon, frozen in N_2 (*l*) and stored at –70 °C until further processing.

4.4.2 Expression of proteins in *E. coli*

The expression with autoinducing media that does not require the addition of Isopropyl-β-D-thiogalactopyranosid (IPTG) and was adapted from Treffon (2019)

For the expression of proteins in *E. coli*, suitable expression plasmid was transformed into BL21 cells by chemical transformation and plated on an LB plate containing the required antibiotic. After incubating the plate over night, multiple colonies were picked and mixed with 5 mL of autoinducing media supplemented with the correct antibiotic for a pre-culture. The pre-culture was shaken with 220 rpm at 37 °C over night. The entire pre-culture was mixed with 400 mL autoinducing media supplemented with the correct antibiotic in a 2 L flask and shaken with 220 rpm at 37 °C for 6 h. The flask was subsequently transferred to 29 °C and shaken with 220 rpm over night. The cell suspension was transferred to a 450 mL ultracentrifuge bottle, tared and centrifuged at 5000 rpm for 20 min at 4 °C with an SLA-3000 rotor. The supernatant was discarded and the pellet was resuspended in 12 mL of the respective wash buffer and transferred in a fresh 50 mL falcon. The sample was frozen in N_2 (*l*) and stored at –70 °C until further processing.

4.4.3 Purification of MBP tagged proteins

The purification of strep-MBP-tagged proteins, mainly strep-MBP-GRXs, was adapted from Treffon (2019), but the buffer system was changed to include GSH as reducing agent. An MBPTrap column and a single step elution was utilized.

strep-MBP-GRX pellets were thawed in a beaker containing cold water and stirred in the cold room. The sample was placed on ice and sonicated with a Sonopuls sonifier equipped with an MS73 sonotrode for 5 min with 30% amplitude and 0.4 s pulses followed by 0.6 s breaks. The lysate was centrifuged at 20000 rpm for 45 min at 4 °C with an SS-34 rotor and the supernatant filtered through a stack of one 1.2 µm sterile filter connected to one 0.45 µm sterile filter. An aliquot of this crude extract was mixed with RPB.

A 5 mL MBPTrap column was connected to the Äkta prime plus chromatography system and equilibrated with MBP+GSH lysis buffer. The crude extract was loaded onto the column via a superloop at a flow rate of 1 $\frac{\text{mL}}{\text{min}}$. 5 mL fractions of the flow through were collected. After absorbance returned to baseline, elution was initiated with a single step changing the buffer to 100% MBP+GSH elution buffer. 2 mL fractions were collected during the elution. Representative fractions from flow through and elution peak are mixed with RPB and analysed by SDS-Page alongside with the crude extract sample. Fractions containing

the protein of interest were pooled.

All buffers were degassed and stored at 4 °C until use.

MBP+GSH lysis

- 20 mM HEPES pH 7.5
- 100 mM NaCl
- 5 mM GSH
- 5% (w/v) glycerol

MBP+GSH elution

- 20 mM HEPES pH 7.5
- 100 mM NaCl
- 5 mM GSH
- 5% (w/v) glycerol
- 100 mM maltose

4.4.4 Purification of HIS tagged proteins

His-tagged roGFP2, TEV and TGA1 was purified with a HISTrap column and an elution gradient similar to the procedure detailed by Treffon (2019) for His-TEV. Sample preparation of His-TGA1 from insect cells was carried out as described for strep-MBP tagged proteins.

His-roGFP2 or His-TEV pellets were thawed in a beaker containing cold water and stirred in the cold room. Lysozyme was added with the tip of a spatula and the samples were incubated for 30 min in the cold room. The sample was placed on ice and sonicated with a Sonopuls sonifier equipped with an MS73 sonotrode for 15 min with 50% amplitude and 1 s pulses followed by 2 s breaks. The lysate was centrifuged at 20000 rpm for 45 min at 4 °C with an SS-34 rotor and the supernatant filtered through a 0.45 µm sterile filter. An aliquot of this crude extract was mixed with RPB.

A 5 mL HISTrap column was connected to the Äkta prime plus chromatography system and equilibrated with the respective wash buffer. The crude extract was loaded onto the column via a superloop at a flow rate of 1 $\frac{\text{mL}}{\text{min}}$. 5 mL fractions of the flow through were collected. After absorbance returned to baseline, elution was initiated with a linear gradient over 40 mL ranging from 0% to 50% elution buffer (250 mM imidazole). 2.5 mL fractions were collected during the

gradient. Afterwards, the proportion of elution buffer is changed to 100% elution buffer in a single step. Representative fractions from flow through and elution peak are mixed with RPB and analysed by SDS-Page alongside with the crude extract sample. Fractions containing the protein of interest were pooled.

All buffers were degassed and stored at 4 ℃ until use.

roGFP wash

- 20 mM Tris-HCl pH 7.5
- 100 mM NaCl

roGFP elution

- 20 mM Tris-HCl pH 7.5
- 100 mM NaCl
- 500 mM imidazole

TEV wash

- 50 mM Tris-HCl pH 8.0
- 150 mM NaCl
- 5% (w/v) glycerol

TEV elution

- 50 mM Tris-HCl pH 8.0
- 150 mM NaCl
- 5% (w/v) glycerol
- 500 mM imidazole

TGA1 wash

- 50 mM KH_2PO_4/Na_2HPO_4 pH 8.0
- 100 mM NaCl
- 2 mM DTT
- 5% (w/v) glycerol

TGA1 elution

- 50 mMKH_2PO_4/Na_2HPO_4 pH 8.0

- 100 mM NaCl
- 2 mM DTT
- 5% (w/v) glycerol
- 500 mM imidazole

4.4.5 TEV cleavage

For cleavage of the strep-MBP tag, the TEV protease was employed. This was either performed with commercially available AcTEV protease according to the manufacturers manual or with self-purified His-TEV. Typically, 0.05 mg of His-TEV per 1 mg strep-MBP tagged GRX were sufficient for cleavage and His-TEV was active over a wide range of buffer conditions, including MBP+GSH elution buffer. After mixing HisTEV and substrate, an aliquot of 20 µL was mixed with 20 µL RPB. The cleavage reaction was initiated by addition of DTT to a final concentration of 2 mM and the samples were incubated for 1 to 3 d at 4 °C. Before further processing, another aliquot of 20 µL was mixed with 20 µL RPB and both samples were analysed by SDS-Page to verify successful cleavage.

4.4.6 Separation after TEV cleavage

To separate TEV cleaved samples, a preparative gel filtration was performed in collaboration with the Tittmann group. For this, 4 mL of cleaved samples were loaded onto a Superdex 200 (10/300 GL) column connected to an ÄKTApure device and 1.5 mL fractions were collected. The same degassed MBP+GSH lysis buffer (25 mM HEPES pH 7.5, 100 mM NaCl, 5% (w/v) glycerol, 5 mM GSH) was employed as for the affinity chromatography. Fractions were analyzed by SDS-Page and those identified to contain tag-free GRXs were pooled and subsequently spin concentrated with a VivaSpin MWCO 3k concentrator at 4000 rpm and 4 °C.

4.4.7 CD spectroscopy

The CD spectroscopy was carried out in collaboration with the Tittmann group. Buffers of the protein samples were exchanged to a compatible CD buffer (20 mM Na_2HPO_4 adjusted to pH 7.5 with H_3PO_4, 50 mM NaF, 5% (w/v) glycerol) containing 1 mM DTT or 0.5 mM GSH as reducing agent. For buffer exchange, a MiniTrap desalting column was equilibrated by washing with CD buffer three times, loading 150 µL protein sample, stacking with 550 µL CD buffer and eluting with 150 µL CD buffer. The protein concentration was determined with the NanoDrop. The samples were handed over to Fabian Rabe

von Pappenheim, who kindly conducted the measurements with the CD spectrometer. For a sample set containing DTT as reducing agent, the thermal stability was assessed. Data was processed by calculating the mean residue ellipticity.

4.5 Protein redox assays

4.5.1 Alkylation-based assays

The alkylation-based assays were adapted from Zannini et al. (2017) and carried out according to a similar basic scheme. Protein samples were prepared, mixed with different redox buffers and incubated for a certain time period. The reactions were stopped by TCA precipitation and the samples were labelled with a suitable alkylation reagent before being subjected to SDS-Page.

mmPEG shift assay

For a simple investigation how a protein reacts to certain redox reagents, recombinant protein samples were pre-reduced by creating a reaction mixture of 10 µL per condition of interest (adding at least 20 µL for pipetting errors), containing 10 mM DTT and 0.5 $\frac{\text{mg}}{\text{mL}}$ recombinant protein. The volume was adjusted with 100 mM HEPES pH 7.0 buffer. A typical volume was 150 µL for 13 treatment conditions and subsequent analysis on a gel with 15 pockets, also including protein ladder and initial untreated protein sample. The reaction mixture was incubated for at least 1 h at RT.

To remove the DTT, the mixture was desalted with a MiniTrap desalting column pre-washed by completely filling the volume above the column material with 100 mM HEPES pH 7.0 buffer and letting it run through the column three times. The total volume of the reaction mixture (e.g. 150 µL) was loaded directly onto the bead bed and allowed to enter the column material. 100 mM HEPES pH 7.0 buffer was stacked to reach a total volume of 700 µL (e.g. adding 550 µL) and allowed to enter the column material. The desalted protein sample was eluted with twice the loaded volume (e.g.300 µL) 100 mM HEPES pH 7.0 buffer, collecting the eluate. The column was subsequently washed three times.

Treatment mixtures were prepared by mixing 20 µL desalted protein sample with 30 µL 100 mM HEPES pH 7.0 buffer containing different redox reagents. The final concentration of the redox reagent was typically 10 mM if not otherwise denoted. The samples were incubated for 2 h at RT if not otherwise denoted, followed by the addition of 50 µL 20% (v/v) TCA. Samples could be stored at –20 °C or directly processed by centrifugation at 11200g for 30 min at 4 °C. The supernatant was removed and the pellet washed by adding 800 µL

cold acetone stored at –20 °C, centrifugation at 11200g for 10 min at 4 °C and removal of the acetone. The pellets were dried under the fume hood for 10 min and resolved in 15 µL alkylation buffer (100 mM Tris-HCl pH 8.0, 1% (w/v) SDS) with or without 5 mM 5 kDa mmPEG. The samples were alkylated for 45 min at RT and subsequently mixed with 15 µL non-reducing RPB and subjected to SDS-Page.

Redox titration

For redox titration assays, samples were prepared as described above with the treatment mixtures containing redox buffers of DTT/dithiane or GSH/GSSG at different redox potentials. Ratios were calculated according to the Nernst Equation utilizing biological standard potentials $E^{0'}$ of –327 mV for DTT/dithiane and –240 mV for GSH/GSSG (Zannini et al., 2017). Concentrations of the two components were calculated to yield a total final concentration of 10 mM within the 50 µL treatment mixture. Due to the buffer system of 100 mM HEPES pH 7.0 buffer, no adjustment according to pH was required.

pH titration

For pH titration assays (Zannini et al., 2017), different buffers with a pH from 2.0 to 10.0 in 0.5 pH steps were prepared at a normality of 0.1 N. For pH 2.0 to 6.0, a citrate buffer system was utilized, for pH 6.5 to 8.0, a KH_2PO_4/Na_2HPO_4 buffer system was utilized and for pH 8.5 to 10.0 a $Na_2B_4O_7$ buffer system was utilized. The pH of the buffers were subsequently checked with the pH electrode and adjusted with NaOH or HCl if necessary.

Protein samples were pre-reduced similar to the mmPEG shift assay, but a concentration of 1 $\frac{\text{mg}}{\text{mL}}$ recombinant protein was utilized. The reaction mixture was desalted against 5 mM HEPES pH 7.0 buffer, which was checked to not affect the final pH of the treatment mixtures. The treatment mixtures contained 40 µL pH buffer, 10 µL of desalted protein and 5 µL 100 mM iodoacetamide (IAM). After 1 h incubation time, 55 µL 20% (v/v) TCA were added and the following steps were carried out as described above.

AMS shift assay

For small proteines, the alkylation reagent was changed from 5 kDa mmPEG to 4-Acetamido-4'-maleimidylstilbene-2,2'-disulfonic acid (AMS), roughly adding 0.5 kDa per thiol. Otherwise, the assay was performed similar to the mmPEG shift assay. AMS-labelled protein samples can be detected after immunoblotting.

4.5.2 HEDS assay

A common assay for catalytic activity of glutaredoxins is the reduction of 2-hydroxyethyl disulphide (HEDS) coupled to the consumption of NADPH via glutathione reductase (GR) (Begas et al., 2015, 2017). For this assay, glutaredoxin samples with a concentration of at least 3 $\frac{\text{mg}}{\text{mL}}$ were pre-reduced with DTT by mixing 180 µL of protein sample with 20 µL 100 mM DTT and incubating for 2 h at RT. GRX samples were subsequently buffer exchanged for 100 mM HEPES pH 7.0 buffer with 5 mM GSH by loading the entire 200 µL reaction mixture onto a MiniTrap desalting column pre-equilibrated with 100 mM HEPES pH 7.0 buffer with 5 mM GSH, stacking with 500 µL 100 mM HEPES pH 7.0 buffer with 5 mM GSH and eluting with 400 µL 100 mM HEPES pH 7.0 buffer with 5 mM GSH. The protein concentration was checked with the NanoDrop and adjusted to 1 $\frac{\text{mg}}{\text{mL}}$ with 100 mM HEPES pH 7.0 buffer with 5 mM GSH.

A mastermix was prepared with all reagents diluted in 100 mM HEPES pH 7.0 buffer.

- 1200 µL 100 mM HEPES pH 7.0 buffer
- 200 µL 10 mM GSH
- 200 µL 2 mM NADPH
- 2.5 µL glutathione reductase (GR) from *S. cerevisiae* 255 U/µL

For each assay reaction, 160 µL mastermix were pipetted into a 200 µL cuvette and absorbance at 340 nm was measured for a 30 s equilibration time in a Jasco UV/Vis spectrometer at the Tittmann group. 20 µL of buffer-exchanged protein at 1 $\frac{\text{mg}}{\text{mL}}$ in 100 mM HEPES pH 7.0 buffer with 5 mM GSH were added into the cuvette, followed by an additional 60 s equilibration time. Finally, 20 µL 8 mM HEDS were added to initiate the assay and absorbance was tracked for 510 s. As a buffer control, 20 µL 100 mM HEPES pH 7.0 buffer with 5 mM GSH were added in the second stage of the measurement. For data representation, the first 30 s of the final measurement were omitted and the absorbance was normalized to the starting point.

4.5.3 CHP assay

CHP has been proposed as a substrate of class III glutaredoxins (Xu et al., 2022). The CHP assay was carried out similar to the HEDS assay with certain adjustments. The amount of GSH was reduced to minimize background reactions and the amount of protein as well as the assay time were increased to enhance the visibility of a potential activity. Pre-reduced GRX samples were

buffer-exchanged to 100 mM HEPES pH 7.0 buffer with 1 mM GSH and concentration adjusted to 1 $\frac{mg}{mL}$.
CHP assay mastermix:

- 450 µL 100 mM HEPES pH 7.0 buffer
- 50 µL 10 mM GSH
- 100 µL 2 mM NADPH
- 2.5 µL glutathione reductase (GR) from *S. cerevisiae* 255 U/µL

For each assay reaction, 80 µL mastermix were pipetted into a 200 µL cuvette and absorbance at 340 nm was measured for a 30 s equilibration time in a Jasco UV/Vis spectrometer at the Tittmann group. 100 µL of buffer-exchanged protein at 1 $\frac{mg}{mL}$ in 100 mM HEPES pH 7.0 buffer with 1 mM GSH were added into the cuvette, followed by an additional 60 s equilibration time. Finally, 20 µL 15 mM CHP were added to initiate the assay and absorbance was tracked for 1110 s. As a buffer control, 20 µL 100 mM HEPES pH 7.0 buffer with 1 mM GSH were added in the second stage of the measurement. For data representation, the first 30 s of the final measurement were omitted and the absorbance was normalized to the starting point.

4.5.4 roGFP assay

The roGFP assay utilizes the artificial roGFP2 substrate, a modified GFP with two cysteines that can form a disulphide catalysed by glutaredoxins (Aller et al., 2013), most likely by glutaredoxin-mediated glutathionylation followed by disulphide exchange (Trnka et al., 2020).

Reference samples were prepared with a final concentration of 2 µM His-roGFP2 and 10 mM DTT or H_2O_2, respectively. Additional His-roGFP2 was reduced by incubating 40 µM His-roGFP2 in the presence of 10 mM DTT and a total volume of 150 µL for 2 h at RT. This sample was desalted against 100 mM HEPES pH 7.0 buffer by loading the entire 150 µL onto a pre-equilibrated MiniTrap desalting column, stacking with 550 µL 100 mM HEPES pH 7.0 buffer and eluting with 300 µL 100 mM HEPES pH 7.0 buffer.

Simultaneously, GRX samples were reduced by incubating 50 µM GRX in the presence of 10 mM DTT and a total volume of 150 µL for 2 h at RT. This sample was desalted against 100 mM HEPES pH 7.0 buffer by loading the entire 150 µL onto a pre-equilibrated MiniTrap desalting column, stacking with 550 µL 100 mM HEPES pH 7.0 buffer and eluting with 300 µL 100 mM HEPES pH 7.0 buffer.

The first three rows of a 96-wells microtiter plate were filled with triplicates of 100 µL 100 mM HEPES pH 7.0 buffer, 100 µL reference samples or samples containing 10 µL desalted His-roGFP2 alongside 10 µL of GRX or 100 mM HEPES pH 7.0 buffer and 70 µL 100 mM HEPES pH 7.0 buffer. 50 µL 500 µM GSSG were added to the lowest row of the 96-wells microtiter plate.

Emission at 528 nm after excitation at 360 nm and 485 nm was measured for each well every minute for an 11 min equilibration period with the Synergy HT plate reader. The assay was initiated by distributing 10 µL from the GSSG containing wells into each sample well with a multichannel pipette. The measurement was continued for 81 min and analyzed by calculating the ratio of emission after excitation at 360 nm and 485 nm.

Alternatively, the GRX samples were buffer exchanged to 100 mM HEPES pH 7.0 buffer with 5 mM GSH. Subsequently, reaction mixtures were prepared by adding GSH and GSSG to generate a redox buffer with a redox potential of –200 mV.

- ”GSSG”: 235.8 µL buffer + 14.2 µL 10 mM GSSG
- ”-200 mV”: 60.8 µL buffer + 14.2 µL 10 mM GSSG + 75 µL 10 mM GSH + 100 µL 100 mM HEPES pH 7.0 buffer with 5 mM GSH
- ”-200 mV+GRX”: 60.8 µL buffer + 14.2 µL 10 mM GSSG + 75 µL 10 mM GSH + 100 µL buffer-exchanged GRX sample in 100 mM HEPES pH 7.0 buffer with 5 mM GSH

10 µL of these reaction mixtures were were added to samples containing 10 µL desalted His-roGFP and 80 µL 100 mM HEPES pH 7.0 buffer after the 11 min equilibration period.

4.5.5 GAPDH assay

The GAPDH assay is based on the reactivation of glutathionylated GAPDH by a glutaredoxin-catalysed deglutathioylation (Zaffagnini et al., 2008). The three step process involves the glutathionylation of GAPDH, the deglutathionylation assay in the presence of GRX and finally measurement of GAPDH activity and was adapted from Treffon (2019).

In this assay, a total of twelve different treatment conditions were typically investigated at five different time points. Four of these conditions were always control treatments of untreated GAPDH, GAPDH-SG, GAPDH-SG reduced by DTT and GAPDH-SG reduced by GSH. To account for pipetting errors, mastermixes were prepared for 70 reactions. Deviating from other experiments, a

100 mM phosphate buffer pH 8.0 (NaH_2PO_4/Na_2HPO_4) was utilized. All reaction mixtures and stocks were protected from light.

Similar to previous experiments, glutaredoxin samples were pre-reduced with DTT by mixing 99 µL of protein sample with 1 µL 1 M DTT and incubating for 2 h at RT. The GRX samples were subsequently desalted against 100 mM phosphate buffer pH 8.0 (loading 100 µL, stacking 600 µL and eluting 200 µL) and concentrations were determined with the NanoDrop.

Simultaneously, a GAPDH stock of 1000 µM ($2\,\frac{mg}{mL}$) was prepared. Glutathionylated GAPDH (GAPDH-SG) was generated in the following reaction mixture:

- 50 µL 1000 µM GAPDH
- 15 µL 100 mM GSH
- 1 µL 700 mM H_2O_2
- 434 µL 100 mM phosphate buffer pH 8.0

After 15 min incubation time at RT, the reaction mixture was desalted by loading the entire 500 µL onto a MiniTrap desalting column pre-equilibrated in 100 mM phosphate buffer pH 8.0 and eluting with 1 mL 100 mM phosphate buffer pH 8.0 into a 15 mL falcon tube. The sample was diluted to a concentration of 12.5 µM GAPDH-SG by adding 3 mL 100 mM phosphate buffer pH 8.0. A 12.5 µM GAPDH was diluted from the stock solution.

For the stopping the deglutathionylation reaction, a quenching mixture was prepared:

- 315 µL 150 mM 3-phosphoglygerate
- 210 µL 100 mM ATP
- 52.5 µL 1 mM $MgCl_2$
- 2.8 µL 3-phosphoglygceric acid phosphokinase 15 U/µL
- 2919.7 µL 100 mM phosphate buffer pH 8.0

The quenching mixture was incubated for at least 15 min at RT to allow for the generation of 1,3-bisphosphoglycerate, the substrate of GAPDH. 50 µL of the quenching mixture were distributed to the first five rows of a 96-wells microtiter plate.

Deglutathionylation reactions were prepared by mixing 250 µL of GAPDH-SG with 50 µL of desalted GRX samples at varying concentrations and 12.5 µL 100 mM GSH. For a negative control, GSH was replaced by 100 mM phosphate

buffer pH 8.0. Additional controls involved 250 µL of GAPDH with 62.5 µL buffer, 250 µL of GAPDH-SG with 62.5 µL buffer, 250 µL of GAPDH with 50 µL buffer and 12.5 µL 1 M DTT as well as 250 µL of GAPDH with 50 µL buffer and 12.5 µL 100 mM GSH. Final GAPDH(-SG) concentrations in these mixtures were 10 µM. Immediately after mixing, 50 µL of each deglutathionylation reaction mixture were removed and distributed into one row of the 96-wells microtiter plate containing the quenching mixture. This procedure was repeated four times at the indicated time points.

To assay GAPDH activity, an additional mastermix was prepared:

- 21 µL 500 mM EDTA
- 105 µL 20 mM NADH
- 3374 µL 100 mM phosphate buffer pH 8.0

After stopping all deglutathionylation reactions, the mastermix was added to the respective wells of the 96-wells microtiter plate and absorbance at 340 nm was measured every minute for 1 h with the Synergy HT plate reader. For each reaction condition, the linear decrease in absorbance was fitted to determine GAPDH activity.

4.5.6 TGA1 glutathionylation assay

The assay with TGA1 was based on the mmPEG shift assay. Both TGA1 and glutaredoxin samples were pre-reduced with 10 mM DTT for 2 h. For this 180 µL of an impure His-TGA1 sample containing roughly 1 $\frac{\text{mg}}{\text{mL}}$ of His-TGA1 were mixed with 20 µL 100 mM DTT. After 2 h incubation at RT, the TGA1 samples were desalted against 100 mM HEPES pH 7.0 buffer by loading the entire 200 µL onto a pre-equilibrated MiniTrap desalting column, stacking with 500 µL 100 mM HEPES pH 7.0 buffer and eluting with 400 µL 100 mM HEPES pH 7.0 buffer.

Glutaredoxins were mixed with 100 mM HEPES pH 7.0 buffer and 20 µL 100 mM DTT to yield reaction mixtures of 180 µL containing 10 mM DTT and 3 $\frac{\text{mg}}{\text{mL}}$ GRX. After 2 h incubation at RT, GRX samples were buffer exchanged for 100 mM HEPES pH 7.0 buffer with 5 mM GSH by loading the entire 150 µL reaction mixture onto a MiniTrap desalting column pre-equilibrated with 100 mM HEPES pH 7.0 buffer with 5 mM GSH, stacking with 550 µL 100 mM HEPES pH 7.0 buffer with 5 mM GSH and eluting with 300 µL 100 mM HEPES pH 7.0 buffer with 5 mM GSH.

Stocks for treatment mixtures were prepared with redox agents diluted in 100 mM HEPES pH 7.0 buffer. The ratio of GSSG and GSH was calculated with the Nernst equation for a redox potential of –200 mV.

- ”DTT”: 350 µL buffer + 50 µL 100 mM DTT
- ”-”: 400 µL buffer
- ”GSSG”: 150 µL buffer + 250 µL 10 mM GSSG
- ”-200 mV”: 21.6 µL buffer + 28.4 µL 10 mM GSSG + 150 µL 10 mM GSH + 200 µL 100 mM HEPES pH 7.0 buffer with 5 mM GSH
- ”-200 mV+GRX”: 21.6 µL buffer + 28.4 µL 10 mM GSSG + 150 µL 10 mM GSH + 200 µL buffer-exchanged GRX sample in 100 mM HEPES pH 7.0 buffer with 5 mM GSH

Treatment mixtures were prepared by mixing 40 µL stock solution with 10 µL desalted TGA1 sample. 50 µL 20% (v/v) TCA were added at indicated time points after 1 min, 5 min, 15 min and 60 min. For the time point of 0 min, 40 µL stock solution was mixed with 50 µL 20% (v/v) TCA before adding 10 µL desalted TGA1 sample. After addition of TCA, samples were stored on ice and after processing all samples, TCA precipitation was carried out as described for the mmPEG shift assay. Samples were separated by SDS-Page and immunoblotting and detected with the αTGA1 antibody.

4.6 Fe-S-cluster investigations

The Fe-S-cluster reconstitution and analysis was carried out in collaboration with the Lill group at the Philipps University in Marburg.

4.6.1 Reconstitution of Fe-S-clusters

The concentration of affinity-purified strep-MBP-ROXY9 samples in MBP+GSH elution buffer containing 5 mM GSH was determined with the NanoDrop and typically ranged between 5 and 10 $\frac{\text{mg}}{\text{mL}}$. 2.5 mL samples were transferred into the anaerobic tent and incubated for 1.5 h on ice. 25 µL of 1 M DTT were added to reduce the sample as well as potentially formed GSSG, and the samples were incubated for 2 h on ice. Ammonium iron(III) citrate was added to a final concentration six-fold as high as the protein concentration. The samples were incubated 20 min at RT. Subsequently, Li_2S was added to a final concentration six-fold as high as the protein concentration in three steps, carefully mixing the samples by inverting between each addition. The samples were incubated 20 min at RT and the colour change was observed. The samples were incubated for further 20 min on ice. To remove unbound iron and sulphide, the samples were desalted against degassed and filtered HPLC buffer (25 mM HEPES pH 7.8, 100 mM NaCl, 5% (w/v) glycerol) by loading 2.5 mL onto a

PD-10 desalting column and eluting 3.5 mL. 3.5 µL of 1 M DTT were added after desalting to protect the samples from oxidation. The samples were spin-concentrated with a VivaSpin MWCO 50k concentrator sealed with parafilm outside the anaerobic tent at 4000 rpm and 4 °C until the sample volume was reduced to 2 mL. Aliquots of the samples were frozen in N_2 (*l*) and stored at −70 °C for longer term storage or kept at 4 °C for short term storage.

The first experiment deviated in the sample preparation. strep-MBP-ROXY9 was purified according to the protocol presented by Treffon (2019) in MBP elution buffer (20 mM HEPES pH 7.5, 300 mM NaCl, 2 mM Na_2-EDTA, 100 mM Maltose, 1 mM DTT, 5% (w/v) glycerol). To remove the Na_2-EDTA, the sample was dialysed three times against dialysis buffer (20 mM HEPES pH 7.5, 300 mM NaCl, 1 mM DTT, 5% (w/v) glycerol) at a ratio of 1:333 sample to dialysis buffer. For the reconstitution, GSH was added to a final concentration four-fold as high as the protein concentration (5 $\frac{mg}{mL}$) and fresh DTT was added to a final concentration six-fold as high as the protein concentration. No DTT was added after desalting and the sample was spin concentrated inside the anaerobic tent.

4.6.2 Analysis of reconstituted samples

Anaerobic gel filtration

Samples after reconstitution as well as reference samples were analysed by gel filtration inside the anaerobic tent. Reference samples were reduced by adding DTT to a final concentration of 10 mM and incubating for 15 to 30 min at RT. 100 µL were injected into a Thermo Scientific UltiMate 3000 UPLC liquid chromatography system connected to a Superdex 200 (10/300) gel filtration column and equilibrated with HPLC buffer (25 mM HEPES pH 7.8, 100 mM NaCl, 5% (w/v). The run was tracked with a diode array detector. The flow rate was 1 to 0.75 $\frac{mL}{s}$. For reconstituted strep-MBP-ROXY9, 0.5 mL fractions were collected around the multimer peak.

In the first experiment, an Äkta prime chromatography system was utilized and absorbance was tracked at 280 nm.

Determination of Fe content

The concentration of iron was determined based on a colorimetric assay with ferene in accordance to an internal manual provided by the Lill group. Two replicates of 100 µL protein samples collected around the multimer peak were prepared alongside with two samples containing 100 µL dH_2O as blanks and seven 100 µL iron standard samples containing 2, 5, 10, 20, 50, 100 and 200 µM $(NH_4)_2Fe(SO_4)_2 \cdot 6\,H_2O$ outside the anaerobic tent. 100 µL 1% (w/v) HCl were added to all samples and the samples were incubated at 80 °C for

10 min. 500 µL 7.5% (w/v) ammonium acetate, 100 µL 4% (w/v) ascorbic acid, 100 µL 2.5% (w/v) SDS and 100 µL 1.5% (w/v) 3-(2-Pyridyl)-5,6-di(2-furyl)-1,2,4-triazine-5',5"-disulfonic acid disodium salt (ferene) were added to each sample sequentially, vortexing after each step. The samples were centrifuged at 13000 rpm and RT for 10 min and absorbance was measured at 593 nm. The iron content of the samples was determined based on the standard calibration curve.

Determination of S content

The concentration of sulphide content was determined based on a colorimetric assay with DMPD in accordance to an internal manual provided by the Lill group. A 2 mM Li_2S standard solution was freshly prepared in 10 mM NaOH. Two replicates of 100 µL protein samples collected around the multimer peak were mixed with 100 µL dH_2O alongside with one replicate containing 100 µL protein sample, 90 µL dH_2O and 10 µL 2 mM Li_2S in 10 mM NaOH. Two samples containing 200 µL dH_2O as blanks and nine 200 µL sulphide standard samples containing 5, 10, 25, 50, 75, 100, 150, 200 and 250 µM Li_2S in 10 mM NaOH were prepared. 600 µL 1% (w/v) Zinc acetate were added to each sample. 50 µL 7% (w/v) NaOH were added, the samples were mixed by inverting and incubated at RT for 15 min followed by a brief centrifugation at low speed. Solutions of 0.1% (w/v) N,N'-Dimethyl-p-phenylenediamine (DMPD) in 5 M HCl and 10 mM $FeCl_3$ in 1 M HCl were prepared. For each sample, 150 µL DMPD solution was carefully pipetted with the tip at the bottom at the reaction tube, immediately followed by the addition of 150 µL $FeCl_3$ solution and vortexing for 30 s. After all samples were treated sequentially, the samples were centrifuged at 13000 rpm and RT for 10 min. Absorbance was measured at 670 nm after 20 min. The sulphide content of the samples was determined based on the standard calibration curve.

5 Results

5.1 Recombinant ROXY9 can be obtained in mg amounts after expression in insect cells.

In order to obtain recombinant ROXY9 for biophysical and biochemical analysis, we expressed the protein in insect cells. Using the baculovirus expression vector system, ROXY9 was expressed as a fusion protein with a Strep-MBP tag at its N-terminus.

The purification process is outlined in figure 4 A. strep-MBP-ROXY9 was purified by affinity chromatography via the MBP tag. The fusion protein was cleaved with the TEV protease and separated from strep-MBP and TEV by gel filtration. All purification steps were done in the presence of GSH.

Figure 4 B and C show a representative affinity purification of wild-type strep-MBP-ROXY9 with a MBPTrap column. A broad flow-through absorbance peak was visible upon loading of the insect cell extracts as shown in the chromatogram in figure 4 B by a blue line. Representative fractions collected during the purification were analysed by SDS-Page alongside with a crude extract (CE) sample as represented in figure 4 C and indicated by green triangles. The first lane from the centre of the flow-through peak contains bands corresponding to differently sized insect proteins that were also present in the CE sample with one exception; a strong band slightly above 55 kDa was present within the CE but not the flow through. The lane containing a fraction collected right after absorbance had dropped to baseline appeared to be void of proteins.

After washing, the buffer was changed in a single step to an elution buffer containing 100 mM maltose to competitively elute proteins bound to the amylose resin column material as indicated by the green line in figure 4 B. During this elution step, a sharp elution peak was observed after approximately one column volume. On the SDS-Page (figure 4 C), fractions collected around the elution peak as indicated by red triangles show a strong protein band at around 55 kDa, that is mainly concentrated within the two main fractions and corresponds nicely to the expected size of strep-MBP-ROXY9, 57 kDa. In these fractions, only very few additional protein bands were visible which indicates a reasonably high purity of the sample.

In order to remove the strep-MBP tag, the affinity purified strep-MBP-ROXY9 sample was mixed with either commercially obtained TEV protease or purified His-TEV protease expressed in *E.coli*. The cleavage reaction with a cysteine protease requires reducing conditions, which should already be present due to the GSH within the strep-MBP-ROXY9 sample; to guarantee reducing conditions after a potential air oxidation during storage, fresh DTT was added to

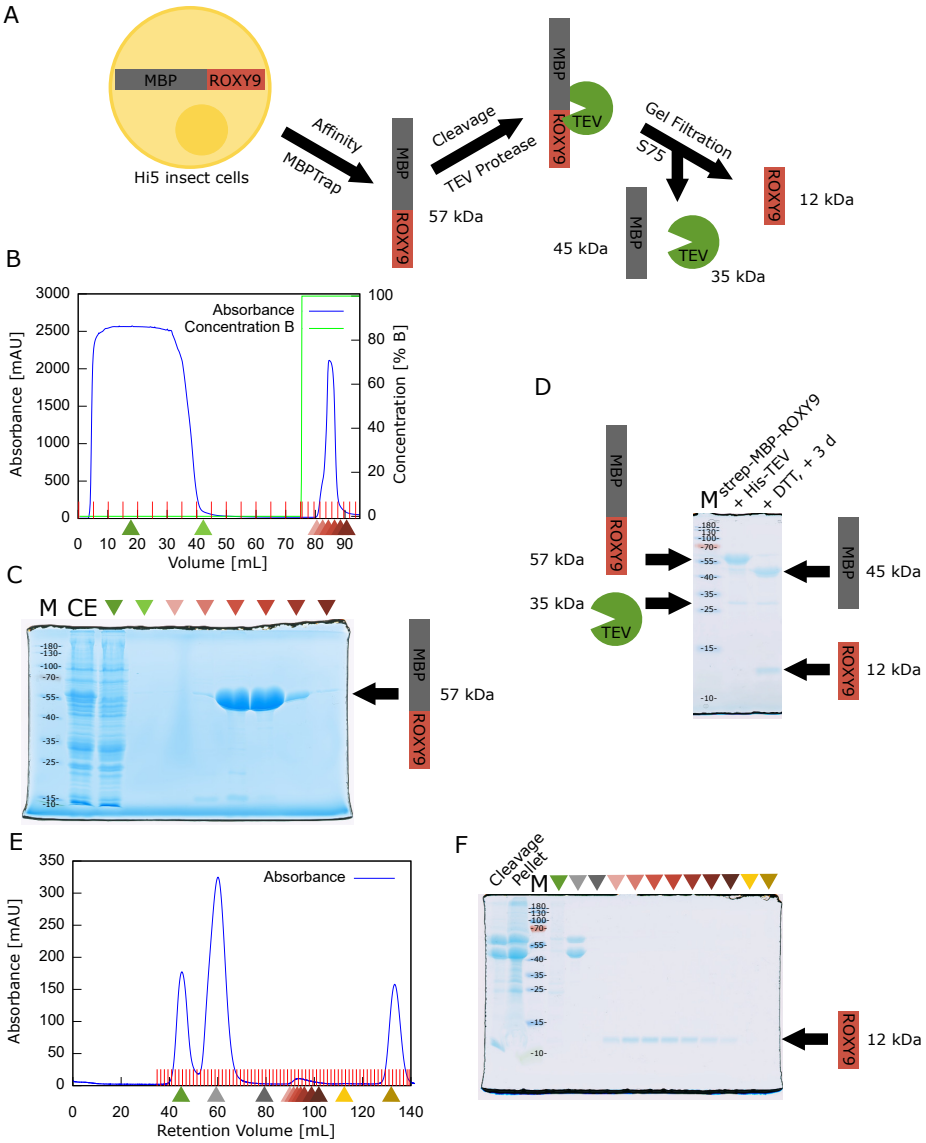

Figure 4: **Purification, TEV cleavage and gel filtration of ROXY9.** (A) Schematic representation of the purification process. (B) and (C) Representative affinity purification of strep-MBP-ROXY9. (B) Extracts from Hi5 insect cells expressing strep-MBP-ROXY9 were loaded onto an MBPTrap column connected to an Äkta prime chromatography system. Absorbance was tracked at 280 nm (blue). After loading and washing, strep-MBP-ROXY9 was eluted by switching to elution buffer containing maltose (green). (C) SDS-Page analysis (12% gel) of fractions indicated by coloured triangles alongside a crude extract (CE) sample. (D) SDS-Page analysis (15% gel) of TEV cleavage. strep-MBP-ROXY9 was mixed with His-TEV protease and incubated for 3 d. (E) and (F) preparative gel filtration after TEV cleavage. (E) Cleavage mixtures were centrifuged to separate precipitated proteins and loaded onto a Sephadex S75 column connected to an Äkta chromatography system. Absorbance was tracked at 280 nm (blue). (F) SDS-Page analysis (15% gel) of fractions indicated by coloured triangles alongside the initial cleavage mixture and a pellet sample from centrifugation.

initiate the cleavage reaction. Reaction mixtures were incubated for three days at 4 ℃ and efficient cleavage was checked by SDS-Page as shown in figure 4 D. After incubation in the presence of DTT, the band corresponding to the fusion protein at 57 kDa disappeared while two bands of the expected products appeared slightly above 40 kDa for strep-MBP and between 10 and 15 kDa for ROXY9. The weak band between 25 and 35 kDa corresponding to His-TEV was present in both lanes.

After cleavage, ROXY9 needed to be separated from strep-MBP and His-TEV. Previous experiments showed that the cleaved strep-MBP surprisingly was neither able to bind to an MBPTrap nor a StrepTrap column (Treffon, 2019). Preliminary experiments with a DEAE ion exchange column, which is routinely used for the purification of glutaredoxins (Couturier et al., 2013a), showed that ROXY9 did not bind to the matrix and passed through the column together with His-TEV. His-TEV could be separated by an additional HISTrap purification step, but with this two-step approach, large amounts of protein were lost (Data not shown).

Therefore, a preparative gel filtration step with a Sephadex S75 column was chosen. After cleavage, the sample had a high turbidity, so it was centrifuged prior to loading onto the column. The chromatogram is shown in figure 4 E, exhibiting three large absorbance peaks at around 45, 60 and 135 mL retention volume as well as a very small peak at around 95 mL. Different fractions were subsequently analysed by SDS-Page alongside the supernatant ("cleavage") and the pellet after centrifugation as presented in figure 4 F. The initial cleavage sample in this particular experiment still contained a noticeable band at 57 kDa corresponding to the full-length strep-MBP-ROXY9, which indicates an incomplete cleavage reaction. The pellet sample largely contained the bands corresponding to full-length strep-MBP-ROXY9 and strep-MBP as well as an unspecific background of proteins larger than 25 kDa, but, reassuringly, no band at 12 kDa. A weak but distinct band was visible in the pellet sample between 25 and 35 kDa at the observed size of His-TEV. This might implicate a certain degree of precipitation of the His-TEV protease, which in turn could be an explanation for the incomplete cleavage.

The fractions from the centre of the large peaks are indicated by green, light grey and ochre tringles in figure 4 E and F. The first peak contained a weak background of larger protein bands and likely aggregates of a high molacular weight. The second peak contained both full-length strep-MBP-ROXY9 and strep-MBP while the last peak, that eluted unusually late, contained no visible protein band. It could correspond to the GSH added within the buffer, possibly in complex with metal ions that lead to absorbance at 280 nm. Fractions from the small peak at around 95 mL retention volume are indicated by

red triangles. In these samples, a band 12 kDa was visible, which indicates successful purification of untagged ROXY9. The low absorbance of the peak at 280 nm can be explained by the absence of tryptophane in the entire peptide sequence of ROXY9 (see figure 2).

Processing a pellet from an infected 600 mL insect cell culture typically yielded 20 to 40 mg of fusion protein after affinity purification. For the run presented in figure 4 B and C, 28 mg were obtained. For the second stage of purification shown in figure figure 4 E and F, 16 mg of fusion protein were employed for cleavage, recovering approximately 1 mg of untagged ROXY9 after gel filtration and concentration. This corresponds to a yield of roughly 30% considering reduced weight after cleavage.

5.2 ROXY9 adopts a thioredoxin fold similar to *A. thaliana* GRXC2

With an established expression system and purification protocol at hand, the question arises whether the protein is correctly folded. For a protein annotated as a glutaredoxin, one would expect the thioredoxin fold consisting of a core structure with a four-stranded β sheet sandwiched by three α helices as detailed in the introduction (See section 2.2). Plant glutaredoxins have an additional, N-terminal α helix. This structure was predicted by modelling ROXY9 with SWISS-MODEL (Waterhouse et al., 2018) and is shown in figure 5 A.

A relatively quick way to obtain structural information is CD spectroscopy. Protein CD spectra give a structural signature based on the secondary structure elements. Tag-free ROXY9 was measured alongside with strep-MBP separated after cleavage and with GRXC2 as reference proteins. GRXC2 is a class I glutaredoxin that is active in classical activity assays like the HEDS Assay (see section 5.5). It was prepared in the same way as ROXY9, expressing strep-MBP-GRXC2 in insect cells followed by MBPTrap affinity purification and cleavage. For all samples, the buffer was replaced by a buffer without chloride ions that contained DTT as a reducing agent. Figure 5 B shows the mean residue ellipticity of ROXY9 (red), GRXC2 (blue) and strep-MBP (grey). The curves align very well for ROXY9 and GRXC2 while strep-MBP deviates, which indicates that similar structural elements are present within ROXY9 and GRXC2.

To further investigate the structural properties of the two glutaredoxins, melting curves were measured by tracking mean residue ellipticity at 222 nm and heating the samples. Results are shown in figure 6 A and C for GRXC2 and ROXY9 respectively. In both cases, ellipticity remained relatively stable over a wide temperature range followed by a loss in amplitude between 60 and

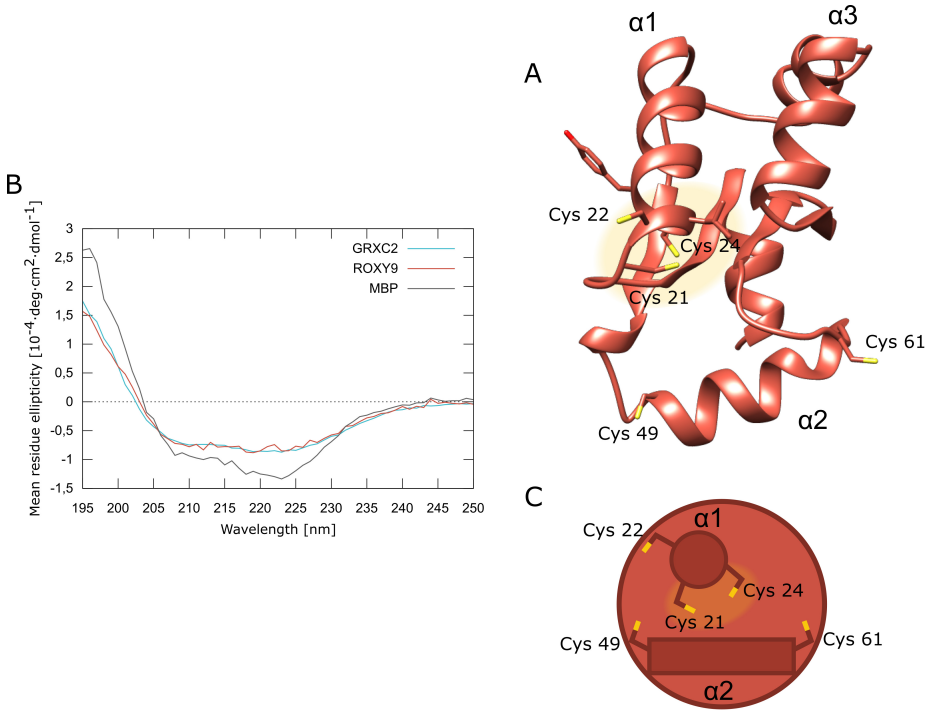

Figure 5: **CD Spectra of ROXY9 and GRXC2 indicate a similar fold.** (A) Model of ROXY9 obtained by SWISS-MODEL (Waterhouse et al., 2018). Secondary structure as well as critical residues are shown, cysteines and α helices are labelled. The active site with the CCLC motif is highlighted by yellow background. (B) CD Spectrum of ROXY9, GRXC2 and strep-MBP after cleavage in the presence of DTT. (C) Simplified schematic representation of ROXY9 showing cysteines on α helices 1 and 2. The putative catalytic cysteine, Cys 21, is highlighted alongside the putative resolving cysteine, Cys 24, by yellow background. Data set is also presented in figures 6, 7 and S1.

80 ℃. The curves were fitted with a logisitc fit and melting temperatures were determined as $T_m = 70.5759\,^{\circ}\mathrm{C}$ for GRXC2 and $T_m = 69.2049\,^{\circ}\mathrm{C}$ for ROXY9. After the heat treatment, full CD spectra were remeasured as shown in figure 6 B and D. For ROXY9 in figure 6 D, the ellipticity was close to zero after heating, which implies an absence of secondary structure elements. For GRXC2 in figure 6 B, however, the curves measured before and after heating to 88 ℃ almost perfectly align. This indicates a refolding of the protein, and the heat treated sample also exhibited activity in the HEDS assay (data not shown).

Glutaredoxins utilize GSH as a cofactor, which is bound by a binding site between the active site and $\alpha 2$ helix (Berndt and Lillig, 2017). This interaction could potentially influence the protein structure, and was thus investigated by measuring CD spectra of ROXY9 and GRXC2 in the presence of GSH instead

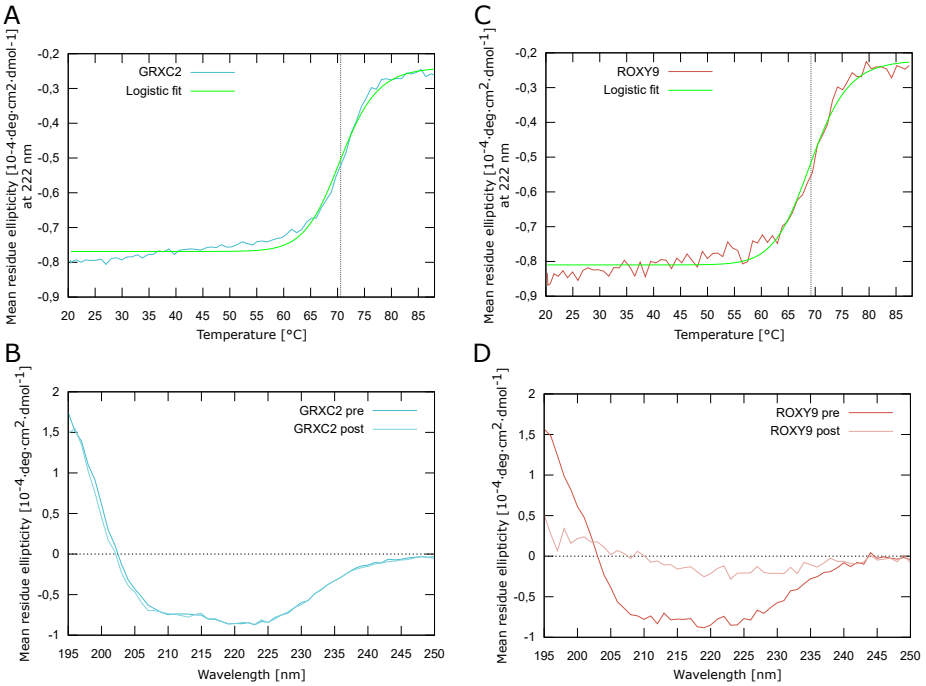

Figure 6: **ROXY9 and GRXC2 show high thermal stability.** (A) Melting curve of GRXC2. GRXC2 was heated and ellipticity was tracked at 222 nm. The curve was fitted logistically ($y = -0.2389 + \frac{-0.5299}{1+\frac{x}{70.5759}^{20.69867}}$, $R^2 = 0.99145$), yielding $T_m = 70.5759\,°C$ as indicated by the dashed line. (B) CD Spectrum of GRXC2 before and after heat treatment. (C) Melting curve of ROXY9. ROXY9 was heated and ellipticity was tracked at 222 nm. The curve was fitted logistically ($y = -0.22094 + \frac{-0.58905}{1+\frac{x}{69.2049}^{19.79758}}$, $R^2 = 0.98684$), yielding $T_m = 69.2049\,°C$ as indicated by the dashed line. (D) CD Spectrum of ROXY9 before and after heat treatment. Data sets before heat treatment are also presented in figures 5, 7 and S1.

of the previously used DTT.

Results are shown in figure 7. The presence of GSH led to a more strongly pronounced ellipticity for both proteins, which could imply a higher degree of structure of the protein. Though the curves for ROXY9 (red) and GRXC2 (blue) align in the presence of DTT, the curves differ to some extent in the presence of GSH, with GRXC2 (dark blue) showing stronger pronounced minima at around 210 and 222 nm than ROXY9 (dark red). This could be a slight indication of a different interaction mode with GSH. In contrast, the CD spectrum of strep-MBP was only marginally influenced by the change from DTT to GSH as shown in supplement figure S1.

In summary, ROXY9 and GRXC2 show a highly similar CD spectrum as well as a similarly high thermal stability. Also, both proteins were influenced by

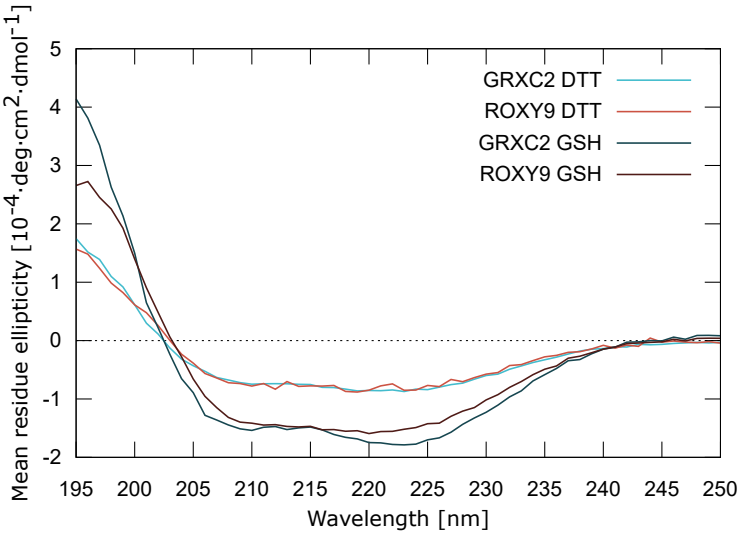

Figure 7: **GSH influences the CD spectrum of GRXC2 and ROXY9.** CD Spectrum of ROXY9 and GRXC2 in the presence of DTT or GSH. Data sets in the presence of DTT are also presented in figures 5, 6 and S1.

GSH. Considering the fact that the GRXC2 sample with these characteristics is catalytically active, this implies that for the ROXY9 sample, structural prerequisites for such an activity should also be met. ROXY9 likely obeys to the thioredoxin fold as shown in the model in figure 5 A. This 3D structure is simplified to the schematic representation in 5 C, which shows all five cysteines located on α helices 1 and 2, and is used subsequently to indicate potential redox states of the different cysteines.

5.3 The N-terminal and the C-terminal cysteines of the ROXY9 active site form a disulphide bond

The results from the CD spectroscopy strongly suggest that recombinant ROXY9 is present in the thioredoxin fold. This would imply that the CCLC active site motif is indeed located at the end of the $\alpha 1$ helix with a close proximity of the putative catalytic cysteine in the first position of the motif, Cys 21, to the cysteine in the last position, Cys 24, as represented in figure 5 A. This proximity should allow for the formation of a disulphide bond between the two cysteines, a feature that is well known from other glutaredoxins with cysteines in corresponding positions, where it is an intermediate state of the dithiol mechanism (Deponte, 2013; Ukuwela et al., 2018).

Furthermore, such a disulphide should be formed or resolved at a physiologically relevant redox potential to have any *in vivo* significance. The redox

potential in plant cells, that is largely dependent on the cellular glutathione pool, was determined at around –320 mV in the untreated cytosol of *A. thaliana* epidermis cells and –225 mV within the ER (Schwarzländer et al., 2008). The midpoint redox potential of poplar class I glutaredoxins was reported between -260 to –240 mV (Couturier et al., 2013a).

A way to determine the redox state of cysteines is the labelling with thiol alkylation reagents (Zannini et al., 2017). These reagents like iodoacetamide or maleimide compounds react with reduced cysteines in the thiolate form and labelling can subsequently be detected by fluorescence or changes in electrophoretic mobility. In a typical experiment, protein samples are incubated under different reducing and oxidizing conditions followed by TCA precipitation and labelling of the reduced cysteines.

To analyse whether ROXY9 can form a disulphide bridge, a redox titration assay was performed (Zannini et al., 2017). strep-MBP-ROXY9 was incubated with DTT and dithiane, the oxidized form of DTT with an intramolecular disulphide, employing either one of the compounds alone or a mixture of both at different redox potentials as calculated by the Nernst equation. The disulphide dithiane can be transferred onto the target protein by a disulphide exchange reaction if electrochemically favourable. In addition, strep-MBP-ROXY9 was incubated with GSSG, which can induce the formation of an intramolecular disulphide but also mixed disulphides between the protein and GSH. After incubation, the samples were processed by TCA precipitation and reduced cysteines were labelled with 5 kDa mmPEG, a maleimide compound conjugated with a 5 kDa polyethylene glycol chain, and separated by SDS-Page under non-reducing conditions. It is worth noting that the strep-MBP-ROXY9 fusion protein only contains the five cysteines of ROXY9 and no further cysteines within the strep-MBP tag.

The redox titration for strep-MBP-ROXY9 with a wild-type active site is shown in figure 8. In the first four lanes, unlabelled samples from the initial purification, desalting as well as DTT- and dithiane treatment were loaded. The main protein band was always at 57 kDa as expected for monomeric strep-MBP-ROXY9. Two thin bands were visible at 115 kDa, which could correspond to a dimer and was most pronounced after the oxidizing dithiane treatment, and below 70 kDa.

For the DTT-treated sample labelled with 5 kDa mmPEG in the fifth lane, the main band was located at 130 kDa. Under these conditions, a fully reduced protein was expected, where all five cysteines were accessible for alkylation as assigned by the sketch on the right, showing a simplified model of ROXY9 with all cysteines conjugated to mmPEG. Interestingly, the addition of five 5 kDa mmPEG moieties to a 57 kDa protein induced a shift of roughly 70 kDa, considerably more than the expected shift by 25 kDa. This phenomenon was pre-

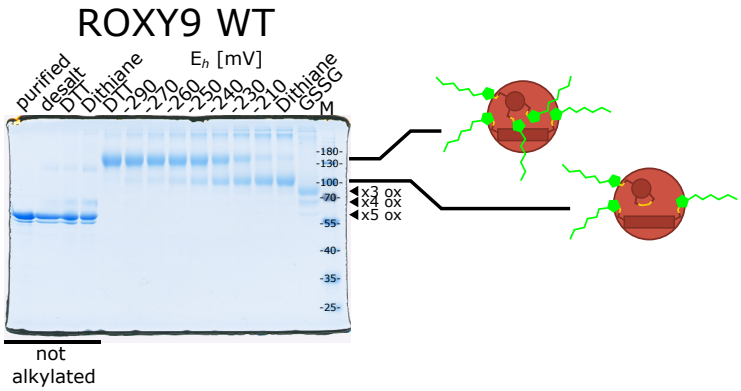

Figure 8: **Redox titration of ROXY9 indicates formation of a disulphide bond between cysteines 21 and 24.** strep-MBP-ROXY9 was pre-reduced, desalted and mixed with DTT, Dithiane, DTT/Dithiane redox buffers at different redox potentials or GSSG as indicated. Samples were incubated at RT for 2 h followed by TCA precipitation. Reduced cysteines were labelled with 5 kDa mmPEG. Samples were separated by non-reducing SDS-Page (10% gel) alongside with untreated protein after purification and desalting. Sketches on the right indicate the likely redox state of proteins, further oxidized species are indicated by triangles.

viously reported for alkylated proteins (Zannini et al., 2017). GRXS16 for instance, a 25 kDa protein, runs at an apparent size of 37 kDa when all three of its thiols are labelled with 2 kDa mmPEG (Zannini et al., 2019). In addition to the monomer band, also some weak multimer bands at the very top of the gel were visible.

The dithiane-treated sample labelled with 5 kDa mmPEG was loaded in the third to last lane in figure 8. A prominent band was located at 100 kDa, while the alleged reduced, 5-fold labelled fraction at 130 kDa was still slightly visible in addition to multimer bands. Dithiane should lead to the formation of disulphide bonds, thereby preventing multiples of two cysteines from being alkylated. Since mmPEG seems to add an apparent molecular weight of 14 kDa in this experimental set up, formation of one disulphide bond in ROXY9 should causes a mobility shift by 42 kDa, leading to an apparent molecular weight of 99 kDa as observed here. The most likely position for this disulphide is between Cys 21 and Cys 24 of the active site, as indicated by the sketch on the right.

The GSSG-treated and labelled sample in the second to last lane contained three distinct bands with the strongest located between 100 and 70 kDa, a weaker band slightly below 70 kDa and a thin band at 57 kDa as indicated by triangles on the right in figure 8. This last band corresponds to an unlabelled protein where all cysteines were prevented from alkylation. This could be ex-

plained by two disulphides and one glutathionylated cysteine, by one disulphide and three glutathionylated cysteines or by five glutathionylated cysteines. The band above this position slightly below 70 kDa likely contains proteins with one alkylated cysteine and either two disulphides or one disulphide and two glutathionylated cysteines, while the band between 100 and 70 kDa likely contains protein with two alkylated cysteines, one disulphide and one glutathionylated cysteine.

The strep-MBP-ROXY9 protein was also incubated with redox buffers containing DTT and dithiane at different ratios to yield different redox potentials as indicated in figure 8. Aside from multimer bands, these samples contained bands both at 130 and 100 kDa, while samples at lower, more reducing redox potentials showed a higher proportion of the assigned 5-fold labelled position, samples at higher, more oxidizing redox potentials mostly contained bands at the alleged 3-fold labelled position. At a redox potential of –240 mV, equal amounts of the two bands were present. This value can thus be taken as an estimate for the midpoint redox potential of the disulphide bond between Cys 21 and Cys 24.

To validate this interpretation, ROXY9 variants with individual cysteines replaced by serines were investigated in the same manner with results presented in figure 9.

For the upper gel, the first cysteine of the active site, Cys 21, was replaced by serine, yielding an SCLC active site motif. With just a point mutation, strep-MBP-ROXY9 SCLC was running as a monomer at 57 kDa similar to the wild-type version in non-alkylated samples. For the dithiane-treated sample in the fifth lane, a slight dimer band was visible at 115 kDa, also in line with observations made with the wild-type. In DTT-treated and labelled sample in the sixth lane, the main band was shifted to a position between 130 and 100 kDa, slightly below the dimer band in the non-labelled sample. This position was assigned to a state were all four of the remaining thiols were reduced and could be alkylated. At higher, more oxidizing redox potentials all the way to a sample incubated only with dithiane, this position remained the most prominent band, indicating overall no disulphide formation. Only treatment with GSSG led to the formation of different bands likely corresponding to non-labelled, 1-fold, 2-fold and possibly also 3-fold labelled protein with the respective oxidation status indicated in figure 9 by triangles.

The gel in the centre of figure 9 shows results for strep-MBP-ROXY9 CSLC with the second cysteine of the active site, Cys 22, replaced by serine. For the non-labelled samples, the familiar band at 57 kDa corresponding to strep-MBP-ROXY9 CSLC was observed, alongside with additional weak bands indicating the presence of a small amount of impurities. All samples contained an addi-

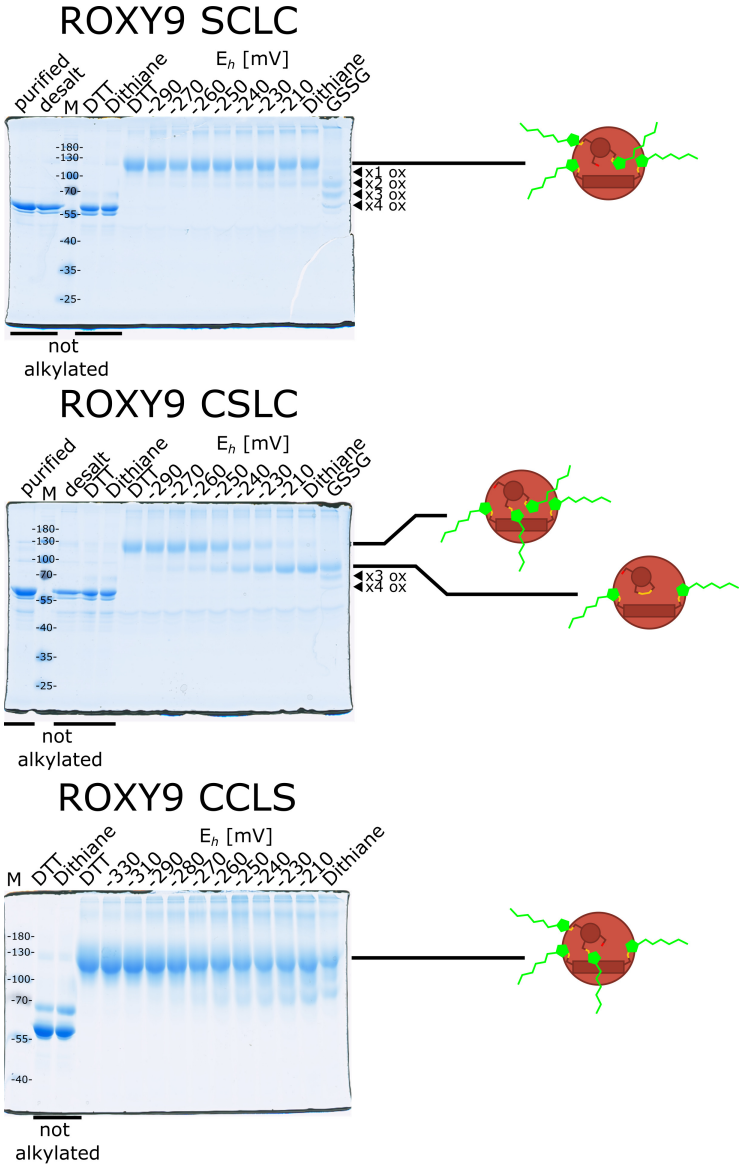

Figure 9: **Redox titration of ROXY9 active site variants indicates formation of a disulphide bond between cysteines 21 and 24.** strep-MBP-ROXY9 SCLC, CSLC and CCLS were pre-reduced, desalted and mixed with DTT, Dithiane, DTT/Dithiane redox buffers at different redox potentials or GSSG as indicated. Samples were incubated at RT for 2 h followed by TCA precipitation. Reduced cysteines were labelled with 5 kDa mmPEG. Samples were separated by non-reducing SDS-Page (10% gel) alongside untreated protein after purification and desalting. Sketches on the right indicate the likely redox state of proteins, further oxidized species are indicated by triangles.

tion protein with an apparent molecular weight of 55 and 40 kDa, which was not alkylated. This might correspond to the thiol-free strep-MBP fragment. After alkylation, the main band of the DTT-treated sample in the sixth lane was shifted to a position between 130 and 100 kDa, which was assigned to a fully reduced, 4-fold labelled state. With the addition of dithiane and thus higher, more oxidizing redox potentials, this band became weaker while a second band between 100 and 70 kDa became increasingly prominent. This position was previously assigned to a 2-fold labelled protein, implying the formation of a disulphide bridge likely between Cys 21 and Cys 24 as indicated by the sketch on the right. At a redox potential of –240 mV, equal amounts of the two bands were present, similar to the wild-type protein. The GSSG-treated sample contained mostly this 2-fold labelled fraction between 100 and 70 kDa, but also two weaker bands for non-labelled and 1-fold labelled protein, indicating varying degrees of glutathionylation. In comparison to the wild-type protein, this is a first implication that Cys 22 might be the main site of glutathionylation.

Results for strep-MBP-ROXY9 CCLS with a mutation in the last position of the active site motif, Cys 24, are shown on the lower gel in figure 9. Band positions were very similar to ROXY9 SCLC, but the unlabelled samples showed a band slightly below 70 kDa in addition to the expected monomer band at 57 kDa, that was only faintly visible in previous, TCA-precipitated samples. All labelled samples mainly exhibited a band between 130 and 100 kDa, that was assigned to a 4-fold labelled protein. Oxidizing conditions led to the formation of weak bands of a lower molecular weight suggesting disulphide bridges between residual cysteines. A GSSG-treatment was not included in this experiment.

Additional results for mutations in the two cysteines outside of the active site motif, Cys 49 and Cys 61, are shown in supplementary figure S3. Though strep-MBP-ROXY9 C61S exhibited a strange double band phenotype, a transition with turning point at around –240 mV was clearly visible for both variants, indicating the formation of a disulphide bond. In summary, the transition depends on the presence of both Cys 21 and Cys 24, while the other three cysteines are dispensable.

The experiments were all conducted using the full-length fusion protein containing the strep-MBP tag. To rule out an influence of the tag, a similar experiment was attempted with cleaved ROXY9 without the strep-MBP tag with results presented in supplementary figure S2. Overall, the patterns were very similar to the respective samples in figure 8 for strep-MBP-ROXY9 indicating no drastic influence of the strep-MBP tag.

5.4 ROXY9 has reactive thiols and tends to form oligomers through intermolecular disulphide bridges

Working with ROXY9 protein samples often led to the observation that the protein is prone to oxidation in the absence of reducing agents or after longer storage even in the presence of either DTT or GSH. For instance, a strep-MBP-ROXY9 sample that was affinity purified and stored in the presence of 5 mM GSH at 4 °C for approximately one week showed a multimer peak in addition to aggregates and the monomer peak as shown by gel filtration analysis in figure 10. After the addition of 10 mM DTT and incubation for 10 minutes, this multimer peak was resolved and only aggregates and the monomer peak were visible (figure 10).

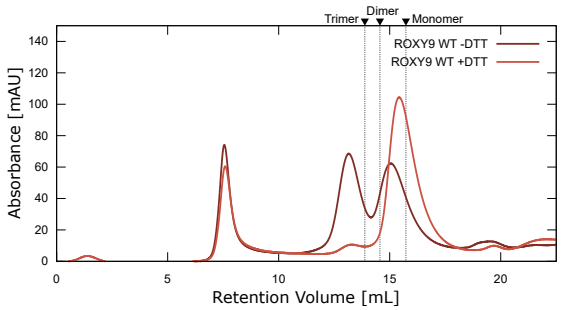

Figure 10: **ROXY9 forms both aggregates and oxidized multimers.** Analytical gel filtration of strep-MBP-ROXY9 by loading both untreated and DTT-reduced samples onto a Sephadex S200 column tracking absorbance at 280 nm. The experiment was carried out under anaerobic conditions in Marburg. The untreated sample was stored in GSH containing buffer for approximately one week at 4 °C. Expected monomer, dimer and trimer retention volumes are 15.73, 14.56 and 13.88 mL respectively as calculated by the provided calibration curve and indicated by dashed lines. This data set is also presented in figures 24 and S6.

It is worth mentioning that the peak positions of the putative monomers (calculated MW: 57 kDa) do not perfectly match the calculated retention volume but were rather calculated to represent a higher weight of 86 kDa for the untreated sample and 68 kDa for the reduced sample. Even if an inaccuracy of the calibration of the column with molecular weight markers is assumed, the different mobilities of the monomers still have to be explained. One option is that the untreated samples might form an intramolecular disulphide or be glutathionylated. Although the molecular weight of GSH is only 0.3 kDa, one would have to postulate that oxidative modifications affect the shape and thereby the mobility of the protein.

In line with this observation, the redox titration assays presented in section

5.3 were found to strictly require pre-reduced protein. In mmPEG labelled samples, a considerable degree of multimerization was visible on the non-reducing gels, that could not be attributed to an individual cysteine when comparing all variants (see figures 8, 9 and S3). Consistent with the gel filtration analysis, these multimers were dissolved on reducing gels (Figure 12). The reactivity of cysteines largely depends on the formation of thiolates, that can serve as nucleophiles (Jensen et al., 2014; Manta et al., 2019). This raises the question how many thiolates are present at a given pH, which was addressed by pH titration assays.

The pH titration assay is an thiol-alkylation approach similar to the redox titration assay (Zannini et al., 2017). Protein samples are incubated at different pH values in the presence of iodoacetamide. This alkylation reagent only reacts with cysteines in their thiolate form, which are present at pH values higher than the specific pKa. These cysteines are blocked and can not be labelled with mmPEG after the TCA precipitation. At pH values lower than the specific pKa, thiols remain protonated and are not blocked by iodoacetamide. After TCA precipitation, which removes remaining iodoacetamide and denatures the proteins, these thiols can be labelled with mmPEG at slightly basic pH. Results for a pH titration assay with wild-type strep-MBP-ROXY9 are shown in figure 11.

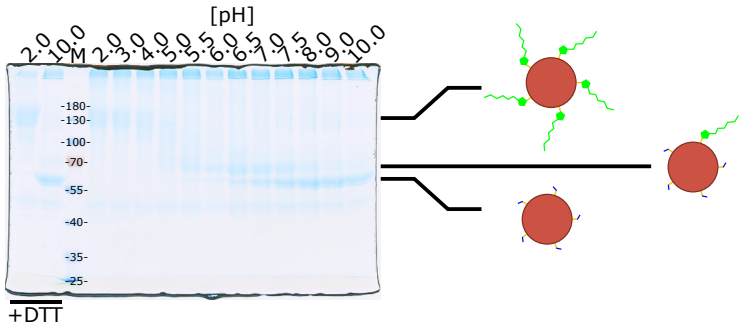

Figure 11: **pH titration of ROXY9 reveals low pKa values for all cysteines.** strep-MBP-ROXY9 was pre-reduced, desalted and incubated with iodoacetamide at different pH values for 1 h to block cysteines present in thiolate form. The samples were subsequently TCA-precipitated and reduced cysteines not blocked by iodoacetamide labelled with 5 kDa mmPEG. Samples were separated by non-reducing SDS-Page (10% gel). For pH 2.0 and 10.0, replicate samples were reduced prior to mmPEG labelling to distinguish between iodoacetamide blocking and a potential air oxidation. Sketches on the right indicate the likely alkylation state of proteins.

At the basic pH of 10.0, a band was present at 57 kDa. This position likely corresponds to a 5-fold iodoacetamide blocked protein that was subsequently

not labelled by 5 kDa mmPEG. Apparently, all five cysteines are reactive thiolates at this pH. At the acidic pH of 2.0, a band was located at 130 kDa, this corresponds to a 5-fold labelled protein where all thiols were protonated and could not be blocked by iodoacetamide. A pH of 6.0 led to a band at slightly below 70 kDa which indicates a 1-fold labelled, 4-fold blocked protein. Between pH 5.5 and 4.0, a ladder of bands leading up to the non-blocked, 5-fold labelled state was visible. The pKa of four thiols seems to be in this range. At physiological conditions between pH 8.0 and 6.5, both 1-fold labelled and non-labelled species were present, indicating that four to five of the thiols were present in the reactive thiolate form. At a pH of 7.5, both bands had roughly the same abundance.

In summary, four cysteines of ROXY9 appear to have a pKa between 5.5 and 4.0 and the fifth cysteine has a pKa around 7.5. To identify which of the cysteines has the highest pKa, pH titrations assays were also performed with the ROXY9 variants with cysteine to serine mutations in the different positions. Results are presented in supplementary figure S4. At first sight, the results looked very similar with double bands present at physiological pH and most changes between 5.5 and 4.0. For ROXY9 C61S, the upper bands was strongly visible at the most basic pH of 10.0. Considering the previous observation that alkylated ROXY9 C61S exhibits a peculiar double band running behaviour (see figure S3), it is the most likely candidate for the higher pKa at around 7.5, implying that all other cysteines have a pKa between 5.5 and 4.0.

The average pKa of a protein cysteine is around 8.5 (Poole, 2015), which implies that the micro-environment around the cysteines of ROXY9 considerably lowers the pKa. This is a known phenomenon for the catalytic cysteine with typical pKa values between 5.5 and 2.5 (Manta et al., 2019). It is thus remarkable, that at least three additional thiols of ROXY9 have a similarly low pKa.

In redox and pH titration assays, varying degrees of multimers were often observed on the non-reducing gels. To investigate the composition of these multimers, a redox titration was repeated and the samples were separated on a reducing gel by utilizing DTT-containing loading buffer. Results are presented in figure 12.

On the reducing gel at the bottom, the multimer band was almost completely absent. Instead, the monomer bands that shift between 5-fold and 3-fold labelled state depending on the redox conditions were supplemented by additional bands at positions expected for 4-fold and 2-fold labelled protein. For the more reducing treatment conditions, these 4-fold labelled species likely formed a dimer connected by an intermolecular disulphide, that was resolved by the reducing loading buffer as indicated by sketches on the left. At more oxidiz-

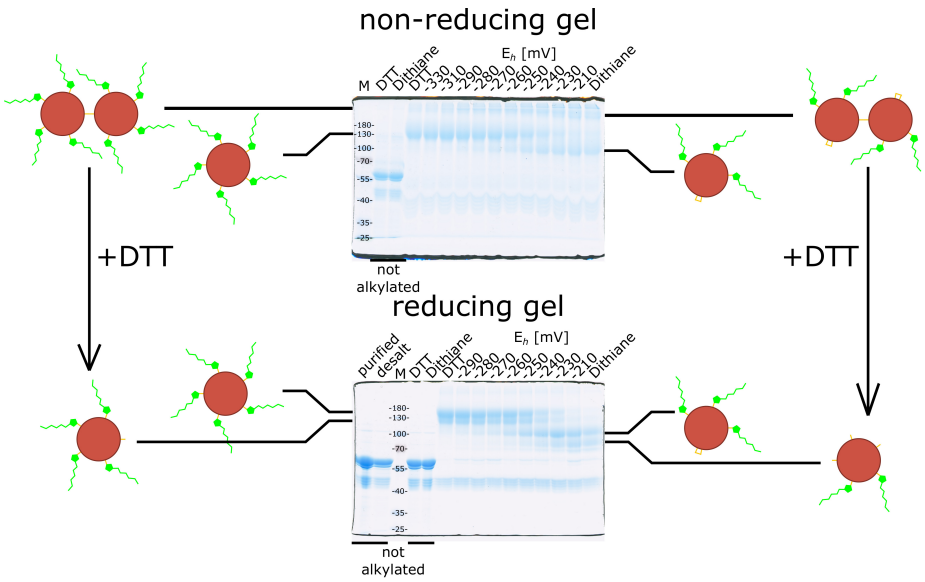

Figure 12: **A considerable amount of the multimer fraction consists of disulphide-linked dimers.** strep-MBP-ROXY9 was pre-reduced, desalted and mixed with DTT, Dithiane or DTT/Dithiane redox buffers at different redox potentials as indicated. Samples were incubated at RT for 2 h followed by TCA precipitation. Reduced cysteines were labelled with 5 kDa mmPEG. For SDS-Page (10% gel), one set of samples is mixed with reducing loading buffer, also including aliquots of untreated protein after purification and desalting (”reducing gel”). A second sample set is mixed with non-reducing loading buffer similar to previous experiments (”non-reducing gel”). Bands likely corresponding to protein without internal disulphide bridge are assigned on the left while bands likely corresponding to protein with internal disulphide bridge are assigned on the right in sketch form.

ing treatment conditions, an intramolecular disulphide was formed. Monomers were subsequently labelled by three moieties of 5 kDa mmPEG while some proteins formed dimers connected by an intermolecular disulphide, leaving only two cysteines to be labelled. Successive reducing treatment resolved all disulphides, giving rise to a 2-fold labelled monomer fraction as indicated by sketches on the right.

At which state the dimers are formed remains an open question. DTT-resolvable multimerization also occurred in samples treated with DTT, indicating that the multimerization took place after removal of DTT, so either during TCA precipitation or labelling. Samples that were not alkylated and instead incubated in buffer without mmPEG alongside with the alkylated samples showed considerably less dimer bands, especially when comparing the DTT treated samples. This suggests that the process of labelling could have an influence

on the multimerization, which is in line with preliminary observations after N-ethylmaleimide (NEM) treatment (data not shown).

5.5 ROXY9 shows little to no reductase activity

With the ROXY9 protein exhibiting the thioredoxin fold and also forming an internal disulphide bridge, which could be part of a catalytic mechanism, the potential activity as reductase was investigated. This is the typical function of class I glutaredoxins.

A commonly used assay for catalytically active glutaredoxins is the HEDS assay, that is outlined in figure 13 A. 2-Hydroxyethyl disulphide (HEDS) serves as an artificial disulphide substrate for glutaredoxins, that is reduced via an intermediate with a mixed disulphide between GSH and 2-mercaptoethanol (βME-SG). Both the formation as well as deglutathionylation of the intermediate are thought to be catalysed by glutaredoxins (Begas et al., 2017). The reaction yields GSSG, and can be coupled to the consumption of NADPH by glutathione reductase (GR), which can be tracked as a decrease of absorbance at 340 nm.

In line with previous observations (Treffon, 2019), strep-MBP-ROXY9 with wild-type active site showed no activity within the HEDS assay (figure 13 B). Activity was not enabled by replacing the active site with CPYC, the consensus active site motif of catalytically active class I glutaredoxins. As a control enzyme, strep-MBP-GRXC2 was utilized, which led to a linear decrease of absorbance at 340 nm until eventually reaching a plateau after 350 s.

In a recent publication, poplar class III glutaredoxins were also found to show no activity within the HEDS assay, but a weak activity towards cumene hydroperoxide (CHP) was reported (Xu et al., 2022). Such a peroxidase activity had been previously observed for yeast glutaredoxins (Collinson et al., 2002).

The assay was carried out similar to the HEDS assay, coupled to NADPH consumption but replacing the HEDS substrate with cumene hydroperoxide (figure 14 A). Results are presented in figure 14 B and C for two sets of experiments.

Figure 14 B shows mean and standard deviation of three experiments with strep-MBP-ROXY9 wild-type, strep-MBP-ROXY9 CPYC and strep-MBP-GRXC2 alongside with the buffer control. For both ROXY9 variants as well as the buffer, a slow decrease in absorbance was measured over the course of the experiment. A slightly steeper decent was measured for strep-MBP-GRXC2. To expose this small difference, which suggests a weak peroxidase activity of GRXC2, the protein amount was increased 5-fold and the reaction time was more than doubled as compared to the HEDS assay.

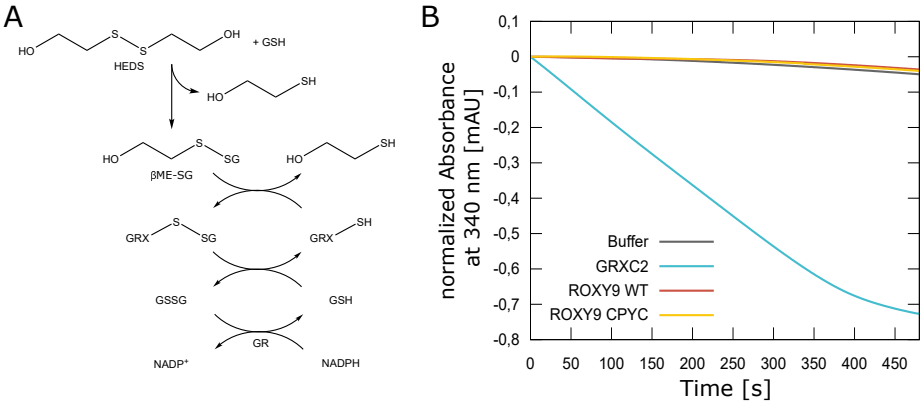

Figure 13: **HEDS Assay shows reductase activity for GRXC2 but not for ROXY9.** (A) Coupled reactions of the HEDS assay. HEDS reacts with GSH either spontaneous or enzymatically via GRXs to the mixed disulphide βME-SG, which is reduced by GRXs using GSH as cofactor. The GSSG formed in this reaction is reduced by GR and NADPH with the consumption of NADPH being tracked at 340 nm. (B) HEDS assay with strep-MBP-GRXC2, strep-MBP-ROXY9-WT and strep-MBP-ROXY9 CPYC. GRX samples were pre-reduced with DTT and the buffer exchanged for buffer containing 5 mM fresh GSH. GRX samples containing 20 µg of protein or GSH-containing buffer as control were added to a buffer containing NADPH and GR. After 60 s mixing and equilibration time, the reaction was started with the addition of the HEDS substrate. The change in absorbance at 340 nm was followed after an additional 30 s mixing and equilibration time for 8 min.

In a second set of experiments with five repetitions presented in figure 14 C, strep-MBP-ROXY9 CPYC was replaced by strep-MBP-ROXY9 SCLC. This constitutes a negative control as the catalytic cysteine in the first position of the active site motif is missing. Again, both ROXY9 variants and the buffer control exhibited a similar decrease in absorbance, while GRXC2 showed a slightly faster decrease. This time, the standard deviation of GRXC2 and the buffer were marginally overlapping. Further repetitions would probably be needed to significantly demonstrate and quantify the peroxidase activity of GRXC2, but no indication of a potential activity of ROXY9 were found.

With ROXY9 showing no reductase activity towards low molecular weight substrates like HEDS or CHP, the focus shifted to potential protein substrates. An established assay system is the deglutathionylation of GAPDH (Zaffagnini et al., 2008). In a three step process, GAPDH is first glutathionylated, which leads to the inactivation of enzymatic activity. Subsequently, the glutathionylated GAPDH (GAPDH-SG) is incubated with GRX to catalyse the deglutathiolylation. Finally, GAPDH activity is measured. Previously, ROXY9 was found to exhibit activity within the GAPDH assay (Treffon, 2019).

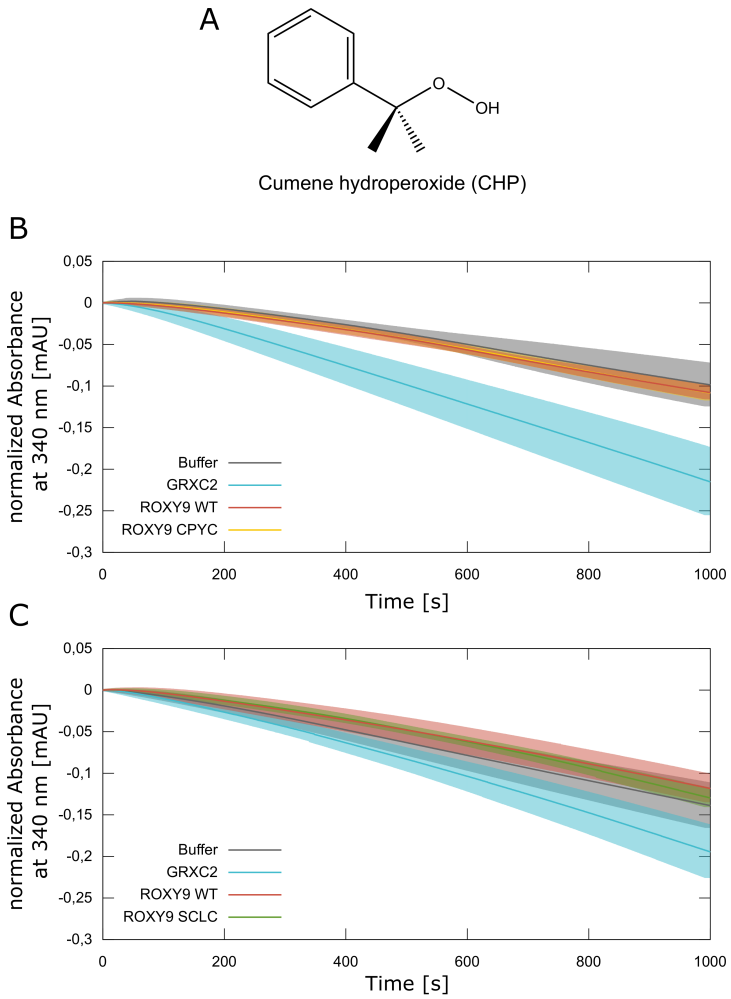

Figure 14: **GRXC2, but not ROXY9, has weak peroxidase activity.** (A) Structure of cumene hydroperoxide. (B) CHP assay with strep-MBP-GRXC2, strep-MBP-ROXY9-WT and strep-MBP-ROXY9 CPYC. GRX samples were pre-reduced with DTT and the buffer was exchanged for buffer containing 1 mM fresh GSH. GRX samples containing 100 µg of protein or GSH-containing buffer as control were added to a buffer containing NADPH and GR. After 60 s mixing and equilibration time, the reaction was started with the addition of the CHP substrate. The change in absorbance at 340 nm was followed after an additional 30 s mixing and equilibration time for 16 min 40 s. Data are displayed as mean and standard deviation of 3 experiments. (C) CHP assay with strep-MBP-GRXC2, strep-MBP-ROXY9-WT and strep-MBP-ROXY9 SCLC as described above. Data are displayed as mean and standard deviation of 5 experiments.

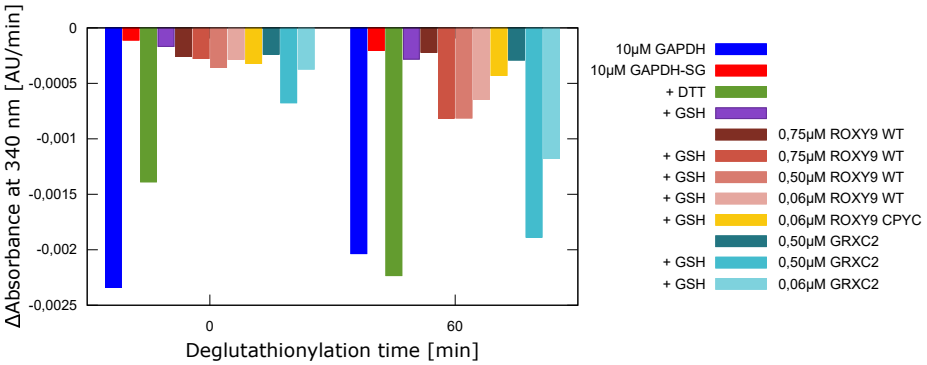

Figure 15: **ROXY9 reduces GAPDH-SG less efficiently than GRXC2.** GRX samples were pre-reduced with DTT and desalted. GAPDH was glutathionylated and desalted. For deglutathionylation, GAPDH-SG was mixed with DTT, GSH, GRX or GRX and GSH combined as indicated in the legend. Directly after mixing and after 60 min, aliquots were withdrawn from the reaction mixtures and deglutathionylation was stopped. In a second step, GAPDH activity of the different samples was determined by measuring NADH consumption and calculating the change in absorbance over time. GAPDH not glutathionylated served as reference.

Figure 15 shows the GAPDH activity after 60 min incubation with strep-MBP-ROXY9 wild-type and CPYC as well as strep-MBP-GRXC2. As control, non-glutathionylated GAPDH was used to measure the initial activity (blue bars). For GAPDH-SG shown in bright red, almost no activity was detected. When adding the reducing agent DTT to GAPDH-SG (green bars), most activity was rapidly restored in the short time after mixing before blocking the reaction and became fully restored after 60 min. In contrast, adding GSH (purple bars) did not notably restore activity, similar to strep-MBP-ROXY9 wild-type (dark red) and strep-MBP-GRXC2 (dark teal) without GSH. Only a combination of varying amounts of glutaredoxins together with GSH led to a restoration of GAPDH activity. For the high concentration of strep-MBP-GRXC2 (teal bars), GAPDH activity could already be detected after a short mixing time and restoration was almost complete after 60 min. ROXY9 wild-type shown in rust red was able to restore GAPDH activity, but only to a lower extent as GRXC2. ROXY9 CPYC (yellow bars) led to the least restored activity, when compared to the same amounts of ROXY9 wild-type and GRXC2, although the results were somewhat inconsistent when also considering intermediate deglutathionylation time points as shown in figure S5.

In summary, ROXY9 wild-type did show the capacity to deglutathionylate GAPDH-SG in line with previous observations (Treffon, 2019), though to a lesser extent than GRXC2. This activity is likely not a one-time transfer by

disulphide exchange between GAPDH-SG and one of the thiols of ROXY9 as it depends on the presence of GSH.

5.6 No oxidase activity detected for ROXY9

While ROXY9 showed a low activity reducing GAPDH-SG, no reductase activity could be observed towards the low molecular weight substrates HEDS and CHP. In recent years, several class II glutaredoxins were found to be inactive in reductase assays, but did exhibit a weak oxidase activity in the roGFP assay. (Trnka et al., 2020), including GRXS15 (Moseler et al., 2015) and GRXS16 (Zannini et al., 2019) from *A. thaliana*. The roGFP assay is based on the artificial roGFP2 substrate, a modified GFP with two cysteines that can form a disulphide catalysed by glutaredoxins (Aller et al., 2013), most likely by glutaredoxin-mediated glutathionylation followed by disulphide exchange (Trnka et al., 2020). The disulphide bridge within roGFP2 has a redox potential of –277.5 mV (Aller et al., 2013), while the active site of ROXY9 has a redox potential of around –240 mV (see figure 8). From a thermodynamic standpoint, oxidized ROXY9 should be able to accept electrons from reduced roGFP2.

The structure of roGFP is shown in figure 16 A for the oxidized form and figure 16 B for the reduced form, with the cysteines upfront. The redox status of roGFP2 influences the excitation spectrum as shown in figure 16 C. The oxidized form exhibits an additional peak at around 400 nm, while emission is lower compared to the reduced form when exciting at around 480 nm. The redox status can thus be determined by measuring emission after excitation at these two wavelengths and calculating the ratio of the two measurements.

Due to the available filters in our lab, excitation wavelengths of 360 nm and 485 nm were utilized for the roGFP assay, yielding a stable ratio of 0.35 for oxidized roGFP2 (bright red) and 0.05 for reduced roGFP2 (blue) as shown in figure 16 D. To assay oxidase activity, reduced roGFP2 was mixed with strep-MBP-ROXY9 wild-type, CPYC or strep-MBP-GRXC2, with or without GSSG. GRXC2, the class I glutaredoxin control enzyme, in combination with GSSG shown in teal led to an increase in the ratio from 0.05 to 0.30 over the course of the assay, indicating a change in the redox state of roGFP2 from reduced to oxidized. Without GSSG, strep-MBP-GRXC2 (dark teal) exhibited only a slow increase in the ratio that aligned with the buffer control (grey), which denotes a certain level of spontaneous oxidation of roGFP2. The addition of GSSG (purple) without glutaredoxins led to a steeper increase of the ratio, indicating non-enzymatic oxidation.

Peculiarly, the addition of ROXY9 with wild-type (rust red) or CPYC (yellow) active site in combination with GSSG led to a slower increase than GSSG

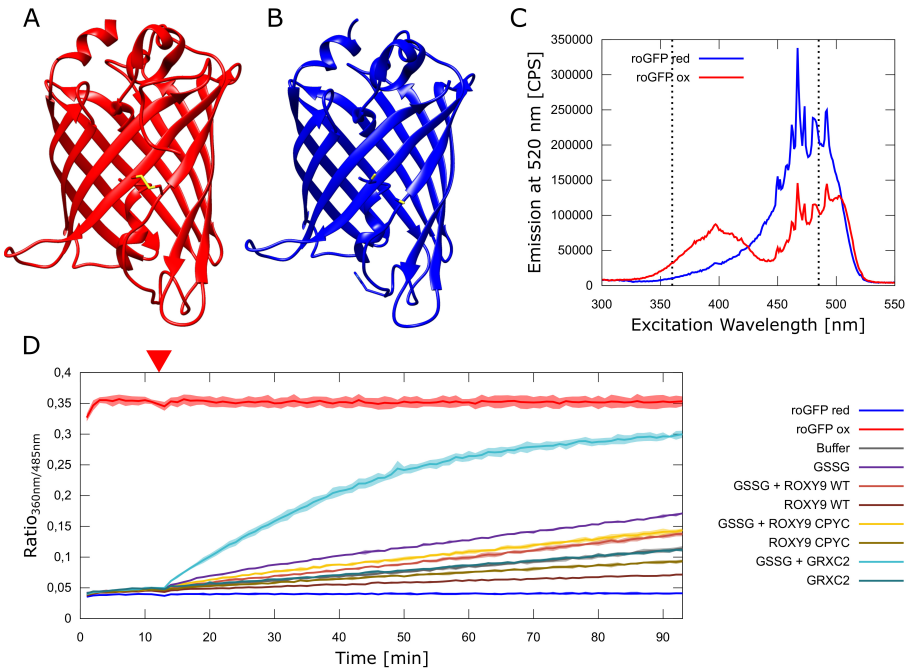

Figure 16: **roGFP Assay shows oxidase activity of GRXC2, but not of ROXY9.** (A) and (B) Structure of roGFP in the oxidized (A, pdb: 2AH8) and reduced (B, pdb: 2AHA) form. (C) Excitation spectrum of His-roGFP2 in the presence of DTT (red) and H_2O_2 (ox), measuring emission at 520 nm. 360 nm and 485 nm are indicated by dashed lines. (D) roGFP assay with strep-MBP-GRXC2, strep-MBP-ROXY9-WT and strep-MBP-ROXY9 CPYC. GRX samples and His-roGFP2 were pre-reduced with DTT and desalted. Reaction mixtures were prepared including GRX protein and/or GSSG. Samples containing roGFP2 were measured for an 11 min equilibration time, the reaction was started with the addition of the reaction mixture at 12 minutes as indicated by the red triangle. Final concentrations were 2 µM roGFP2, 2.5 µM GRX and 50 µM GSSG respectively. The assay was followed for 81 min by measuring emission at 528 nm after excitation at 360 nm and 485 nm every minute. As reference, roGFP2 samples containing 10 mM DTT (red), 10 mM H_2O_2 (ox) or buffer were included. Data is displayed as mean and standard deviation of the ratio after excitation at 360 nm and 485 nm of 3 replicates.

alone. Similar observations were made with the respective control treatment without GSSG (dark red and ochre), also exhibiting a slower increase than the buffer. The ROXY9 variants did not catalyse the oxidation of roGFP2 and rather seemed to prevent the oxidation, both decelerating non-enzymatic oxidation by GSSG and spontaneous oxidation. Previous results indicated the high reactivity of the thiols of ROXY9 (section 5.4), with incubation with GSSG leading to the putative glutathionylation of one or more thiols aside from the disulphide within the active site (see figure 8). This gives rise to the speculation that the

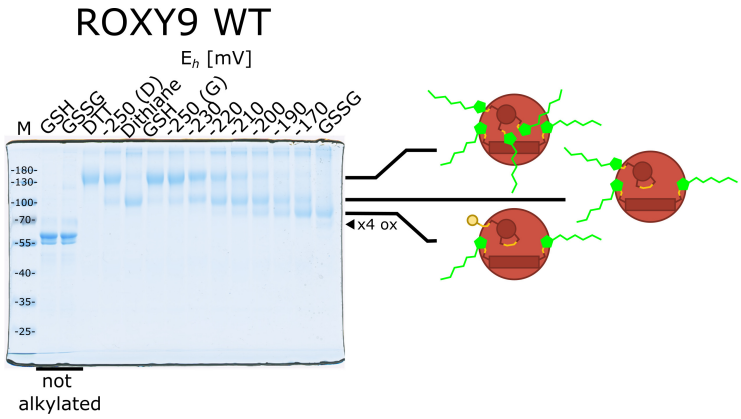

Figure 17: **Redox titration assay of ROXY9 active site variants with GSH and GSSG hints at a potential glutathionylation at cysteine 22.** strep-MBP-ROXY9 was pre-reduced with DTT, desalted and mixed with GSH, GSSG, DTT, Dithiane, DTT/Dithiane redox buffer at a redox potential of –250 mV ("D") or GSH/GSSG redox buffers ("G") at different redox potentials as indicated. Samples were incubated at RT for 2 h followed by TCA precipitation. Reduced cysteines were labelled with 5 kDa mmPEG. Samples were separated by SDS-Page (10% gel). Sketches on the right indicate the likely redox state of proteins, including glutathionylated species, further oxidized species are indicated by triangles.

incubation of GSSG with ROXY9 and roGFP2 leads to an over-oxidation of ROXY9, potentially blocking the accessibility of the active site, which in turn could prevent the oxidation of roGFP2.

To elucidate the oxidation modes of ROXY9 in the presence of GSSG, a redox titration assay was performed utilizing redox buffers containing GSH and GSSG. Results for strep-MBP-ROXY9 wild-type are presented in figure 17. As a reference, DTT, dithiane and a DTT/dithiane redox buffer at –250 mV were included, with similar results as shown in figure 8. ROXY9 was shifted from a 5-fold labelled position to a 3-fold labelled position upon incubation with dithiane. The GSH-treated sample exhibited a band at the 5-fold labelled position as well as a very weak band at the 3-fold labelled position. The sample containing the GSH/GSSG redox buffer at –250 mV looked very similar to the respective DTT/dithiane sample. With increasing shares of GSSG, the protein was increasingly shifted to the 3-fold-labelled position. Starting with –200 mV, also a 2-fold labelled position was observed. GSSG alone lead mostly to the 2-fold labelled position, but also a weak band at a 1-fold labelled position could be detected similar to previous observations (see figure 8).

The 2-fold labelled position observed at –200 to –170 mV indicates the presence of both disulphide within the active site as well as additional glutathiony-

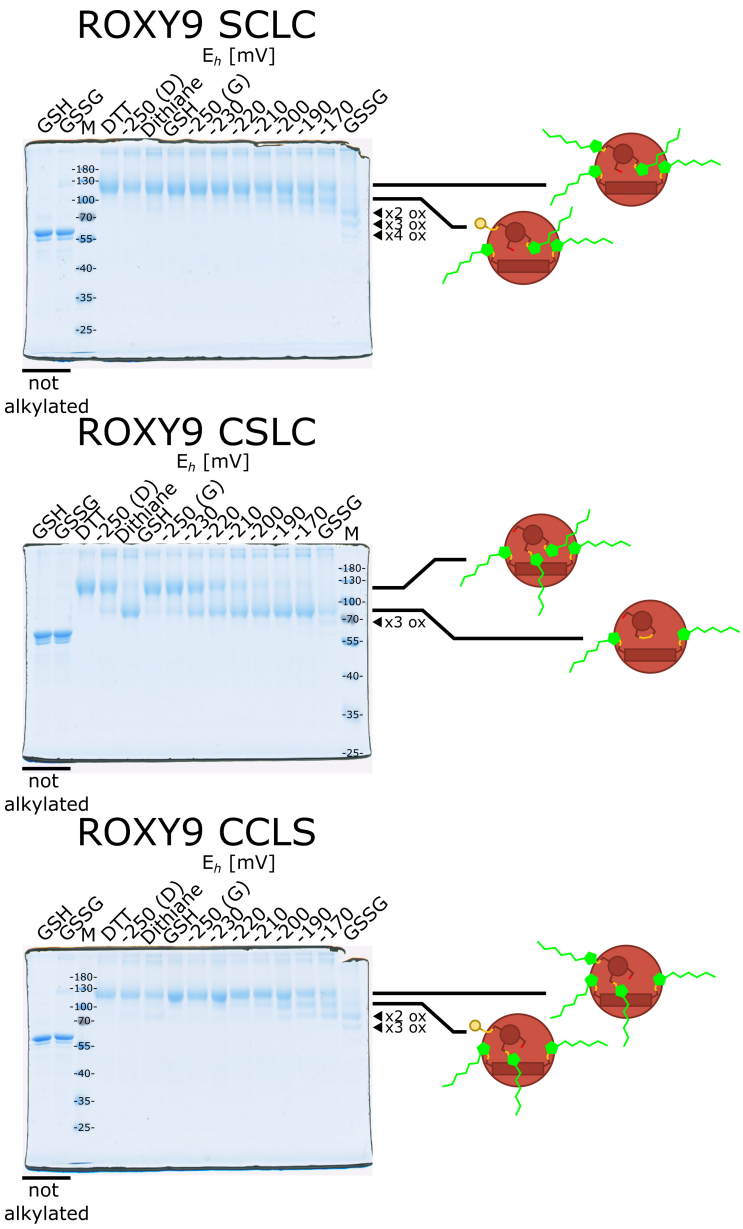

Figure 18: **Redox titration assay of ROXY9 active site variants with GSH hints at a potential glutathionylation at cysteine 22.** strep-MBP-ROXY9 SCLC, CSLC and CCLS were pre-reduced with DTT, desalted and mixed with GSH, GSSG, DTT, Dithiane, DTT/Dithiane redox buffer at a redox potential of −250 mV ("D") or GSH/GSSG redox buffers ("G") at different redox potentials as indicated. Samples were incubated at RT for 2 h followed by TCA precipitation. Reduced cysteines were labelled with 5 kDa mmPEG. Samples were separated by SDS-Page (10% gel). Sketches on the right indicate the likely redox state of proteins, including glutathionylated species, further oxidized species are indicated by triangles.

lation. To assign this additional glutathionylation to one of the cysteines, the GSH/GSSG redox titration was repeated with ROXY9 variants similar to previous experiments (figure 9). Results are shown in figure 18 for strep-MBP-ROXY9 SCLC, CSLC and CCLS.

For the DTT, dithiane and DTT/dithiane redox buffer, similar observations were made as before. ROXY9 CSLC was able to form a disulphide within the active site indicated by a shift from a 4-fold labelled to a 2-fold labelled position upon addition of dithiane, while both ROXY9 SCLC and CCLS remained at the 4-fold labelled position. For these two samples, this position was also predominant after treatment with the different GSH/GSSG redox buffers. At –200 to –170 mV, also bands at a 3-fold and, for ROXY9 CCLS, 2-fold labelled positions were visible, indicating glutathionylation of one to two of the cysteines. For ROXY9 CSLC, increasingly oxidizing conditions conveyed by the GSH/GSSG redox buffer lead to a shift to a 2-fold labelled position, but in contrast to ROXY9 wild-type (figure 17), no additional 1-fold labelled species was visible at –200 to –170 mV. This strongly implies cysteine 22 as the target of glutathionylation under these conditions. Such a gluathionylation at the active site motif might prevent the interaction of substrates or additional GSH with the catalytic cysteine 21.

To circumvent the alleged blocking of the active site by over-oxidation, the roGFP assay was repeated with a redox buffer consisting of GSH and GSSG at a redox potential of –200 mV. At this redox potential, most of the ROXY9 protein contains an oxidized active site while not being further glutathionylated according to the pattern observed in figure 17. Results are presented in figure 19, the addition of strep-MBP-ROXY9 wild-type with the –200 mV redox buffer showed a slow increase of the ratio, that is even slightly slower compared to the different buffer controls and ROXY9 CPYC, that all exhibit a very similar increase. The addition of strep-MBP-GRXC2 with the –200 mV redox buffer led to an increase in the ratio of emission after excitation at the two different wavelengths, indicating the oxidation of roGFP2. This oxidation was slower if compared to the previous experiment in figure 19 D, due to the lower effective concentration of GSSG, which was approximately 5-fold lower.

At all conditions tested thus far, ROXY9 showed no oxidase activity within the roGFP assay. In the light of the weak activity detected towards GAPDH-SG, it can be reasoned that if the ROXY9 protein has a meaningful catalytic activity related to the *in vivo* function, it likely has a narrow set of substrates. One of the known interaction partners of ROXY9 *in planta* is the TGA transcription factor TGA1 (Li et al., 2019). Intriguingly, TGA1 contains four cysteines and was reported to be redox-modulated with the reduced form showing a stronger binding to DNA and the co-activator NPR1 (Després et al., 2003), though also

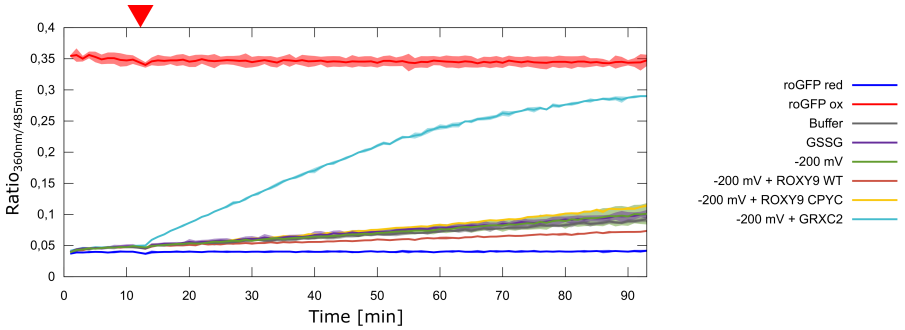

Figure 19: **Refined roGFP Assay shows oxidase activity of GRXC2, but not of ROXY9.** roGFP assay with strep-MBP-GRXC2, strep-MBP-ROXY9-WT and strep-MBP-ROXY9 CPYC at –200 mV GSH/GSSG redox potential. GRX samples and His-roGFP2 were pre-reduced with DTT and His-roGFP2 desalted. The buffer of the GRX samples was exchanged for fresh GSH and reaction mixtures were prepared by adding GSH and GSSG to generate a redox buffer with a redox potential of –200 mV. Samples containing roGFP2 were measured for an 11 min equilibration time, the reaction was started with the addition of the reaction mixture at 12 minutes as indicated by the red triangle. Final concentrations were 2 µM roGFP2, 2.5 µM GRX, 11 µM GSSG and 100 µM GSH respectively. The assay was followed for 81 min by measuring emission at 528 nm after excitation at 360 nm and 485 nm every minute. As reference, roGFP2 samples containing 10 mM DTT (red), 10 mM H_2O_2 (ox) or buffer were included. Data is displayed as mean and standard deviation of the ratio after excitation at 360 nm and 485 nm of 3 replicates.

somewhat conflicting data had been published (Lindermayr et al., 2010). Ectopically expressed ROXY9 over-expression interferes TGA1-dependent transcription (Li et al., 2019), leading to the hypothesis that ROXY9 might oxidize TGA1 as a repressory mechanism.

To test this hypothesis, His-tagged TGA1 was expressed in the insect system and purified by immobilized metal affinity chromatography. After one step of purification, the protein sample was not entirely pure. In order to identify TGA1 in alkylation analysis, immunoblot analysis with the αTGA1 antibody was performed.

At first, the redox properties of TGA1 were investigated by thiol alkylation, similar to the redox titration assay. To this aim, the TGA1 sample was incubated under different redox conditions for different time spans, TCA-precipitated and free thiols were labelled with 5 kDa mmPEG. After immunoblotting, the labelled protein bands could be detected, but the blotting efficiency was much lower as compared to non-alkylated controls (see supplement figure S7).

The main observation is presented in figure 20 A. His-TGA1- when not being alkylated - has an apparent molecular weight between 40 kDa and 55 kDa,

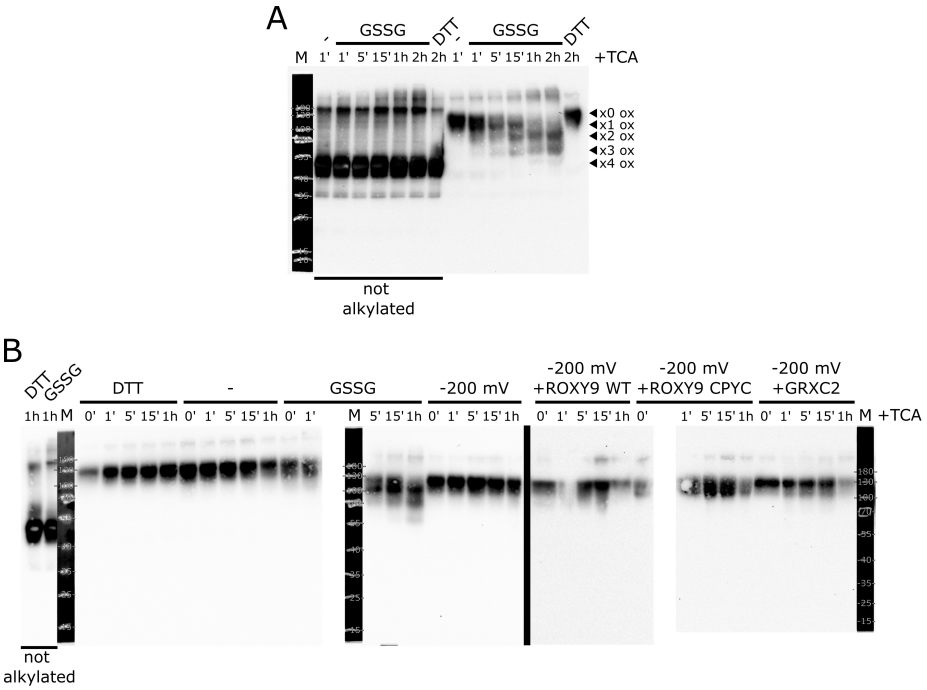

Figure 20: **Oxidation of TGA1 is not enhanced by either ROXY9 or GRXC2.** (A) Oxidation time course of His-TGA1 with GSSG. HisTGA1 was pre-reduced with DTT, desalted and mixed with buffer, GSSG or DTT as indicated. Samples was incubated at RT and reactions were stopped by addition of TCA at indicated time points. The samples were subsequently precipitated and reduced cysteines labelled with 5 kDa mmPEG. Samples were separated by SDS-Page (10% gel), immunoblotted and detected with αTGA1 antibody. Likely number of oxidized cysteines is indicated on the right. (B) Oxidation time course of His-TGA1 with strep-MBP-GRXC2, strep-MBP-ROXY9-WT and strep-MBP-ROXY9 CPYC at –200 mV GSH/GSSG redox potential. GRX samples were pre-reduced with DTT, buffer exchanged for buffer containing fresh GSH and GSH and GSSG are added to generate a redox buffer with at redox potential of –200 mV. HisTGA1 was pre-reduced with DTT, desalted and mixed with the different treatment buffers as indicated. Subsequent steps were carried out as described above. Blot detection time was extended for samples containing GRXs.

and was shifted to a position at around 130 kDa after immediate TCA precipitation of the untreated sample after 1 min or after incubation in the presence of DTT for 2 h. Given the presence of four cysteines, this position likely corresponds to a fully reduced, 4-fold alkylated state. When incubated with GSSG, the protein was shifted to lower positions over time, likely corresponding to a 3-fold, 2-fold, 1-fold and possibly non-labelled state. After 5 min, the protein shifted predominantly to the 3-fold labelled state. After 15 min, the 2-fold and 1-fold labelled positions became more pronounced and after 1 h, the protein was mostly shifted to these positions, with the biggest fraction at the 2-fold labelled position. For both alkylated and non-alkylated samples, GSSG treatment also lead to an increase in multimer bands. Taken together, this is an indication of an oxidation due to non-enzymatic glutathionylation over the course of the incubation time.

To test whether this oxidation is accelerated by glutaredoxins, the experiment was repeated in the presence of strep-MBP-ROXY9 wild-type, CPYC or

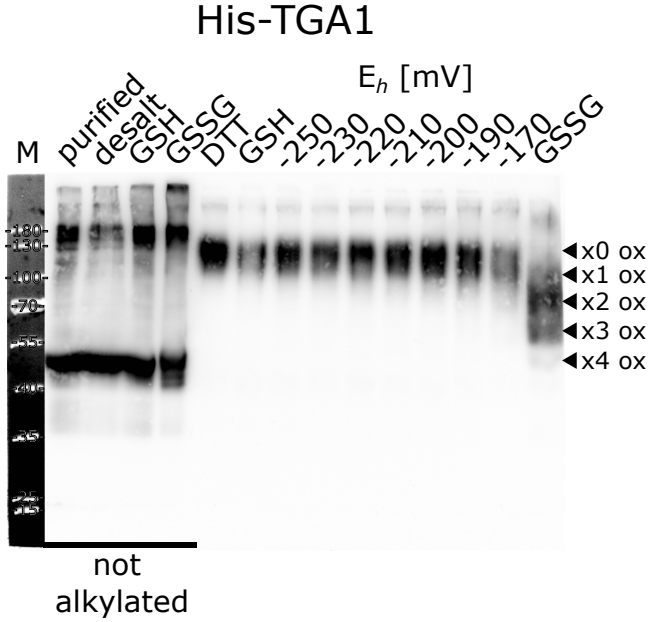

Figure 21: **Redox titration of TGA1 with GSH indicates a relatively high redox potential required for glutathionylation.** HisTGA1 was pre-reduced with DTT, desalted and mixed with GSH, GSSG, GSH/GSSG redox buffers at different redox potentials or DTT as indicated. Samples were incubated at RT for 2 h followed by addition of TCA. The samples were subsequently precipitated and reduced cysteines labelled with 5 kDa mmPEG. Samples were separated by SDS-Page (10% gel), immunoblotted and detected with αTGA1 antibody. Likely number of oxidized cysteines is indicated on the right.

strep-MBP-GRXC2 over a time span of 1 h. To prevent over-oxidation of the glutaredoxins, buffers at –200 mV GSH/GSSG redox potential were utilized. Results are presented in figure 20 B. Both in the presence of DTT as well as for the buffer control, HisTGA1 was shifted to the same, likely 4-fold labelled position at all time points. Incubation with pure GSSG led to the known shift to positions with a lower degree of labelling over time. Interestingly, the incubation with the redox buffer at –200 mV did not lead to a similar shift with bands rather resembling the DTT or untreated samples.

TGA1 seems to require more oxidizing conditions, which lead to the over-oxidation of ROXY9, making a redox modulation unlikely. To further investigate the redox potential required for oxidation of TGA1, a redox titration with His-TGA1 and GSH/GSSG was performed with results shown in figure 21. At most conditions tested, TGA1 was shifted to the 4-fold labelled position. A 3-fold labelled position became slightly visible at the lowest tested redox potential of –170 mV and only pure GSSG treatment led to a shift to more oxidized positions. This confirms that fairly high redox potentials are required for the oxidation of TGA1.

5.7 ROXY9 shows a lower reactivity towards GSH as compared to GRXC2

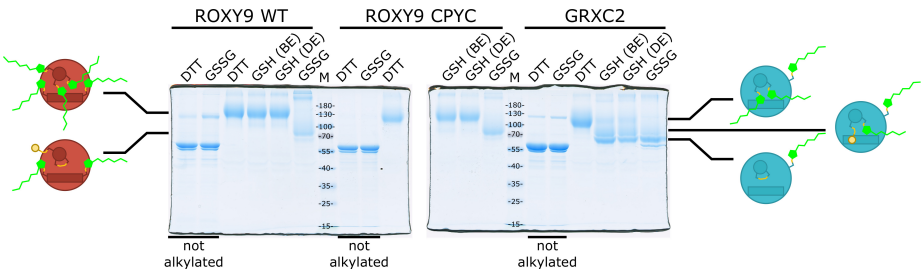

Figure 22: **ROXY9 shows a lower reactivity towards GSH as compared to GRXC2.** strep-MBP-ROXY9 WT, CPYC and strep-MBP-GRXC2 were pre-reduced with DTT, desalted (DE) and mixed with DTT, GSH or GSSG, or buffer exchanged (BE) for GSH containing buffer as indicated. Samples were incubated at RT for 2 h followed by TCA precipitation. Reduced cysteines were labelled with 5 kDa mmPEG. Samples were separated by SDS-Page (10% gel). Sketches on the right indicate the likely redox state of proteins, including glutathionylated species.

In an experiment originally intended at investigating how long ROXY9 remains reduced in the absence of a reducing agent after desalting, strep-MBP-ROXY9 wild-type, CPYC and strep-MBP-GRXC2 samples were pre-reduced

and either desalted and subsequently mixed with GSH or buffer exchanged for GSH containing buffer. The results after mmPEG labelling presented in figure 22 show that both ROXY9 wild-type as well as ROXY9 CPYC remain fully reduced after DTT- and the two GSH-treatments, unaffected by a short incubation time without reducing agent after desalting.

However, for the GRXC2 samples on the right side of figure 22, an interesting observation was made. GRXC2, which contains three cysteines, was fully shifted to a likely 3-fold labelled position when incubated with DTT. For the two different GSH treatments, multiple bands at different positions were visible. The 3-fold labelled position was still present as a weak band but the majority of the protein was shifted to a 2-fold or 1-fold labelled position. This can be explained by a glutathionylation and a disulphide respectively. Pure GSSG treatment led to a 1-fold labelled and non-labelled position.

At first sight, these results are not easily explainable, because the samples should initially contain reduced GSH and reduced GRXC2, but GRXC2 was oxidized to a certain degree after the incubation time. It has to be assumed, that a small fraction of oxidized components, likely GSSG, was present, either already within the freshly prepared GSH buffer or during the incubation time of two hours at room temperature. Under these conditions, GRXC2 apparently has the tendency to become oxidized.

In the different oxidoreductase assays described above, usually a robust activity was observed for GRXC2, while ROXY9 was mostly inactive. Even the adjustment of the buffer conditions to a GSH/GSSG redox buffer at –200 mV did not improve the oxidase activity of ROXY9 (figures 15 and 20). However in principle, ROXY9 does exhibit some properties that could enable activity like the capability to form a disulphide within the active site at a reasonable redox potential. The different observations for GRXC2 and ROXY9 with regard to the redox state in the presence of GSH could lead to a potential explanation of the differing enzymatic activities. To more closely examine the interaction of GSH with GRXC2, a GSH/GSSG redox titration was performed with results shown in figure 23.

When analysing GRXC2 under the same conditions as ROXY9 (figure 17), similar observations were made regarding samples treated with DTT, dithiane and a DTT/dithiane redox buffer at –250 mV. After DTT-treatment, GRXC2 exhibited a band at a 3-fold labelled position while after dithiane-treatment, a 1-fold labelled position was observed. This indicates the formation of a disulphide between the two cysteines of the CPYC active site. At –250 mV, mostly the 3-fold labelled position was detected, indicating that the redox potential of this disulphide is somewhat lower.

In contrast, at all conditions involving GSH or the GSH/GSSG redox buffers

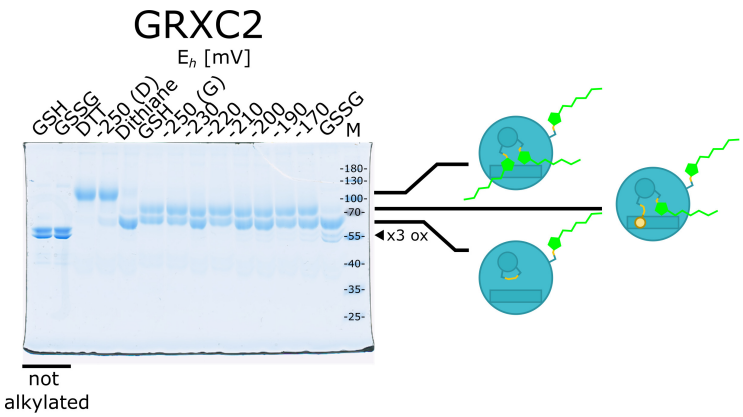

Figure 23: **GRX2 is oxidized over a wide range of redox potentials.** strep-MBP-GRXC2 was pre-reduced with DTT, desalted and mixed with GSH, GSSG, DTT, Dithiane, DTT/Dithiane redox buffer at a redox potential of −250 mV ("D") or GSH/GSSG redox buffers ("G") at different redox potentials as indicated. Samples were incubated at RT for 2 h followed by TCA precipitation. Reduced cysteines were labelled with 5 kDa mmPEG. Samples were separated by SDS-Page (10% gel). Sketches on the right indicate the likely redox state of proteins, including glutathionylated species, further oxidized species are indicated by triangles.

at different redox potentials, the same pattern was observed. The GRXC2 protein was evenly distributed to a 2-fold and 1-fold labelled species, indicating a glutathionylation or a disulphide, respectively. This glutathionylation is most likely located at the N-terminal, catalytic cysteine of the active site, as this is a known intermediate during catalytic activity (Begas et al., 2017). Pure GSSG mostly led to the formation of the 1-fold labelled species as well as a weak fraction at a non-labelled position. Noticeably, this non-labelled position exhibited a double band in both the GSSG-treated sample as well as the non-alkylated samples on the non-reducing gel, which can be an indication for a disulphide bridge.

5.8 ROXY9 dimerizes upon addition of Fe and S

Class II glutaredoxins, as well as some class I glutaredoxins have the capability to bind Fe-S-clusters. Typically, one 2Fe-2S-cluster is bound by two glutaredoxins, the cluster is coordinated by the thiols from the catalytic cysteines as well as two molecules of GSH, each bound by one glutaredoxin. To investigate whether ROXY9 can also bind Fe-S-clusters, *in vitro* reconstitution experiments were performed under anaerobic conditions in the lab of Prof. Lill at the Philipps University Marburg. For these experiments, strep-MBP-ROXY9 was incubated

with GSH, iron- and sulphide-ions under reducing conditions followed by desalting, which led to a brownish staining of the sample. A total of four independent reconstitution experiments were carried out over the course of this thesis. The reconstitution was always evaluated by gel filtration to check for the formation of dimers.

In a first experiment displayed in figure 24 A, strep-MBP-ROXY9 wild-type was analysed after reconstitution, desalting and spin concentration under strictly anaerobic conditions. In the gel filtration, three peaks were observed, one corresponding to aggregates at a retention volume of around 7.5 mL. A second peak at 14.4 mL corresponds to a monomer of strep-MBP-ROXY9 according to the calibration. The highest absorbance was measured for a peak at around 11.3 mL, which corresponds to a dimer of strep-MBP-ROXY9 according to the calibration. A shoulder was observed at higher retention volumes indicating that the presumed dimer is not reflected by a homogenous protein species. It may be speculated, dimers without the Fe-S-cluster might have been generated during the reconstitution experiments. Still, these results were a first hint that ROXY9 could potentially bind iron and sulphur, leading to a dimerization.

In a second experiment, the sample preparation was altered. After reconstitution and desalting, the sample was spin concentrated outside the anaerobic tent. The subsequent analytical gel filtration showed mostly a mixture of different higher order multimers (data not shown), which was attributed to the exposure to air, potentially leading to oxidation and disulphide-linked multimers in addition to a potentially formed holoprotein.

For the third experiment, the sample preparation was again modified. DTT was added to the samples after desalting to prevent a potential oxidation during spin concentration. Results for the gel filtration are shown in figure 24 B. In this experiment, reduced apo strep-MBP-ROXY9 was also analysed to serve as a reference. Two peaks were detected for this sample, one corresponding to aggregates and another one close to the expected retention volume of the monomer. After reconstitution, a higher proportion of aggregates was detected. In addition, a second peak was detected, with a maximum at a position corresponding to a size slightly bigger than the expected dimer, but with a broad shoulder at higher retention volumes, likely also containing some monomeric protein and maybe dimers of the apoprotein.

The experiment was repeated a forth time, again adding DTT to the samples after desalting (figure 24 C). For the reduced apo protein, a small fraction of aggregates was detected as well as a large peak located at a retention volume slightly lower than expected for the monomer based on the provided calibration curve. After reconstitution, a considerable amount of the sample was detected at these two positions, in addition to a third broad peak at a lower retention

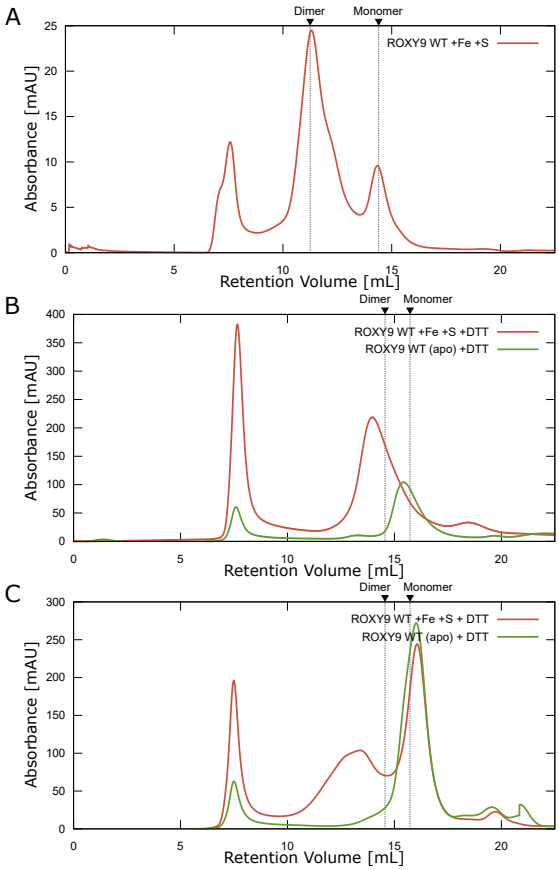

Figure 24: **ROXY9 forms dimers after Fe-S-cluster reconstitution experiments.** (A), (B) and (C) Analytical gel filtration of strep-MBP-ROXY9 after Fe-S-cluster reconstitution with a Sephadex S200 column tracking absorbance at 280 nm. The experiments were carried out under anaerobic conditions in Marburg. For reconstitution, strep-MBP-ROXY9 wild-type was reduced by DTT, incubated with GSH, ammonium iron(III) citrate and Li_2S followed by desalting and spin concentration. The results of three independent experiments are shown. (A) Expected monomer and dimer retention volumes are 14.40 and 11.25 mL, respectively, as calculated by the provided calibration curve and indicated by dashed lines. (B) and (C) strep-MBP-ROXY9 apo samples are included in the analysis and DTT was added to all samples. Expected monomer and dimer retention volumes are 15.73 and 14.56 mL, respectively, as calculated by the provided calibration curve and indicated by dashed lines. The data set of (B) is also presented in figures 10 and S6

volume than the expected dimer position. In contrast to the third experiment shown in figure 24 B, this peak was broader reflecting a number of different unknown multimers of either the expected holo protein, unknown complexes of Strep-MBP-ROXY9 with different Fe or S combinations, and the apoprotein.

In summary, the reconstitution procedure led to a multimerization in all experiments, though to a varying degree. In the first and third experiment (figure 24 A and B), most of the non-aggregated protein formed multimers while in the forth experiment (figure 24 C), the majority of the non-aggregated protein remained at the monomer position. Also, the exact multimer status is not clear. In the first experiment (figure 24 A), the peaks almost perfectly aligned with the expected retention volumes for dimer and monomer based on the calibration. In the third and forth experiment (figure 24 B and C), the multimer peak was observed at a lower retention volume than expected for a dimer, indicating potentially a higher order of multimerization.

Observations so far showed that the reconstitution procedure led to a brownish staining of the sample and induced multimerization, which hints at the binding of iron and possibly the formation of an Fe-S-cluster. To further elucidate the properties of the bound iron, the UV/vis absorbance was taken into account as presented in figure 25. Bound iron typically absorbs at around 320 nm, for Fe-S-cluster also absorbance at around 420 nm is typical. Figure 25 A shows the absorbance at these two wavelengths along with the absorbance at 281 nm that indicates the presence of proteins over the course of the analytical gel filtration introduced in figure 24 C. Absorbance at 320 and 420 nm was detected for the aggregate peak and the multimer peak, but not at the monomer peak. A more detailed representation is provided by the heat map in figure 25 B. At the aggregate and multimer/dimer peak, absorbance spanned large parts of the visual spectrum, while the monomer peak was restricted to wavelengths below 300 nm. This demonstrates that the brownish colour and thus the bound iron associates with aggregates and the multimer.

Figure 25 C shows the UV/vis spectra at the position of the multimer and monomer peak. While the monomer spectrum only showed absorbance at around 280 nm, the multimer spectrum exhibits a broad shoulder around 420 nm. This spectrum is typical for 4Fe-4S-clusters, while spectra of 2Fe-2S-clusters usually bound by glutaredoxins show more distinct peaks (Azam et al., 2020).

Three fractions around the multimer peak were collected during the gel filtration and the iron and sulphur content was determined by colorimetric assays. Together with the determined protein concentrations of the different samples, the amount of iron and sulphur per protein monomer was calculated as presented in figure 25 D. All measured concentrations were low and close to the detection limit due to the dilution by the gel filtration, leading to a high standard

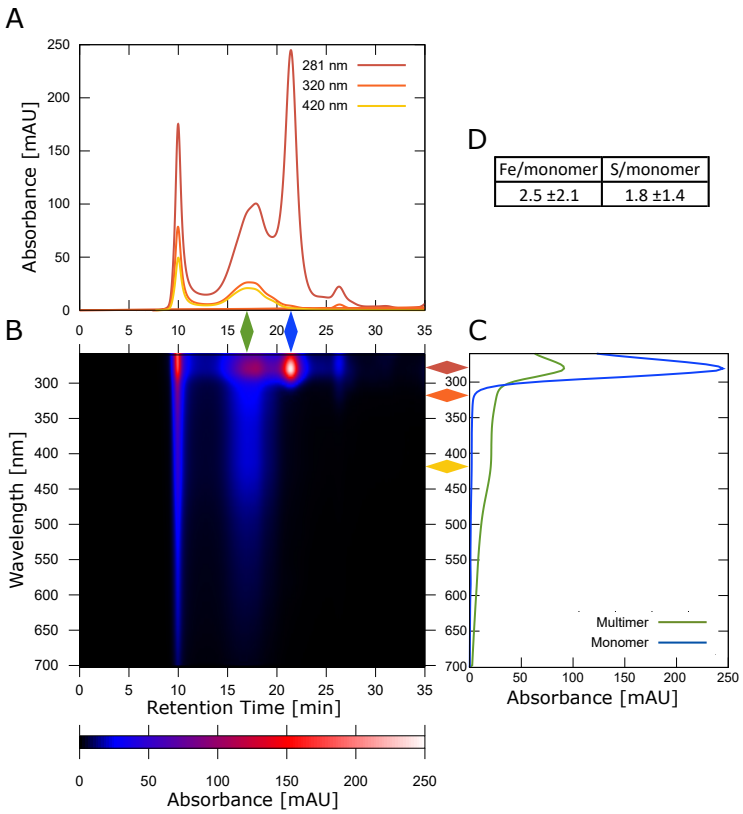

Figure 25: **Gel filtration of ROXY9 after Fe-S-Cluster reconstitutions shows broad UV/vis absorbance of the multimer peak indicating the presence of iron.** (A), (B) and (C) Analytical gel filtration of strep-MBP-ROXY9 holo with a Sephadex S200 column. The experiment was carried out under anaerobic conditions in Marburg and introduced in figure 24 C. (A) Absorbance at 281, 320 and 420 nm against retention time. (B) Heat map showing absorbance at different wavelengths against retention time. (C) Full absorbance spectrum at the multimer and monomer peaks. (D) Fe and S determination. The amount of iron and sulphur of three fractions around the multimer peak was determined and related to the amount of protein including standard deviation. Fe content was determined with ferene while S content was determined with DMPD.

deviation. While the results surely not provide definite proof of a 4Fe-4S-cluster bound by a dimer, the values around two iron and sulphur per monomer do not exclude this interpretation either.

To further elucidate the binding mode of the potential Fe-S-cluster bound by ROXY9 after reconstitution, different active site variants had been included in the third and forth reconstitution experiments. Glutaredoxins are known to bind Fe-S-clusters with the N-terminal, catalytic cysteine of the active site. Class I glutaredoxins with a CPYC active site motif are incapable to bind an Fe-S-

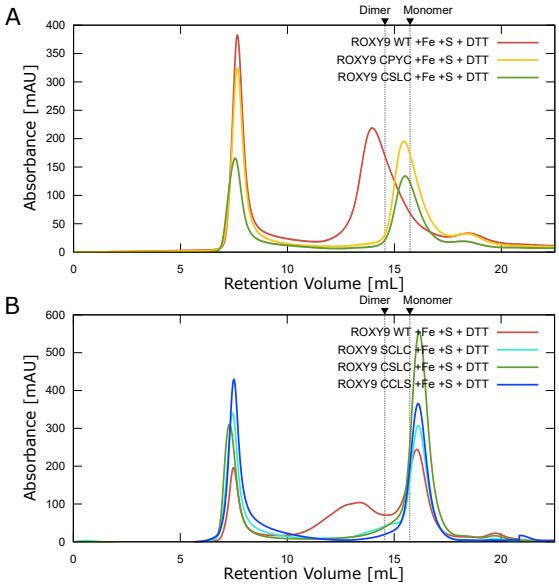

Figure 26: **Gel filtration of ROXY9 active site variants after two independent Fe-S-Cluster reconstitutions reveals importance of the unaltered active site motif for multimerization.** (A) and (B) Analytical gel filtration of strep-MBP-ROXY9 active site variants after Fe-S-Cluster reconstitution with a Sephadex S200 column tracking absorbance at 280 nm. The experiments were carried out under anaerobic conditions in Marburg. For reconstitution, strep-MBP-ROXY9 wild-type was reduced by DTT, incubated with GSH, ammonium iron(III) citrate and Li_2S followed by desalting and spin concentration. Expected monomer and dimer retention volumes are 15.73 and 14.56 mL respectively as calculated by the provided calibration curve and indicated by dashed lines. (A) strep-MBP-ROXY9 WT, CPYC and CSLC are analysed. ROXY9 WT was also presented in figure 24 B. (B) strep-MBP-ROXY9 WT, SCLC, CSLC and CCLS are analysed. ROXY9 WT was also presented in figure 24 C.

cluster, which led to the expectation that ROXY9 SCLC and CPYC should also not bind a cluster.

Surprisingly, all samples turned brownish after reconstitution. As expected, Strep-MBP-ROXY9 derivatives containing the active sites SCLC or CPYC did not form multimers (figure 26 A and B). The same was observed for variants containing a CSLC and the CCLS motif. Thus, the multimerization of strep-MBP-ROXY9 upon reconstitution of Fe-S-clusters relies on an unaltered active site. In contrast, the high molecular weight fractions were brownish for all variants, indicating unspecific binding of at least Fe in the aggregates of all ROXY variants. The mulimerization of ROXY9 relies on the presence of an unaltered active site.

5.9 An N-terminal HA-tag traps ROXY9 in the reduced state

The redox titration analysis shown in figures 8, 9, 17 and 18 were performed with mmPEG as an alkylating agent. Alkylation with mmPEG leads to somehow diffuse bands and is not compatible with immunoblot analysis, at least regarding ROXY9. Moreover, mmPEG alkylation leads to interference with the detection of target proteins with similar mobility. To obtain sharper bands with lower amounts of protein, it was aimed to perform the analysis with AMS, which leads to a mobility shift of 500 Da per cysteine. Since such a small mobility shift can only be detected with small proteins, a strep-MBP-HA-ROXY9 fusion protein with a TEV cleavage site between strep-MBP and HA-ROXY9 was designed and expressed in the insect cell system.

Unexpectedly, the results deviated strongly for strep-MBP-HA-ROXY9 as compared to strep-MBP-ROXY9. Figure 27 shows a transition at around –240 mV between a 5-fold labelled and a 3-fold labelled position for strep-MBP-ROXY9 while GSSG-treatment led to the oxidation of additional cysteines as presented in detail in section 5.3.

For strep-MBP-HA-ROXY9 shown at the bottom of figure 27, however, a band at 130 kDa was present in all samples treated with DTT and/or Dithiane. In the GSSG-treated sample, the band was shifted to lower molecular weight indicating oxidation of some of the thiols. The detection of 5-fold labelled protein even after Dithiane treatment implies that these conditions were not able to induce the formation of a disulphide in strep-MBP-HA-ROXY9 while the same conditions were sufficient for disulphide bridge formation in strep-MBP-ROXY9.

A potential explanation why the addition of the HA tag impedes the ability of ROXY9 to form an intramolecular disulphide was found when comparing strep-MBP-ROXY9 and strep-MBP-HA-ROXY9 by gel filtration with results presented in figure 28.

While DTT-treated strep-MBP-ROXY9 was mainly present as a monomer and a small fraction of aggregates, strep-MBP-HA-ROXY9 was almost completely aggregated. This aggregation could potentially prevent dithiane from physically interacting with the active site and performing a disulphide exchange reaction. Aggregation was not affected by DTT, which was utilized to pre-treat the sample for gel filtration. When separated by non-reducing SDS-Page (see figure 27), the protein was mostly present in monomeric form. This implies that the aggregation is likely caused by strong protein-protein interactions, possibly due to a misfolding of parts of the protein, that can be resolved by SDS.

To rule out any effect of the strep-MBP tag in combination with 3xHA as the reason for this aggregation, strep-MBP-HA-ROXY9 was cleaved by the TEV protease and HA-ROXY9 was separated by gel filtration. Noticeably, the TEV

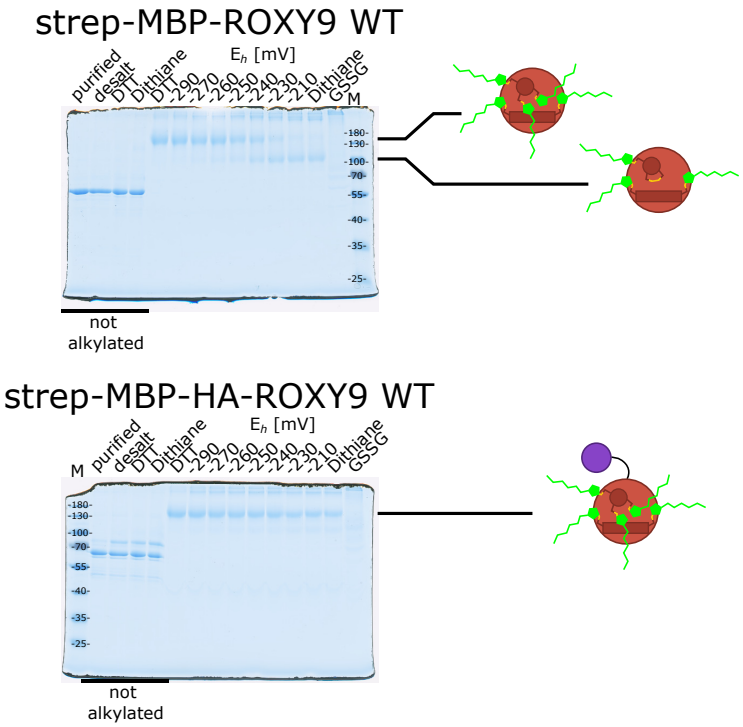

Figure 27: **HA-ROXY9 remains in a reduced state under conditions oxidizing ROXY9.** strep-MBP-ROXY9 and strep-MBP-HA-ROXY9 were pre-reduced, desalted and mixed with DTT, Dithiane, DTT/Dithiane redox buffers at different redox potentials or GSSG as indicated. Samples were incubated at RT for 2 h followed by TCA precipitation. Reduced cysteines were labelled with 5 kDa mmPEG. Samples were separated by non-reducing SDS-Page (10% gel) alongside with untreated protein after purification and desalting. Sketches on the right indicate the likely redox state of proteins.

cleavage reaction was not very efficient even after extended incubation times, further supporting the notion of an impaired accessibility in this case for the TEV protease. During gel filtration, the cleaved protein was collected in the initial, high molecular weight peak (data not shown), implying that it was still aggregated. The sample was further analysed by incubation under different redox conditions and labelling with 4-acetamido-4'-maleimidylstilbene-2,2'-disulfonic acid (AMS), which adds roughly 0.5 kDa per labelled cysteine. The samples were separated by SDS-Page, immunoblotted and HA-ROXY9 was detected with an αHA antibody.

In the AMS shift experiment shown in figure 29, the protein was shifted to the exact same position in all samples after AMS labelling. This implies, that HA-ROXY9 was similarly unaffected by oxidizing treatments as previously observed for the full length strep-MBP-HA-ROXY9 fusion protein.

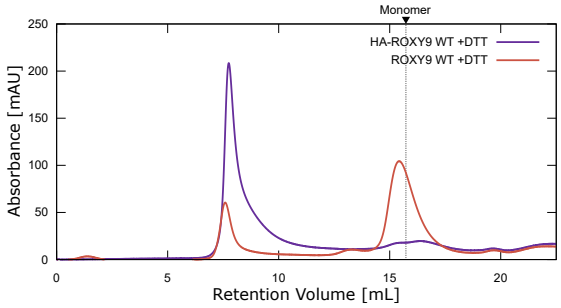

Figure 28: **HA-tagged ROXY9 has a much higher tendency to form aggregates than ROXY9.** Analytical gel filtration of strep-MBP-ROXY9 and strep-MBP-HA-ROXY9 pre-reduced by DTT with a Sephadex S200 column tracking absorbance at 280 nm. The experiment was carried out under anaerobic conditions in Marburg. The expected monomer retention volumes is 15.73 mL as calculated by the provided calibration curve and indicated by a dashed line. strep-MBP-ROXY9 WT was also presented in figure 24 B.

The peptide sequence of the recombinant HA-ROXY9 protein is almost identical to the construct expressed in transgenic plants, with just three additional amino acids at the N-terminus originating from the TEV cleavage site. AMS shift experiments with plant extracts aimed at detecting the *in vivo* redox state of ROXY9 showed that the protein was exclusively found in a reduced state even upon treatment of plants with 10 mM H_2O_2 (Li, unpublished). Originally, this was attributed to a potential strong anti-oxidative system that might keep ROXYs in the reduced state. In the light of the new observations that recombinant HA-ROXY9 had a tendency to aggregate and was unable to form an intramolecular disulphide, the HA tag might rather have a negative influence *in planta*. Over-expression of HA-ROXY9 led to a stringent repression of hyponastic growth (Li et al., 2019), which could potentially be related to the the artificial aggregation of the protein *in planta*.

In order to construct a new HA-tagged ROXY9 for in planta expression, the peptide sequence of the strep-MBP-HA-ROXY9 fusion protein was closely examined and compared to strep-MBP-ROXY9 as displayed in figure 30 A. The addition of an N-terminal fusion did not per se alter the redox properties as strep-MBP-ROXY9 showed a similar behaviour in redox titration assays as tag-free ROXY9 (see figures 8 and S2). The HA-ROXY9 sequence contained a linker between the last HA epitope of the 3xHA tag and the N-terminus of ROXY9 shown in black in figure 30 A. This was mostly predetermined by the sequence of the attachment site utilized for gateway cloning. Both sequences can be speculated to not constitute an enclosed fold motif and might thus potentially influence the fold of the adjacent protein regions.

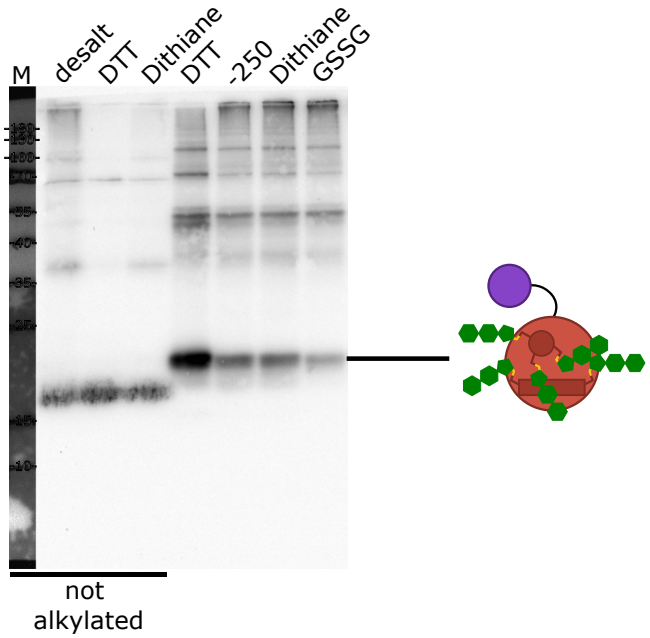

Figure 29: **HA-ROXY9 remains in a reduced state after removal of strep-MBP.** HA-ROXY9 after TEV cleavage was pre-reduced, desalted and mixed with DTT, Dithiane, DTT/Dithiane redox buffer at a redox potential of –250 mV or GSSG as indicated. Samples were incubated at RT for 2 h followed by TCA precipitation. Reduced cysteines were labelled with AMS. Samples were separated by non-reducing SDS-Page (15% gel) alongside with desalted protein, immunoblotted and detected with αHA antibody. Sketches on the right indicate the likely redox state of proteins.

To test this hypothesis, three new constructs were generated by inserting a linker containing three repeats of GGGGS followed by asparagine and alanine. The new linker, shown in yellow in figure 30 A, was inserted between attachment site and ROXY9 N-terminus (”HA-A-L-ROXY9”), between HA-tag and attachment site (”HA-L-A-ROXY9”) and as a replacement for the attachment site (”HA-L-ROXY9”). The new constructs were expressed in insect cells, affinity purified and analysed by redox titration alongside with strep-MBP-ROXY9 and strep-MBP-HA-ROXY9 with results shown in figure 30 B.

For strep-MBP-ROXY9, the typical pattern was observed with a 5-fold labelled position after DTT treatment, both a 5-fold and 3-fold labelled position at –250 mV DTT/dithiane and 3-fold labelled position after dithiane treatment. GSSG treatment mostly lead to a 2-fold labelled protein. The same pattern was also observed for strep-MBP-HA-A-L-ROXY9 and strep-MBP-HA-L-ROXY9 indicating no influence of the tag on the redox properties. However, strep-MBP-HA-L-A-ROXY9 showed a similar pattern as strep-MBP-HA-ROXY9 with just

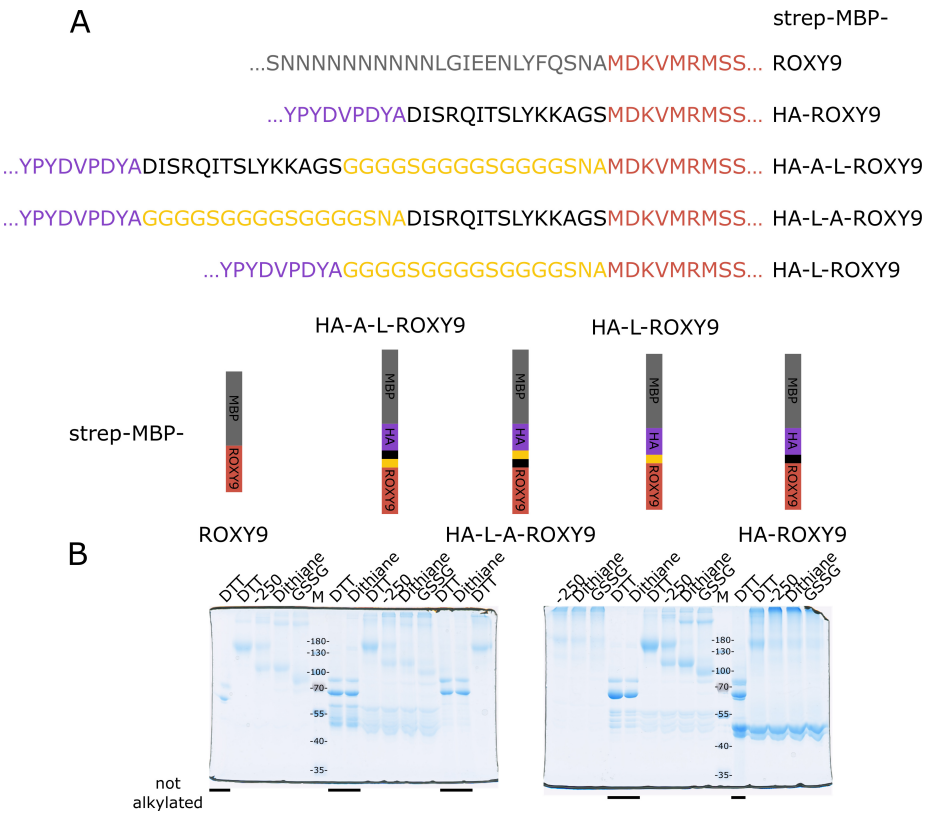

Figure 30: **Insertion of a linker peptide between the HA-tag and ROXY9 restores the midpoint redox potential.** (A) Peptide sequence around the N-Terminus of ROXY9 as well as schematic representations of strep-MBP-ROXY9, strep-MBP-HA-ROXY9, strep-MBP-HA-A-L-ROXY9, strep-MBP-HA-L-A-ROXY9 and strep-MBP-HA-L-ROXY9 showing strep-MBP in grey, 3xHA-tag in purple, the pre-existing linker encoded by the attachment site in black, the new linker in yellow and ROXY9 in red. (B) Redox titration assay of the linker variants. strep-MBP-ROXY9, strep-MBP-HA-ROXY9, strep-MBP-HA-A-L-ROXY9, strep-MBP-HA-L-A-ROXY9 and strep-MBP-HA-L-ROXY9 were pre-reduced, desalted and mixed with DTT, Dithiane, DTT/Dithiane redox buffers at a redox potential of –250 mV or GSSG as indicated. Samples were incubated at RT for 2 h followed by TCA precipitation. Reduced cysteines were labelled with 5 kDa mmPEG. Samples were separated by non-reducing SDS-Page (10% gel).

the 5-fold labelled position in all samples regardless of treatment. In summary, the direct connection of the peptide encoded by the attachment site and the N-terminus of ROXY9 seems to cause the altered redox properties.

Based on these analyses, new over-expression lines were generated with the HA-A-L-ROXY9 construct. However, these have not been analysed yet. .

6 Discussion

6.1 ROXY9 from insect cells has properties expected for glutaredoxin proteins

The main goal of this thesis was to characterize the glutaredoxin-like protein ROXY9 with respect to the known activities of class I glutaredoxins (oxidoreductases) and class II glutaredoxins (Fe-S-cluster binding). Therefore, recombinant ROXY9 protein was required both in good quality as well as quantity.

Class III glutaredoxins are notoriously hard to express in *E. coli* (Couturier et al., 2010; Oberdiek, 2018; Xu et al., 2022). In contrast, the insect cell-based baculovirus expression vector system (Luckow and Summers, 1988; Kost et al., 2005; Jarvis, 2009) was identified as a suitable expression system to obtain soluble, recombinant protein. The initial baculovirus for the expression of wild-type strep-MBP-ROXY9 was generated by Isaac Fianu (Department for Molecular Biology, Prof. Dr. Patrick Cramer, MPI for Biophysical Chemistry, Göttingen) (Treffon, 2019). Subsequently, and as a part of this thesis, the expression system including *T. ni* and *S. frugiperda* cell culture lines was established in the Gatz lab. The expression in insect cells proved to be very successful. Typically, 350 to 700 nmol ROXY9 was obtained from 600 mL insect cells. CD spectroscopy of ROXY9 as compared to class I glutaredoxin GRXC2 confirmed that ROXY9 adopted the predicted thioredoxin fold. The CD spectra of ROXY9 and GRXC2 were not only very similar, but the two proteins also unfolded at a similarly high temperature of around 70 °C (figure 6). The relatively high thermal stability is not uncommon for thioredoxin proteins, as demonstrated by one of the first thioredoxin purification protocols which involved heating *E. coli* extracts to 85 °C and collecting proteins that did not precipitate under these conditions (Holmgren, 1976). In contrast, most A. thaliana proteins unfold between 40 and 50 °C (Jarzab et al., 2020). After cooling, GRXC2 even folded back and exhibited activity in the HEDS assay. Overall, these observations strongly suggest a similar folding of GRXC2 and ROXY9, which is a prerequisite for the investigation to which extent ROXY9 exhibits of typical functions of class I and II glutaredoxin.

ROXY9 was expressed as a fusion protein with an N-terminal strep-MBP tag. A recent publication reported successful expression of poplar class III glutaredoxins in *E. coli* also employing an MBP tag, which underlines the beneficial properties of this type of tag (Xu et al., 2022). A procedure to cleave off and remove the MBP tag was established (figure 4), though it was connected with 70% of the protein. Due to this low yield and due to weak staining of the protein in commassie gels, which were required for the analysis of the redox

state, we preferred to carry out experiments with the full length fusion protein. This decision required to be carefully validated by cross-comparing key properties of strep-MBP-ROXY9 and tag-free ROXY9 as well as strep-MBP-GRXC2 and tag-free GRXC2.

Both, the fusion protein and untagged ROXY9, showed the same alkylation pattern in redox titration assays, indicating formation of a disulfide bond at a midpoint redox potential of –240 mV and oxidation of three cysteines upon GSSG treatment. (figures 8 and S2). Both proteins were inactive in the HEDS assay while the GRXC2 variants were active (figure 13 and Treffon (2019)). Taken together, these results indicate that the strep-MBP-tag has no strong effect on the properties of ROXY9. Xu et al. (2022) also utilized MBP-tagged class III glutaredoxins in their analysis because the proteins became unstable after removal of the tag, an observation not made with ROXY9 from insect cells. The MBP-tag reduced the specific enzymatic activity of class I glutaredoxins in the HEDS assay by 50%, again supporting the notion that the MBP tag does not completely interfere with the function of GRXs. (Xu et al., 2022). It is worth pointing out, that the HA-tag had a far stronger effect on the ROXY9 protein (section 5.9).

ROXY9 forms a disulphide bridge between Cys 21 and Cys 24 of the active site with a midpoint redox potential of around –240 mV (figures 8 and 9). Such a disulphide within the active site is a well known property of catalytically active class I glutaredoxins, where it is involved in the catalytic mechanism when reducing bulky substrates or when GSH obtains an unfavourable orientation Deponte (2013). The midpoint redox potential is very close to the biological standard redox potential $E^{0'}$ of the GSH/GSSG redox couple (Zannini et al., 2017) and relatively close to physiologically relevant redox potentials. The formation of a disulphide at this position is also a further confirmation that ROXY9 adopts the thioredoxin-fold, which locates the two cysteines in close proximity on the $\alpha 1$ helix. of the thioredoxin fold where the two cysteines are located in close proximity on an α helix.

Taken together, ROXY9 and also the strep-MBP-ROXY9 fusion protein seems to have a lot of the properties one would expect from a glutaredoxin. This allowed for a further analysis regarding a potential oxidoreductase function or Fe-S-cluster binding capability.

6.2 Differences in the redox state of ROXY9 and GRXC2 under different GSH/GSSG ratios might be related to the low or lacking oxidoreductase activity of ROXY9

A number of experiments were carried out to determine whether strep-MBP-ROXY9 can function as an oxidoreductase similar to class I glutaredoxins. While a weak deglutathionylation activity was observed towards GAPDH (figure 15), ROXY9 was not able to reduce the low molecular weight substrates HEDS and CHP (figures 13 and 14) or oxidize the protein substrate roGFP2 (figures 16 and 19). As a control, GRXC2 was used, which was functional in all assays except for only a very weak activity as a CHP peroxidase. Especially the results regarding CHP were surprising, as this substrate was recently proposed as a substrate of class III glutaredoxins as well as CPYC-type glutaredoxins from poplar (Xu et al., 2022). Stil, it has to be noted that the reported specific activity in the order of 0.1 µmol/s perµmol was approximately 2000-fold lower as compared to yeast CHP peroxidase activity (Collinson et al., 2002) and some of the tested poplar class III glutaredoxins also showed no activity (Xu et al., 2022).

Since the most obvious difference between the three classes of glutaredoxins is the difference in the active site, several approaches have been initiated to test whether altering the active site can restore or abolish activities (Couturier et al., 2010; Trnka et al., 2020). For instance, replacing the CGFS active site of human GRX5, a class II glutaredoxin with only minor oxidase activity towards roGFP2, by CSYC led to a sevenfold increase in this activity, which was even threefold higher than the oxidase activity of the class II glutaredoxin GRX2. Moreover, gain of reductase activity towards roGFP2 and HEDS was observed. However this reached only 1.8% (roGFP) and 2.5% (HEDS) of the activity of GRX2 (Trnka et al., 2020). In this work, replacing the CCLC active site of ROXY9 with CPYC, the canonical active site motif of class I glutaredoxins, did not lead to a gain of activity, it rather reduced the deglutathionlyation activity towards GAPDH (figure 15). The notion that CC-type glutaredoxins might not exhibit strong reductase activity is supported by previous observations with the poplar CPYC-type GRXC4, which showed a 50-fold decrease in the HEDS assay when the active site was exchanged against the CCMC motif(Couturier et al., 2010). In summary, answering the central question, how this difference in activity between ROXY9 and GRXC2 can be explained, goes beyond the amino acid sequence of the active site motif.

Catalytically active glutaredoxins like GRXC2 are thought to perform glutathionylation and deglutathionylation reactions with a monothiol mechanism that includes a dithiol side reaction (Ukuwela et al., 2017; Deponte, 2013). The

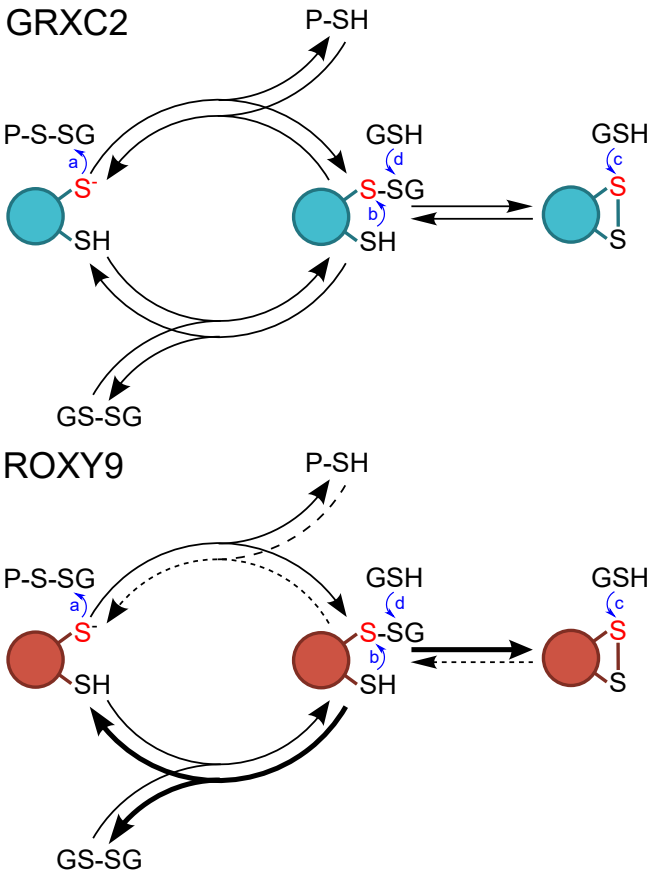

Figure 31: **Glutathionylated active site of ROXY9 appears highly unstable.** Simplified monothiol reaction mechanism of GRXC2 and ROXY9 with dithiol side reaction. The catalytic cysteine of the active site is shown in red while the steps of a deglutathionylation reaction are indicated by blue arrows. In the first step (a), the active site cysteine in the thiolate form performs a nucleophilic attack on the glutathionylated substrate. The glutathione moiety is transferred onto the glutaredoxin and the reduced substrate is released. In a side reaction (b), the second cysteine of the active site can form a disulphide with the first cysteine, thereby releasing the reduced glutathione. To reduce this disulphide (c), reduced glutathione has to perform the reverse reaction. The reduced glutaredoxin can be restored (d) with a second moiety of reduced glutathione, forming oxidized glutathione in the process. For ROXY9, prevalence of the different steps is indicated by thick or dashed arrows as discussed. The scheme was adapted from Ukuwela et al. (2017).

general mechanism of a deglutathionylation, e.g. of GAPDH-SG or βME-SG, involves a transfer of the glutathione from the substrate (P-S-SG) onto the catalytic cysteine of the glutaredoxin (figure 31 (a)). The glutathionylated glutaredoxin shown in the centre of figure 31 can either form a disulphide bridge with

the second cysteine of the active site in an equilibrium reaction (figure 31 (b) and (c)) or be reduced by a second moiety of GSH (figure 31 (d)). For the reverse reaction, the catalytic cysteine needs to be glutathionylated by GSSG. The glutathione can subsequently be transferred onto a target protein. Oxidation of roGFP is argued to include transfer of a glutathione from glutathionylated GRX to one of the cysteines, that leads to the formation of an intramolecular disulphide via a spontaneous disulphide exchange reaction (Trnka et al., 2020).

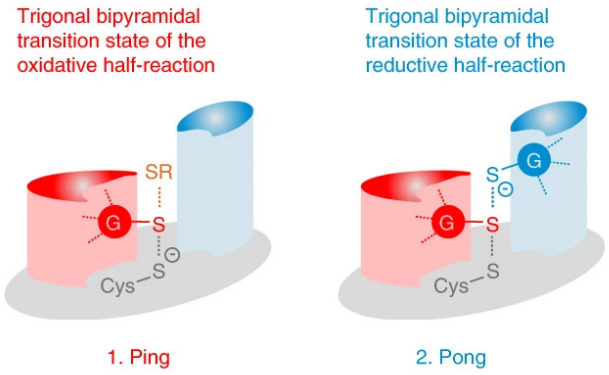

Figure 32: **Enzymatically active Grx have two distinct glutathione-interaction sites.** Predicted transitions states of the glutaredoxin-catalyzed reduction of glutathionylated substrates (GSSR) by GSH which can be separated into an oxidative (red, Ping) and reductive (blue, Pong) half-reaction. During the oxidative half-reaction, the glutathione moiety of GSSR binds to the scaffold site, which positions the sulphur in a way that favours the nucleophilic attack of the thiolate of the catalytic cysteine. During the reductive half-reaction, the glutathione binds to the activator site, favouring the nucleophilic attack for the thiolate of GSH on the disulphide bond. The resulting GSSG dissociates from the protein. (Figure taken from Liedgens et al. (2020)

Figure 32 displays the ping-pong reaction that is operational for the deglutathionylation activity routinely tested in the HEDS assay (Begas et al., 2017; Liedgens et al., 2020). According to this model, glutaredoxins bind the glutathionylated substrates through a scaffold binding site. In this position, the nucleophilic attack of the catalytic cysteine is sterically favoured and glutathione is transferred to this cysteine. Glutathionylation can be resolved by either a second cysteine encoded by the glutaredoxin or by a second glutathione that binds to a second binding site, the so called activator site.

Consequently, a major prerequisite for efficient deglutathionylation activity is the binding to the glutathione moiety of the substrate to the scaffold site. Indeed, one of the differences between GRXC2 and ROXY9 concerns the in-

teraction with glutathione. Both the CD spectra of ROXY9 and GRXC2 were affected by the addition of glutathione, but GRXC2 showed more pronounced peaks in the presence of glutathione (figure 7). The most striking difference was observed when comparing the redox titration assays with GSH and GSSG. ROXY9 was predominantly reduced in the presence of GSH and increasing amounts of GSSG led to a transition towards an oxidized species containing a disulphide bridge and, at higher redox potentials, also additional glutathionylated cysteines (figure 17). In contrast, the majority of GRXC2 was either glutathionylated or contained a disulphide bridge over the whole spectrum of redox potentials investigated (figure 23). Noticeably, ROXY9 and GRXC2 did show a similar pattern for the redox titration assay with DTT and dithiane (left side of figures 17 and 23). The oxidation state of GRXC2 at –250 mV was still highly reduced with a portion of the protein having formed a disulphide bridge. ROXY9 also was in the reduced and oxidized state at this redox potential. When the redox potential of –250 mV was adjusted by GSH/GSSG, GRXC2 was oxidized. In contrast, for ROXY9, the relative ratio of reduced versus disulphide bond containing proteins was the same, independent of whether the rodox potential of –250 mV was adjusted by DTT/Dithiane or GSH/GSSG.

Especially the pattern observed for GRXC2 after the GSH-treatment in figures 22 and 23 is not easily explainable. The experiments were started with a protein that had been reduced with DTT. DTT was exchanged against freshly prepared GSH, but after the incubation time of 2 h at RT, most of the protein appears to be oxidized either by glutathionylation or disulphide bridge formation. The electrons of the reduced glutaredoxin must have been transferred onto some oxidized component, potentially a small fraction of GSSG formed by spontaneous oxidation under aerobic conditions. Interestingly, evidence for the same phenomenon can be found in Hatori et al. (2012), with figure 3 showing a GSH/GSSG redox titration assay with human GRX1 (see supplement figure S10). The main band observed after treatment with the highest GSH content was visible at a lower position as compared to treatment with the reducing agent TCEP.

Obviously, the redox status of ROXY9 was not affected by the traces of GSSG that can lead to the oxidation of GRXC2. With the pKa value for the reactive cysteine being in the same range (beween pH4 and pH5, figure 11) as in class I glutaredoxins (Couturier et al., 2013a) the catalytic cysteine has a similar reactivity towards alkylating agents. The lack of oxidation under conditions that already lead to the oxidation of GRXC2 might be due to the fact that the glutathione moiety does not perfectly fit into the glutathione-scaffold site shown in figure 32. This would result in a dominant back-reaction at a high ratio of GSH over GSSG (step d in figure 31). Therefore, we postulate that

the activator site is not compromised. As soon as GSSG amounts increase, the presumed unstable glutathionylated intermediate is replaced by the disulphide bridge (figure 17, step b in figure 31). Remarkably, ROXY9 CCLS with a mutation in the last cysteine of the active site remained predominantly in the reduced form at redox potentials that led to an almost complete disulphide formation in the wild-type protein (figure 18). This supports the notion that the glutathionylated protein is prone to degluathionylation either by GSH or by the resolving cysteine. The weak additional band emerging at redox potentials of −200 mV and below was also present in ROXY9 SCLC and likely indicates a glutathionylation of the cysteine in the second position of the active site motif. This supports the assumption that glutathionylation of the active site is not stable, and is readily resolved by either GSH in the case of ROXY9 CCLS or by GSH and the second cysteine in ROXY9, depending on the excess of GSH over GSSG.

Now, the question arises whether the described differences in the reactivity towards GSSG can explain why GRXC2 shows oxidoreductase activity in various assays, while only a weak deglutathionylation activity with GAPDH has been observed for ROXY9. At first site, it seemed counter-intuitive, that GRXC2, which is oxidized in a buffer that contains freshly prepared GSH, has reductase activity, while ROXY9, which has remained reduced under these conditions is inactive. However, it has to be kept in mind, that a GSH-regenerating system was installed in some of the enzyme assays. The reduced state of GRXC2 was also observe to some degree in the presence of GSH in one experiment (figure 22). Thus, sufficient reduced GRXC2 is probably available to accept the glutathione of glutathionylated substrates, like HEDS, roGFP and GAPDH.

One explanation for the low oxidoreductase activity of ROXY9 is the binding mode of the glutathione moiety of the substrate to the scaffold site. Differences in this binding mode, which exist between class I and class II glutaredoxins, have been shown to determine whether a glutaredoxin can have oxidoreductase activity (Deponte, 2013; Begas et al., 2017; Liedgens et al., 2020). An unfavourable scaffold site in ROXY9 might already explain why GSSG, which also binds to the scaffold site with one of its glutathione moieties, is less efficient as an oxidant than for GRXC2. This binding site might be even less efficient for βME-SG, while the interaction with GAPDH-SG might still be possible due to favourable protein-protein interactions. Saying that, it cannot be excluded that ROXY9 might have deglutathionylation activity in combination with specific substrates like TGA1.

The orientation of glutathione within the scaffold site has been shown to be strongly influenced by the loop length between a conserved lysine (dark blue

Figure 33: **Alignment of ROXY9 and GRXC2**. Protein sequences of ROXY9 and GRXC2 were aligned by COBALT (Papadopoulos and Agarwala, 2007). The active site position is highlighted by yellow background. Important residues are indicated by stars; dark blue for conserved lysine prior to active site, light blue for additional residues involved in glutathione binding for GRXC5 (Berndt and Lillig, 2017).

star in figures 2 and 33) and the active site motif, with large-scale influences on the binding direction of Fe-S-cluster (Trnka et al., 2020). Both ROXY9 and GRXC2 carry the same, short version of this loop, which is conserved in class I glutaredoxins and five amino acids longer in class II glutaredoxins. Additional residues involved in binding of glutathione have been shown to influence the catalytic properties (Liedgens et al., 2020). Some of the key residues according to Berndt and Lillig (2017) are highlighted in figures 2 and 33 by light blue stars. GRXC2 contains a conserved glutamine located on the $\alpha 2$ helix, while ROXY9 carries a charged glutamic acid at this position. Class II glutaredoxins contain an arginine or lysine in this position. Another deviation is observed in the beginning of the $\alpha 3$ helix, where the GCD motif of GRXC2 is changed to STN in ROXY9. However, this motif is not very different between class I and class II glutaredoxins. All these alterations could potentially explain an altered position of glutathione in the scaffold site that leads to lower reactivity towards glutathionylated substrates. Moreover, the newly formed disulphide bond might be under a strong tension in ROXY9, so that it is more readily resolved by the second cysteine than in GRXC2. For further analysis, it would be beneficial to investigate the potential binding modes of glutathione to ROXY9 and GRXC2 by molecular dynamics simulations, similar to the recent literature (Liedgens et al., 2020; Trnka et al., 2020). Based on this, critical residues could potentially be determined and their influence on the redox properties in GSH/GSSG titration experiments and enzymatic can be investigated in recombinant mutant proteins *in vitro*.

While an assumed altered binding mode of glutathione to the scaffold site in ROXY9 explains the low or lacking oxidoreductase activity, the efficient resolution of such an intermediate by the resolving cysteine would not necessarily explain the low oxidoreductase activity, unless the disulphide bond cannot be reduced by GSH. Indeed, the efficiency of the reduction of the disulphide bridge by GSH (step c in figure 31) has remained an open question. GSH/GSSG

buffers at reducing redox potentials of −250 mV did not lead to a high proportion of disulphide-bridged proteins (figure 17) over the incubation time of 2 h, which could indicate an equilibrium also involving the reduction of the disulphide bridge. But for a clear answer, whether the equilibrium was reached within the two hours, the effect of an extension of the incubation time has to be addressed. If the formation of the disulphide bond is irreversible, it would be expected that its proportion increases over longer time periods. Alternatively, the oxidized species with the disulphide bond would have to be desalted and subsequently incubated with GSH as already described in Couturier et al. (2013a).

A glutathionylation activity of ROXY9, for instance with reduced roGFP2, could not be detected in this thesis. This can be attributed to the transient nature of the glutathionylated catalytic cysteine, that quickly reacts to the reduced or disulphide-bridged state before a transfer of the glutathione onto roGFP is possible.

An important question concerns whether the observed properties of ROXY9 and GRXC2 are representative for other members of class I and class III glutaredoxins. As mentioned above, in the case of class I glutaredoxins, a predominantly glutathionylated species in the presence of GSH has likely been observed before for human GRX1 (Hatori et al., 2012) (see supplement figure S10). Still one difference exists: for GRXC2, the relative amounts of gluathionylated protein and protein with a disulfide bridge were highly similar over a wide range of redox potentials (figure 23), while slight effects of the GSSG/GSH ratio on the relative amounts of the two oxidized protein species were detected (Hatori et al., 2012). It would be of interest to investigate how other members of the class I glutaredoxins perform in this regard.

6.3 TGA1 is unlikely to be a target of redox modulation

Yeast two hybrid experiments and co-immunoprecipitation experiments have shown that ROXY9 interacts with the transcription factor TGA1 (Li et al., 2019). TGA1 was also reported to be redox modulated, with Després et al. (2003) reporting a reduction of a disulphide between cysteines 260 and 266 in plants treated with the defense hormone salicylic acid (SA). This reduction was essential for the interaction between TGA1 and the SA receptor NPR1 and led to the enhancement of the DNA-binding affinity of TGA1 in the presence of NPR1. Consistent with the notion that TGA1 contains redox-active cysteines, Lindermayr et al. (2010) reported glutathionylation of recombinant TGA1 upon treatment with GSNO. H_2O_2 treatment presumably led to a disulphide bond, however not between C260 and C266. GSNO excluded the formation of the

disulphide bond and promoted the DNA binding activity in the presence of NPR1. To reconcile both manuscripts, one would have to postulate that in SA-treated plants, the subsequent observed increase in the GSH/GSSG ratio leads to reduction and thus activation of TGA1, whereas other conditions might lead to a gluathionylation to increase TGA1 activity. In any of these two cases, ROXY9 and potentially other ROXYs might be required to catalyse these changes.

In this work, it was observed that recombinantly expressed TGA1 becomes non-enzymatically oxidized by GSSG over a time span of over 15 min. However, this process was not accelerated by ROXY9 (figure 20). In fact, TGA1 remains reduced at redox potentials high enough to oxidize the active site of ROXY9 (figure 21). It is concluded that it is unlikely that ROXY9 acts as an oxidase. However, it might act as a reductase on glutathionylated TGA1. Experiments to test this options failed so far for technical reasons, and should be repeated. Since glutathionylated TGA1 is suggested to be more active than the reduced or the disulphide containing protein, a deglutathionylation function for ROXY9 would be compatible with its function as a repressor.

Preliminary attempts to establish an assay for a potential deglutathionylation of TGA1 were unsuccessful. During the process of reducing TGA1 by DTT to start the assay at defined conditions, desalting, oxidation with GSSG, again desalting and finally mixing the samples with GSH and ROXY9, TGA1 was diluted to a point were it could not be detected after immuno-blotting. But even if a reductase activity of ROXY9 towards TGA1 could be identified *in vitro*, a functional integration of such an activity as a repressory mechanism is difficult due to the lack of a known pathway and the contradiction with the reductive activation proposed by Després et al. (2003).

This scenario would imply the existance of glutathionylated TGA1 in vivo at some stage, which seems to require high amounts of GSSG over GSH at a redox potential of −170 mV or higher. (figure 21). In contrast, the cytosolic redox potential is maintained at around −320 mV (Schwarzländer et al., 2008) and even after treatment with 50 to 200 mM H_2O_2, cytosolic redox potentials remained at −280 mV in leaves (Jubany-Mari et al., 2010), though roots seem to be more sensitive, going as high as −250 mV at 200 µM H_2O_2 (Jiang et al., 2006) and −260 mV after treatment with 1 mM buthionine sulphoximine (BSO), a GSH-synthesis inhibitor (Schnaubelt et al., 2015). A redox potential of −170 mV has been linked to apoptosis (Schafer and Buettner, 2001). Oxidized TGA1 thus either requires an *in vivo* micro-environment with a redox potential considerably deviating from its surrounding or it has to be regarded as an *in vitro* artefact that can only be formed by physiologically irrelevant pure GSSG treatment.

Recently, TGA1 complementation lines with all four cysteines replaced to the respective amino acid in TGA2 were found to neither be pre-induced nor be un-inducible with regard to the regulation of typical TGA1-dependent defence genes in SA-treated plants (Budimir et al., 2021). This argues against a functional relevance of redox modulation for TGA1 in the context of SA-mediated defense reactions.

In contrast, a functional significance of the redox modulation of a TGA factor by a class III glutaredoxin was found in the regulation of meristem size in maize (Yang et al., 2021a). These findings are based on the concept that the maintenance of undifferentiated cells and their differentiation are regulated by the redox state of the cells. TGA factor FEA4 is important to limit meristem size. In its oxidized state as in the corresponding grx mutant, it is hyperactive and meristems are small. In its reduced state, which is facilitated by GRX, it is less active and wild-type meristem size is established. Experiments showed electron transfer from GRX to oxidized FEA4. However, this experiment was conducted in the absence of GSH. Moreover, the redox potentials of FEA4 and the corresponding GRX are unknown. Importantly, the interaction between both proteins depends on the GRX active center. This is completely different from the mode of interaction between ROXY9 and TGA1, which is independent of the active center (Li et al., 2019). It therefore still remains to be elucidated in which functional contexts TGA1 is regulated by ROXY9 and/or other ROXYs and how this regulation is mechanistically achieved.

6.4 Fe-S-cluster binding capability requires further investigation

Class II glutaredoxins are known for their role in Fe-S-cluster binding and transfer (Li and Outten, 2012; Rouhier et al., 2010). Some class I glutaredoxins also bind Fe-S-clusters (Rouhier et al., 2010), a prerequisite being that the canonical CPYC motif is altered in all but one known examples (Roret et al., 2021). Apparently, CPYC-type glutaredoxins typically cannot bind Fe-S-clusters due to the proline in the second position. At least for human GRX2 with a CSYC active site motif, it has been speculated that the oxidoreductase activity of hGRX2 is activated upon release of the Fe-S-cluster under oxidative conditions (Lillig et al., 2005). Thus, it was interesting to analyse whether the class III glutaredoxin ROXY9 with a cysteine in the second position would be able to coordinate such a cluster. Multiple experiments were carried out in the Lill lab in Marburg.

In a first experiment, Fe-S-cluster reconstitution clearly induced the formation of a dimer (figure 24 A). Moreover, the sample showed a brownish colour as in all other experiments. However, since the aggregates that are present in

all samples tend to unspecifically bind iron, no clue on the identity of the postulated Fe-S-cluster in the dimer was obtained. Based on these promising data, further experiments were pursued. However, in all subsequent experiments, no clear dimer peak was detected, but rather a broad peak with yet undefined protein species was formed. Still, in contrast to the high molecular weight aggregates, which are formed by ROXY9 irrespective of the active center, the formation of this multimer depended on the wild-type active site . Future experiments have to re-establish the conditions of the first experiment, where a clear dimerisation was observed. The most obvious difference between the experiments was that the amount of GSH and DTT in the later experiments was more than 10-fold higher than in the initial experiment.

The UV/Vis absorbance spectrum and the iron and sulphur content of the putative multimer peak hint at the presence of an 4Fe-4S-cluster (figure 25), though further repetitions are clearly required to validate this assumption. So far, class I and II glutaredoxins have mostly been observed to bind 2Fe-2S-clusters (Couturier et al., 2015; Berndt et al., 2021), but the class II glutaredoxin GRX5 from *S. cerevisiae* was shown to bind 4Fe-4S-clusters alongside with linear 3F-4S clusters after *in vitro* reconstitution (Zhang et al., 2013).

The mode of cluster binding has been shown to depend on the orientation of the GSH involved in coordinating the cluster (Trnka et al., 2020). Though ROXY9 was not glutathionylated in the presence of glutathione (figure 17), glutathione did influence the CD spectrum (figure 7), which implies a non-covalent binding, potentially in a different orientation as compared to catalytically active glutaredoxins, which is oxidized upon GSH treatment (figure 23). Moreover, it also contains the additional cysteine in the second position of the active site. A cluster binding mode that deviates from class I and II glutaredoxins and enables the binding of 4Fe-4S-clusters might be realized in ROXY9. Based on complementation experiments, Anja Pelizaeus could already show that the active site is not important for the function of ROXY9 as an activator of nitrate response genes in roots. Thus, at least for this function, neither Fe-S-cluster binding nor oxidoreductase activity are required. Analysis of the active site variant with respect to hyponastic growth (figure 3) has shown that the CCLS is functional, though it does not form the FeS containing multimer peak. Thus FeS binding is unlikely to be important for the two *in vivo* functions of ROXY9 that we analysed. Still, given the strong conservation of the active site motif, it cannot be excluded that either Fe-S-cluster binding or weak or specific oxidoreductase activity is required for a subset of yet unknown ROXY9 functions or for other class III glutaredoxins.

Class III glutaredoxins have a nucleocytoplasmic localization (Li et al., 2009; Xu et al., 2022). While Fe-S-cluster biogenesis is located in the mitochon-

dria and chloroplasts (Lill and Mühlenhoff, 2008; Couturier et al., 2013b) and most Fe-S-cluster proteins are found in chloroplasts, a considerable share of Fe-S-cluster proteins is also present in the cytosol and the nucleus (Przybyla-Toscano et al., 2021). 4Fe-4S-clusters are required for the activity of cytosolic enzymes involved in metabolism like aconitase (Bernard et al., 2009, 2013), and several nucleic acid processing enzymes like helicases, polymerases and DNA repair enzymes (White and Dillingham, 2012; Wu and Brosh Jr, 2012). A potential function of Fe-S-cluster binding class III glutaredoxins could thus be the transfer of 4Fe-4S-clusters, supporting the only cytosolic class II glutaredoxin, GRXS17. GRXS17 was found to bind 2Fe 2S-clusters, associate with other components of the cytosolic Fe-S-cluster assembly pathway (Iñigo et al., 2016) and homologues in yeast and vertebrates were found to be essential (Mühlenhoff et al., 2010; Haunhorst et al., 2013). However, the *grxs17* mutant was viable and not severely impaired in aconitase activity (Knuesting et al., 2015), suggesting the existence of redundant factors for cluster transfer.

7 Supplementary

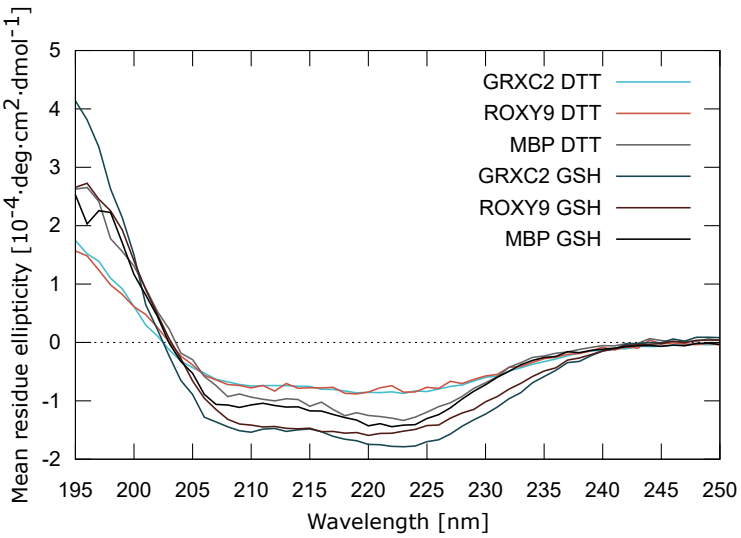

Figure S1: GSH influences the CD spectrum of GRXC2, ROXY9 and MBP. CD Spectrum of ROXY9, GRXC2 and strep-MBP in the presence of DTT or GSH. This figure supports figure 7.

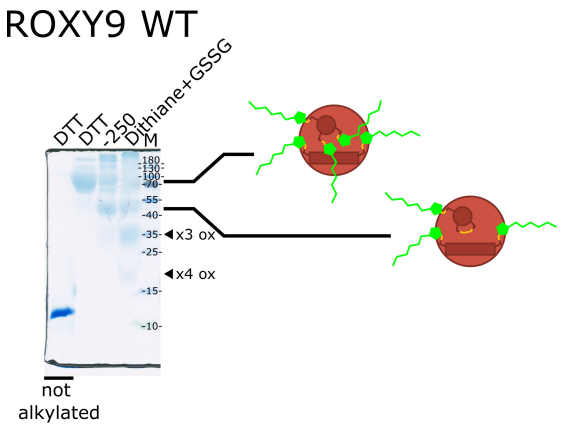

Figure S2: Untagged ROXY9 shows the same midpoint redox potential as Strep-MBP-ROXY9. Due to limited amount of available sample, ROXY9 after TEV cleavage in a GSH containing buffer was directly mixed with fresh DTT, DTT/Dithiane redox buffer at a redox potential around –250 mV or a mixture of Dithiane and GSSG as indicated. Samples were incubated at RT for 2 h followed by TCA precipitation. Reduced cysteines were labelled with 5 kDa mmPEG. Samples were separated by non-reducing SDS-Page. Sketches on the right indicate the likely redox state of proteins, further oxidized species are indicated by triangles. The 12 kDa protein was shifted to a position above 70 kDa when labelling with 5 kDa mmPEG. With the redox buffer at –250 mV, two bands above 70 kDa and between 55 and 40 kDa were visible along with multimer bands. The combined dithiane and GSSG-treatment led to the formation of a ladder that contained bands at the same positions as well as additional bands at 35 kDa and 20 kDa. This figure supports figure 8.

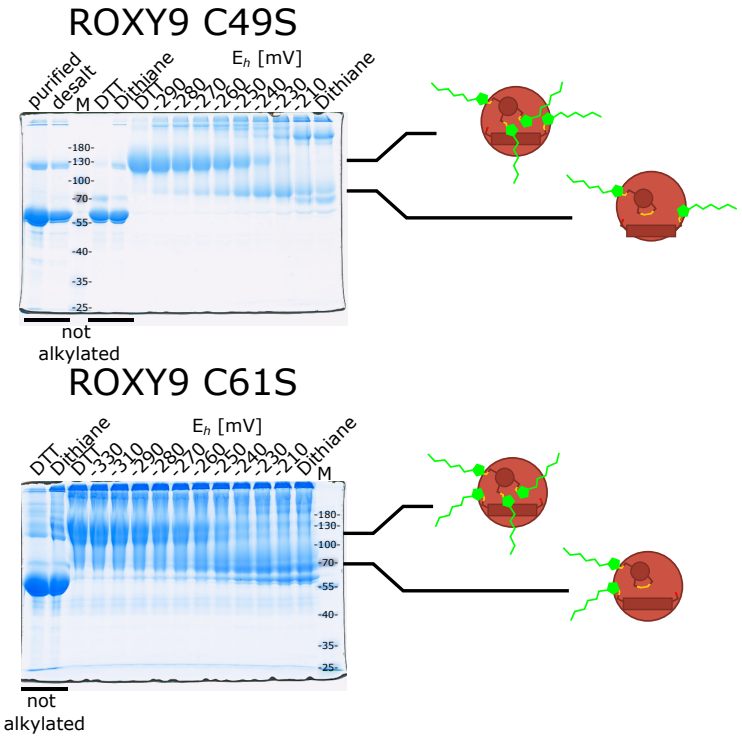

Figure S3: Redox titration assay of ROXY9 variants with mutations in cysteines 49 and 61. strep-MBP-ROXY9 C49S and C61S were pre-reduced, desalted and mixed with DTT, Dithiane and DTT/Dithiane redox buffers at different redox potentials as indicated. Samples were incubated at RT for 2 h followed by TCA precipitation. Reduced cysteines were labelled with 5 kDa mmPEG. Samples were separated by non-reducing SDS-Page alongside untreated protein after purification and desalting. Sketches on the right indicate the likely redox state of proteins. strep-MBP-ROXY9 C61S exhibited a strange double band phenotype for the dimer band as well as labelled fractions while for strep-MBP-ROXY9 C49S, the oxidizing treatment lead to the formation of a considerable dimer band in labelled samples while in previous experiments multimer bands could not be unambiguously assigned. This figure supports figures 8 and 9.

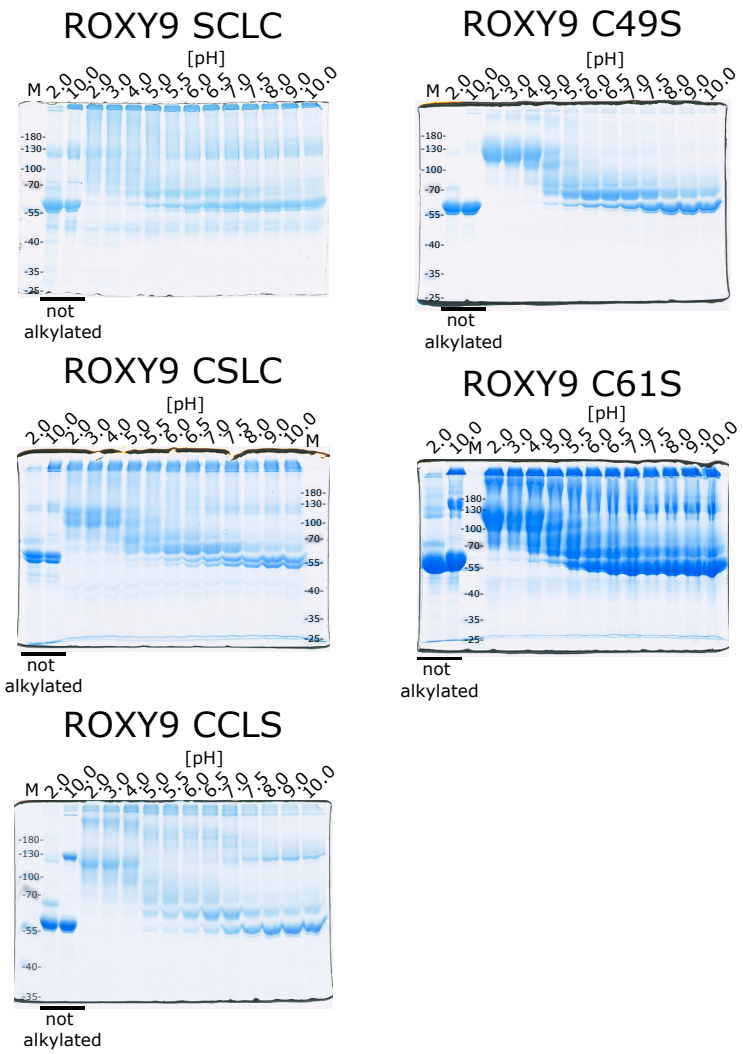

Figure S4: pH titration assay of ROXY9 cysteine mutants. strep-MBP-ROXY9 SCLC, CSLC, CCLS, C49S and C61S were pre-reduced, desalted and incubated with iodoacetamide at different pH values for 1 h to block cysteines present in thiolate form. The samples were subsequently TCA-precipitated and reduced cysteines not blocked by iodoacetamide labelled with 5 kDa mmPEG. Samples were separated by non-reducing SDS-Page. For pH 2.0 and 10.0, replicate samples are not labelled with mmPEG to better identify the non-labelled running position. This figure supports figure 11.

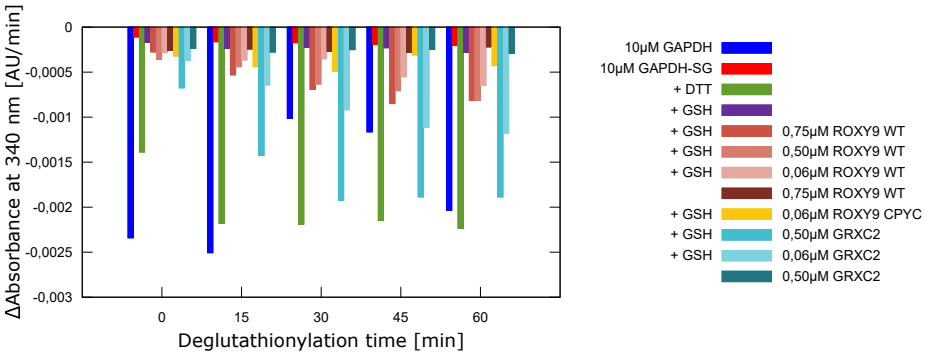

Figure S5: ROXY9 reduces GAPDH-SG less efficiently than GRXC2. GRX samples were pre-reduced with DTT and desalted. GAPDH was glutathionylated and desalted. For deglutathionylation, GAPDH-SG was mixed with DTT, GSH, GRX or GRX and GSH combined as indicated in the legend. Directly after mixing and at indicated time points, aliquots were withdrawn from the reaction mixtures and deglutathionylation was stopped. In a second step, GAPDH activity of the different samples was determined by measuring NADH consumption and calculating the change in absorbance over time. GAPDH not glutathionylated served as reference. This figure supports figure 15.

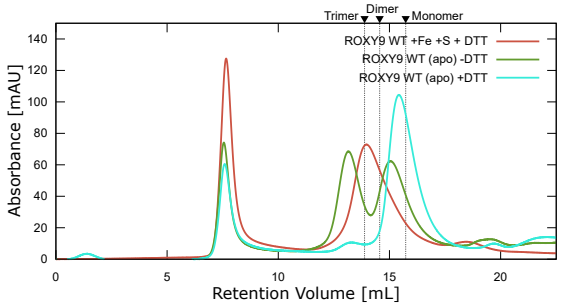

Figure S6: Gel filtration of ROXY9 before and after reduction with DTT or after Fe-S-cluster reconstitution shows differing multimer positions. Analytical gel filtration of strep-MBP-ROXY9 by loading untreated, DTT-reduced and Fe-S-cluster reconstituted holo samples onto a Sephadex S200 column tracking absorbance at 280 nm. The experiment was carried out under anaerobic conditions in Marburg. For reconstitution, strep-MBP-ROXY9 wild-type was reduced by DTT, incubated with GSH, ammonium iron(III) citrate and Li_2S followed by desalting, addition of DTT and spin concentration. Expected monomer, dimer and trimer retention volumes are 15.73, 14.56 and 13.88 mL respectively as calculated by the provided calibration curve and indicated by dashed lines. This figure supports figures 10 and 24, where this data set is also presented.

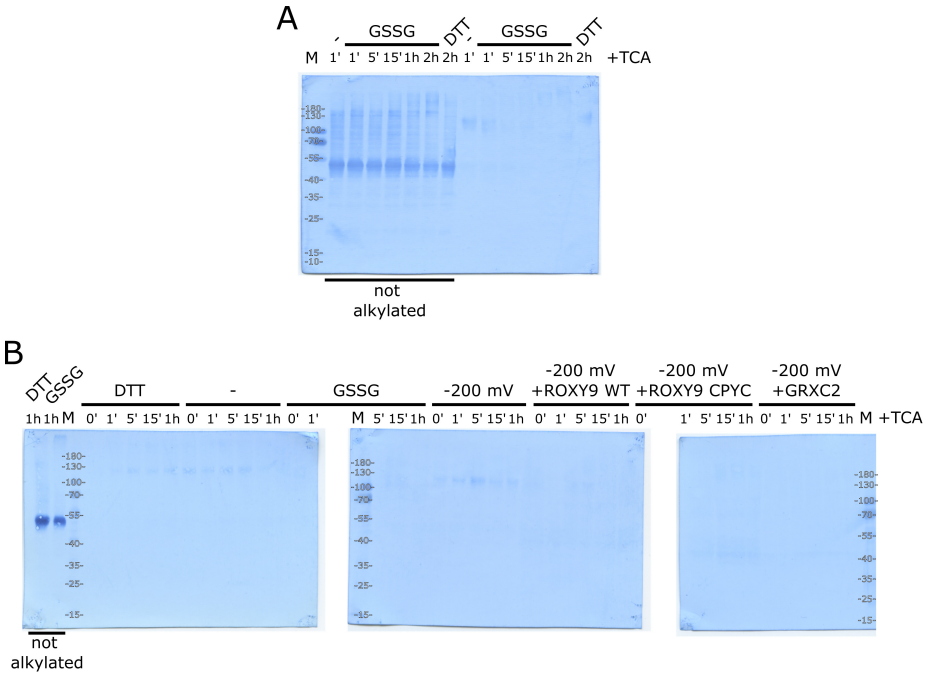

Figure S7: Coomassie stained membranes for oxidation of TGA1 with GSSG. (A) stained membrane for oxidation time course of His-TGA1 with GSSG. (B) Stained membranes for Oxidation time course of His-TGA1 with strep-MBP-GRXC2, strep-MBP-ROXY9-WT and strep-MBP-ROXY9 CPYC at –200 mV GSH/GSSG redox potential. This figure supports figure 20.

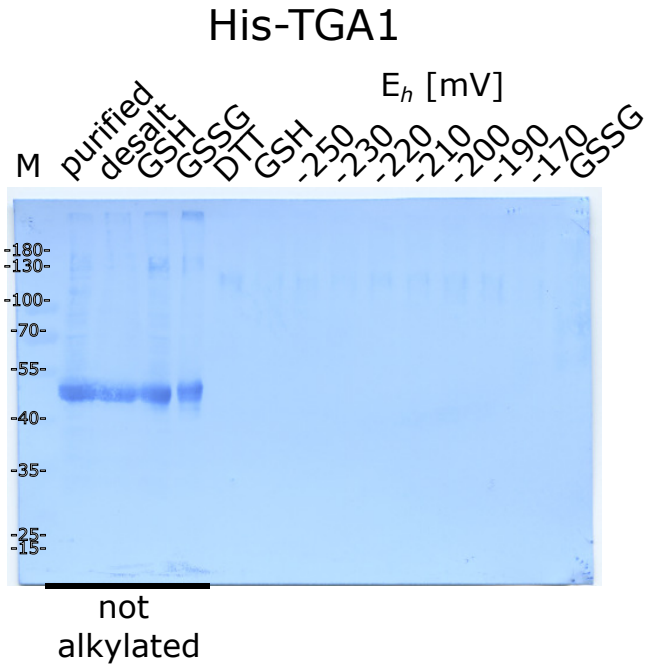

Figure S8: Coomassie stained membrane for redox titration of TGA1 with GSH. This figure supports figure 21.

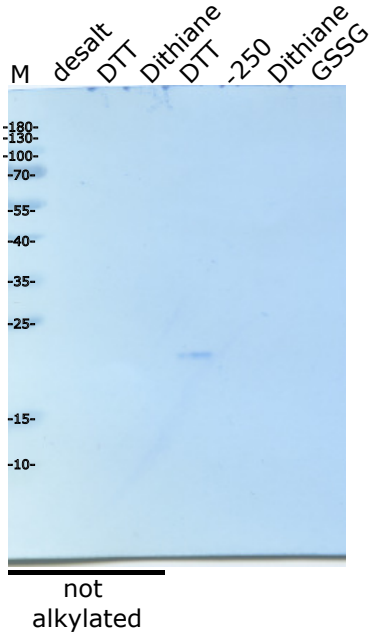

Figure S9: Coomassie stained membrane for AMS-shift assay with HA-ROXY9. This figure supports figure 29.

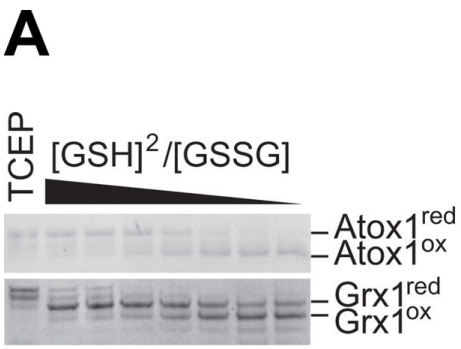

Figure S10: GSH/GSSG redox titration with human GRX1 and ATOX1. Figure taken from Hatori et al. (2012)

References

Isabel Aller, Nicolas Rouhier, and Andreas J Meyer. Development of rogfp2-derived redox probes for measurement of the glutathione redox potential in the cytosol of severely glutathione-deficient rml1 seedlings. *Frontiers in Plant Science*, 4:506, 2013.

Louise E Anderson and Toh-chin Lim. Chloroplast glyceraldehyde 3-phosphate dehydrogenase: light-dependent change in the enzyme. *FEBS letters*, 27(2): 189–191, 1972.

Tiziana Anelli and Roberto Sitia. Protein quality control in the early secretory pathway. *The EMBO journal*, 27(2):315–327, 2008.

Christian Appenzeller-Herzog and Lars Ellgaard. The human pdi family: versatility packed into a single fold. *Biochimica et Biophysica Acta (BBA)-Molecular Cell Research*, 1783(4):535–548, 2008.

Richard N Armstrong. Glutathione s-transferases: reaction mechanism, structure, and function. *Chemical research in toxicology*, 4(2):131–140, 1991.

Holly J Atkinson and Patricia C Babbitt. An atlas of the thioredoxin fold class reveals the complexity of function-enabling adaptations. *PLoS computational biology*, 5(10):e1000541, 2009a.

Holly J Atkinson and Patricia C Babbitt. Glutathione transferases are structural and functional outliers in the thioredoxin fold. *Biochemistry*, 48(46):11108–11116, 2009b.

Farnaz Zahedi Avval and Arne Holmgren. Molecular mechanisms of thioredoxin and glutaredoxin as hydrogen donors for mammalian s phase ribonucleotide reductase. *Journal of Biological Chemistry*, 284(13):8233–8240, 2009.

Tamanna Azam, Jonathan Przybyla-Toscano, Florence Vignols, Jérémy Couturier, Nicolas Rouhier, and Michael K Johnson. The arabidopsis mitochondrial glutaredoxin grxs15 provides [2fe-2s] clusters for isca-mediated [4fe-4s] cluster maturation. *International journal of molecular sciences*, 21(23):9237, 2020.

Doris Baier and Erwin Latzko. Properties and regulation of c-1-fructose-1, 6-diphosphatase from spinach chloroplasts. *Biochimica et Biophysica Acta (BBA)-Bioenergetics*, 396(1):141–147, 1975.

Sibali Bandyopadhyay, Filipe Gama, Maria Micaela Molina-Navarro, José Manuel Gualberto, Ronald Claxton, Sunil G Naik, Boi Hanh Huynh, Enrique Herrero, Jean Pierre Jacquot, Michael K Johnson, et al. Chloroplast monothiol glutaredoxins as scaffold proteins for the assembly and delivery of [2fe–2s] clusters. *The EMBO journal*, 27(7):1122–1133, 2008.

Marie-Christin Baune, Hannes Lansing, Kerstin Fischer, Tanja Meyer, Lennart Charton, Nicole Linka, and Antje von Schaewen. The arabidopsis plastidial glucose-6-phosphate transporter gpt1 is dually targeted to peroxisomes via the endoplasmic reticulum. *The Plant Cell*, 32(5):1703–1726, 2020.

Patricia Begas, Verena Staudacher, and Marcel Deponte. Systematic re-evaluation of the bis (2-hydroxyethyl) disulfide (heds) assay reveals an alternative mechanism and activity of glutaredoxins. *Chemical science*, 6(7): 3788–3796, 2015.

Patricia Begas, Linda Liedgens, Anna Moseler, Andreas J Meyer, and Marcel Deponte. Glutaredoxin catalysis requires two distinct glutathione interaction sites. *Nature communications*, 8(1):1–13, 2017.

Kyle W Bender, Xuejun Wang, George B Cheng, Hyoung Seok Kim, Raymond E Zielinski, Steven C Huber, et al. Glutaredoxin atgrxc2 catalyses inhibitory glutathionylation of arabidopsis bri1-associated receptor-like kinase 1 (bak1) in vitro. *Biochem. J*, 467:399–413, 2015.

Delphine G Bernard, Youfa Cheng, Yunde Zhao, and Janneke Balk. An allelic mutant series of atm3 reveals its key role in the biogenesis of cytosolic iron-sulfur proteins in arabidopsis. *Plant physiology*, 151(2):590–602, 2009.

Delphine G Bernard, Daili JA Netz, Thibaut J Lagny, Antonio J Pierik, and Janneke Balk. Requirements of the cytosolic iron–sulfur cluster assembly pathway in arabidopsis. *Philosophical Transactions of the Royal Society B: Biological Sciences*, 368(1622):20120259, 2013.

Carsten Berndt and Christopher Horst Lillig. Glutathione, glutaredoxins, and iron. *Antioxidants & Redox Signaling*, 27(15):1235–1251, 2017.

Carsten Berndt, Christoph Hudemann, Eva-Maria Hanschmann, Rebecca Axelsson, Arne Holmgren, and Christopher Horst Lillig. How does iron–sulfur cluster coordination regulate the activity of human glutaredoxin 2? *Antioxidants & redox signaling*, 9(1):151–157, 2007.

Carsten Berndt, Loïck Christ, Nicolas Rouhier, and Ulrich Mühlenhoff. Glutaredoxins with iron-sulphur clusters in eukaryotes-structure, function and impact

on disease. *Biochimica et Biophysica Acta (BBA)-Bioenergetics*, 1862(1): 148317, 2021.

Simon Black, Eileen M. Harte, Blondel Hudson, and Leonard Wartofsky. A specific enzymatic reduction of l(-) methionine sulfoxide and a related non-specific reduction of disulfides. *Journal of Biological Chemistry*, 235(10): 2910–2916, 1960. ISSN 0021-9258.

Jade R Bleau and Steven H Spoel. Selective redox signaling shapes plant–pathogen interactions. *Plant physiology*, 186(1):53–65, 2021.

Bob B Buchanan. The path to thioredoxin and redox regulation in chloroplasts. *Annual review of plant biology*, 67:1–24, 2016.

Jelena Budimir, Katrin Treffon, Aswin Nair, Corinnna Thurow, and Christiane Gatz. Redox-active cysteines in tgacg-binding factor 1 (tga1) do not play a role in salicylic acid or pathogen-induced expression of tga1-regulated target genes in arabidopsis thaliana. *New Phytologist*, 230(6):2420–2432, 2021.

Alexandra P Carvalho, Pedro A Fernandes, and Maria J Ramos. Similarities and differences in the thioredoxin superfamily. *Progress in biophysics and molecular biology*, 91(3):229–248, 2006.

Francisco Javier Cejudo, Valle Ojeda, Víctor Delgado-Requerey, Maricruz González, and Juan Manuel Pérez-Ruiz. Chloroplast redox regulatory mechanisms in plant adaptation to light and darkness. *Frontiers in plant science*, 10:380, 2019.

Ning-Hui Cheng. Atgrx4, an arabidopsis chloroplastic monothiol glutaredoxin, is able to suppress yeast grx5 mutant phenotypes and respond to oxidative stress. *FEBS letters*, 582(6):848–854, 2008.

Ning-Hui Cheng and Kendal D Hirschi. Cloning and characterization of cxip1, a novel picot domain-containing arabidopsis protein that associates with cax1. *Journal of Biological Chemistry*, 278(8):6503–6509, 2003.

Ning-Hui Cheng, Jian-Zhong Liu, Amanda Brock, Richard S Nelson, and Kendal D Hirschi. Atgrxcp, an arabidopsis chloroplastic glutaredoxin, is critical for protection against protein oxidative damage. *Journal of Biological Chemistry*, 281(36):26280–26288, 2006.

Ning-Hui Cheng, Jian-Zhong Liu, Xing Liu, Qingyu Wu, Sean M Thompson, Julie Lin, Joyce Chang, Steven A Whitham, Sunghun Park, Jerry D Cohen, et al. Arabidopsis monothiol glutaredoxin, atgrxs17, is critical for

temperature-dependent postembryonic growth and development via modulating auxin response. *Journal of Biological Chemistry*, 286(23):20398–20406, 2011.

Emma J Collinson, Glen L Wheeler, Ester Ocón Garrido, Angela M Avery, Simon V Avery, and Chris M Grant. The yeast glutaredoxins are active as glutathione peroxidases. *Journal of Biological Chemistry*, 277(19):16712–16717, 2002.

Michael J Considine and Christine H Foyer. Redox regulation of plant development. *Antioxidants & redox signaling*, 21(9):1305–1326, 2014.

Shelley D Copley, Walter RP Novak, and Patricia C Babbitt. Divergence of function in the thioredoxin fold suprafamily: evidence for evolution of peroxiredoxins from a thioredoxin-like ancestor. *Biochemistry*, 43(44):13981–13995, 2004.

Jérémy Couturier, Jean-Pierre Jacquot, and Nicolas Rouhier. Evolution and diversity of glutaredoxins in photosynthetic organisms. *Cellular and Molecular Life Sciences*, 66(15):2539–2557, 2009a.

Jeremy Couturier, Cha San Koh, Mirko Zaffagnini, Alison M Winger, Jose Manuel Gualberto, Catherine Corbier, Paulette Decottignies, Jean-Pierre Jacquot, Stéphane D Lemaire, Claude Didierjean, et al. Structure-function relationship of the chloroplastic glutaredoxin s12 with an atypical wcsys active site. *Journal of Biological Chemistry*, 284(14):9299–9310, 2009b.

Jérémy Couturier, Claude Didierjean, Jean-Pierre Jacquot, and Nicolas Rouhier. Engineered mutated glutaredoxins mimicking peculiar plant class iii glutaredoxins bind iron–sulfur centers and possess reductase activity. *Biochemical and biophysical research communications*, 403(3-4):435–441, 2010.

Jérémy Couturier, Elke Ströher, Angela-Nadia Albetel, Thomas Roret, Meenakumari Muthuramalingam, Lionel Tarrago, Thorsten Seidel, Pascale Tsan, Jean-Pierre Jacquot, Michael K Johnson, et al. Arabidopsis chloroplastic glutaredoxin c5 as a model to explore molecular determinants for iron-sulfur cluster binding into glutaredoxins. *Journal of Biological Chemistry*, 286(31):27515–27527, 2011.

Jérémy Couturier, Jean-Pierre Jacquot, and Nicolas Rouhier. Toward a refined classification of class i dithiol glutaredoxins from poplar: biochemical basis for the definition of two subclasses. *Frontiers in plant science*, 4:518, 2013a.

Jérémy Couturier, Brigitte Touraine, Jean-François Briat, Frédéric Gaymard, and Nicolas Rouhier. The iron-sulfur cluster assembly machineries in plants: current knowledge and open questions. *Frontiers in Plant science*, 4:259, 2013b.

Jérémy Couturier, Jonathan Przybyla-Toscano, Thomas Roret, Claude Didierjean, and Nicolas Rouhier. The roles of glutaredoxins ligating fe–s clusters: sensing, transfer or repair functions? *Biochimica et Biophysica Acta (BBA)-Molecular Cell Research*, 1853(6):1513–1527, 2015.

Agnès Delaunay, Delphine Pflieger, Marie-Bénédicte Barrault, Joelle Vinh, and Michel B Toledano. A thiol peroxidase is an h2o2 receptor and redox-transducer in gene activation. *Cell*, 111(4):471–481, 2002.

Marcel Deponte. Glutathione catalysis and the reaction mechanisms of glutathione-dependent enzymes. *Biochimica et Biophysica Acta (BBA)-General Subjects*, 1830(5):3217–3266, 2013.

Charles Després, Catherine Chubak, Amanda Rochon, Rena Clark, Terry Bethune, Darrell Desveaux, and Pierre R Fobert. The arabidopsis npr1 disease resistance protein is a novel cofactor that confers redox regulation of dna binding activity to the basic domain/leucine zipper transcription factor tga1. *The Plant Cell*, 15(9):2181–2191, 2003.

Shuangcheng Ding, Fengyu He, Wenlin Tang, Hewei Du, and Hongwei Wang. Identification of maize cc-type glutaredoxins that are associated with response to drought stress. *Genes*, 10(8):610, 2019.

Jelena Dumanović, Eugenie Nepovimova, Maja Natić, Kamil Kuča, and Vesna Jaćević. The significance of reactive oxygen species and antioxidant defense system in plants: A concise overview. *Frontiers in plant science*, 11:552969, 2021.

Robert Edwards, David P Dixon, and Virginia Walbot. Plant glutathione s-transferases: enzymes with multiple functions in sickness and in health. *Trends in plant science*, 5(5):193–198, 2000.

Ahmad Ehrary, Miguel Rosas, Sophia Carpinelli, Oscar Davalos, Craig Cowling, Francisco Fernandez, and Matthew Escobar. Glutaredoxin atgrxs8 represses transcriptional and developmental responses to nitrate in arabidopsis thaliana roots. *Plant direct*, 4(6):e00227, 2020.

Ashraf El-Kereamy, Yong-Mei Bi, Kashif Mahmood, Kosala Ranathunge, Mahmoud W Yaish, Eiji Nambara, and Steven J Rothstein. Overexpression of

the cc-type glutaredoxin, osgrx6 affects hormone and nitrogen status in rice plants. *Frontiers in plant science*, 6:934, 2015.

Aristi Potamitou Fernandes and Arne Holmgren. Glutaredoxins: glutathione-dependent redox enzymes with functions far beyond a simple thioredoxin backup system. *Antioxidants and Redox Signaling*, 6(1):63–74, 2004.

Christine H Foyer and Graham Noctor. Redox homeostasis and antioxidant signaling: a metabolic interface between stress perception and physiological responses. *The Plant Cell*, 17(7):1866–1875, 2005.

Christine H Foyer and Graham Noctor. Redox regulation in photosynthetic organisms: signaling, acclimation, and practical implications. *Antioxidants & redox signaling*, 11(4):861–905, 2009.

Christine H Foyer and Graham Noctor. Redox signaling in plants, 2013.

Debra E Frederickson Matika and Gary J Loake. Redox regulation in plant immune function. *Antioxidants & redox signaling*, 21(9):1373–1388, 2014.

Xing-Huang Gao, Mirko Zaffagnini, Mariette Bedhomme, Laure Michelet, Corinne Cassier-Chauvat, Paulette Decottignies, and Stéphane D Lemaire. Biochemical characterization of glutaredoxins from chlamydomonas reinhardtii: kinetics and specificity in deglutathionylation reactions. *FEBS letters*, 584(11):2242–2248, 2010.

Elisabeth Gasteiger, Christine Hoogland, Alexandre Gattiker, Marc R Wilkins, Ron D Appel, Amos Bairoch, et al. Protein identification and analysis tools on the expasy server. *The proteomics protocols handbook*, pages 571–607, 2005.

Christiane Gatz. From pioneers to team players: Tga transcription factors provide a molecular link between different stress pathways. *Molecular Plant-Microbe Interactions*, 26(2):151–159, 2013.

Stephen A Gravina and John J Mieyal. Thioltransferase is a specific glutathionyl mixed-disulfide oxidoreductase. *Biochemistry*, 32(13):3368–3376, 1993.

Nora Gutsche and Sabine Zachgo. The n-terminus of the floral arabidopsis tga transcription factor perianthia mediates redox-sensitive dna-binding. *PLoS One*, 11(4):e0153810, 2016.

Nora Gutsche, Corinna Thurow, Sabine Zachgo, and Christiane Gatz. Plant-specific cc-type glutaredoxins: functions in developmental processes and stress responses. *Biological Chemistry*, 396(5):495–509, 2015.

Yuta Hatori, Sara Clasen, Nesrin M Hasan, Amanda N Barry, and Svetlana Lutsenko. Functional partnership of the copper export machinery and glutathione balance in human cells. *Journal of Biological Chemistry*, 287(32): 26678–26687, 2012.

Petra Haunhorst, Eva-Maria Hanschmann, Lars Bräutigam, Oliver Stehling, Bastian Hoffmann, Ulrich Mühlenhoff, Roland Lill, Carsten Berndt, and Christopher Horst Lillig. Crucial function of vertebrate glutaredoxin 3 (picot) in iron homeostasis and hemoglobin maturation. *Molecular biology of the cell*, 24(12):1895–1903, 2013.

Fanglian He. Laemmli-sds-page. *Bio-protocol*, pages e80–e80, 2011.

Enrique Herrero and María Angeles de la Torre-Ruiz. Monothiol glutaredoxins: a common domain for multiple functions. *Cellular and molecular life sciences*, 64(12):1518–1530, 2007.

Arne Holmgren. Hydrogen donor system for escherichia coli ribonucleoside-diphosphate reductase dependent upon glutathione. *Proceedings of the National Academy of Sciences*, 73(7):2275–2279, 1976.

Arne Holmgren. Thioredoxin. *Annual review of biochemistry*, 54:237–271, 1985.

Arne Holmgren. Thioredoxin structure and mechanism: conformational changes on oxidation of the active-site sulfhydryls to a disulfide. *Structure*, 3 (3):239–243, 1995. ISSN 0969-2126.

Arne Holmgren and Fredrik Aslund. [29] glutaredoxin. In *Biothiols Part B: Glutathione and Thioredoxin: Thiols in Signal Transduction and Gene Regulation*, volume 252 of *Methods in Enzymology*, pages 283–292. Academic Press, 1995.

Md Faruq Hossain, Yana Bodnar, Calvin Klein, Clara Ortegón Salas, Elias SJ Arnér, Manuela Gellert, and Christopher Horst Lillig. Molecular basis for the interactions of human thioredoxins with their respective reductases. *Oxidative medicine and cellular longevity*, 2021, 2021.

Li-Jun Huang, Ning Li, Corinna Thurow, Markus Wirtz, Rüdiger Hell, and Christiane Gatz. Ectopically expressed glutaredoxin roxy19 negatively regulates the detoxification pathway in arabidopsis thaliana. *BMC plant biology*, 16(1): 1–12, 2016.

Sabrina Iñigo, Astrid Nagels Durand, Andrés Ritter, Sabine Le Gall, Martin Termathe, Roland Klassen, Takayuki Tohge, Barbara De Coninck, Jelle

Van Leene, Rebecca De Clercq, et al. Glutaredoxin grxs17 associates with the cytosolic iron-sulfur cluster assembly pathway. *Plant Physiology*, 172(2): 858–873, 2016.

Thomas Iwema, Antoine Picciocchi, Daouda AK Traore, Jean-Luc Ferrer, Franck Chauvat, and Lilian Jacquamet. Structural basis for delivery of the intact [fe2s2] cluster by monothiol glutaredoxin. *Biochemistry*, 48(26):6041–6043, 2009.

Donald L Jarvis. Baculovirus–insect cell expression systems. *Methods in enzymology*, 463:191–222, 2009.

Anna Jarzab, Nils Kurzawa, Thomas Hopf, Matthias Moerch, Jana Zecha, Niels Leijten, Yangyang Bian, Eva Musiol, Melanie Maschberger, Gabriele Stoehr, et al. Meltome atlas—thermal proteome stability across the tree of life. *Nature methods*, 17(5):495–503, 2020.

Kristine Steen Jensen, Jeppe T Pedersen, Jakob R Winther, and Kaare Teilum. The p k a value and accessibility of cysteine residues are key determinants for protein substrate discrimination by glutaredoxin. *Biochemistry*, 53(15): 2533–2540, 2014.

Keni Jiang, Christian Schwarzer, Elizabeth Lally, Shibo Zhang, Steven Ruzin, Terry Machen, S James Remington, and Lewis Feldman. Expression and characterization of a redox-sensing green fluorescent protein (reduction-oxidation-sensitive green fluorescent protein) in arabidopsis. *Plant physiology*, 141(2):397–403, 2006.

T Jubany-Mari, L Alegre-Batlle, K Jiang, and LJ Feldman. Use of a redox-sensing gfp (c-rogfp1) for real-time monitoring of cytosol redox status in arabidopsis thaliana water-stressed plants. *FEBS letters*, 584(5):889–897, 2010.

Ji-Yul Jung, Ji Hoon Ahn, and Daniel P Schachtman. Cc-type glutaredoxins mediate plant response and signaling under nitrate starvation in arabidopsis. *BMC plant biology*, 18(1):1–13, 2018.

Meenu Kesarwani, Jungmin Yoo, and Xinnian Dong. Genetic interactions of tga transcription factors in the regulation of pathogenesis-related genes and disease resistance in arabidopsis. *Plant physiology*, 144(1):336–346, 2007.

Johannes Knuesting, Christophe Riondet, Carlos Maria, Inga Kruse, Noëlle Bécuwe, Nicolas König, Carsten Berndt, Sébastien Tourrette, Jocelyne Guilleminot-Montoya, Enrique Herrero, et al. Arabidopsis glutaredoxin s17

and its partner, the nuclear factor y subunit c11/negative cofactor 2α, contribute to maintenance of the shoot apical meristem under long-day photoperiod. *Plant physiology*, 167(4):1643–1658, 2015.

Takanori Kobayashi, Haruka Shinkawa, Atsushi J Nagano, and Naoko K Nishizawa. The basic leucine zipper transcription factor osbzip83 and the glutaredoxins osgrx6 and osgrx9 facilitate rice iron utilization under the control of oshrz ubiquitin ligases. *The Plant Journal*, 2022.

Thomas A Kost, J Patrick Condreay, and Donald L Jarvis. Baculovirus as versatile vectors for protein expression in insect and mammalian cells. *Nature biotechnology*, 23(5):567–575, 2005.

Sylvain La Camera, Floriane L'Haridon, Jérémy Astier, Mark Zander, Eliane Abou-Mansour, Gonzague Page, Corinna Thurow, David Wendehenne, Christiane Gatz, Jean-Pierre Métraux, et al. The glutaredoxin atgrxs13 is required to facilitate botrytis cinerea infection of arabidopsis thaliana plants. *The Plant Journal*, 68(3):507–519, 2011.

Martha CA Laboissiere, Stephen L Sturley, and Ronald T Raines. The essential function of protein-disulfide isomerase is to unscramble non-native disulfide bonds. *Journal of Biological Chemistry*, 270(47):28006–28009, 1995.

Anna M Łasica and Elżbieta K Jagusztyn-Krynicka. The role of dsb proteins of gram-negative bacteria in the process of pathogenesis. *FEMS microbiology reviews*, 31(5):626–636, 2007.

Torvard C Laurent, E Colleen Moore, and Peter Reichard. Enzymatic synthesis of deoxyribonucleotides: Iv. isolation and characterization of thioredoxin, the hydrogen donor from escherichia coli b. *Journal of Biological Chemistry*, 239 (10):3436–3444, 1964.

Samuel Lee, Soo Min Kim, and Richard T Lee. Thioredoxin and thioredoxin target proteins: from molecular mechanisms to functional significance. *Antioxidants & redox signaling*, 18(10):1165–1207, 2013.

Stéphane D Lemaire. The glutaredoxin family in oxygenic photosynthetic organisms. *Photosynthesis Research*, 79(3):305–318, 2004.

Haoran Li and Caryn E Outten. Monothiol cgfs glutaredoxins and bola-like proteins:[2fe-2s] binding partners in iron homeostasis. *Biochemistry*, 51(22): 4377–4389, 2012.

Lenong Li, Ninghui Cheng, Kendal D Hirschi, and Xiaoqiang Wang. Structure of arabidopsis chloroplastic monothiol glutaredoxin atgrxcp. *Acta Crystallographica Section D: Biological Crystallography*, 66(6):725–732, 2010.

Ning Li. *Plant-specific glutaredoxin ROXY9 regulates hyponastic growth by inhibiting TGA1 function*. PhD thesis, Niedersächsische Staats-und Universitätsbibliothek Göttingen, 2017.

Ning Li, Martin Muthreich, Li-Jun Huang, Corinna Thurow, Tongjun Sun, Yuelin Zhang, and Christiane Gatz. Tgacg-binding factors (tgas) and tga-interacting cc-type glutaredoxins modulate hyponastic growth in arabidopsis thaliana. *New Phytologist*, 221(4):1906–1918, 2019.

Shutian Li, Andrea Lauri, Mark Ziemann, Andrea Busch, Mrinal Bhave, and Sabine Zachgo. Nuclear activity of roxy1, a glutaredoxin interacting with tga factors, is required for petal development in arabidopsis thaliana. *The Plant Cell*, 21(2):429–441, 2009.

Shutian Li, Nora Gutsche, and Sabine Zachgo. The roxy1 c-terminal l** ll motif is essential for the interaction with tga transcription factors. *Plant physiology*, 157(4):2056–2068, 2011.

Linda Liedgens, Jannik Zimmermann, Lucas Wäschenbach, Fabian Geissel, Hugo Laporte, Holger Gohlke, Bruce Morgan, and Marcel Deponte. Quantitative assessment of the determinant structural differences between redox-active and inactive glutaredoxins. *Nature communications*, 11(1):1–18, 2020.

Roland Lill and Ulrich Mühlenhoff. Maturation of iron-sulfur proteins in eukaryotes: mechanisms, connected processes, and diseases. *Annu. Rev. Biochem.*, 77:669–700, 2008.

Christopher Horst Lillig, Carsten Berndt, Olivia Vergnolle, Maria Elisabet Lönn, Christoph Hudemann, Eckhard Bill, and Arne Holmgren. Characterization of human glutaredoxin 2 as iron–sulfur protein: a possible role as redox sensor. *Proceedings of the National Academy of Sciences*, 102(23):8168–8173, 2005.

Christopher Horst Lillig, Carsten Berndt, and Arne Holmgren. Glutaredoxin systems. *Biochimica et Biophysica Acta (BBA)-General Subjects*, 1780(11): 1304–1317, 2008.

Christian Lindermayr, Simone Sell, Bernd Müller, Dario Leister, and Jörg Durner. Redox regulation of the npr1-tga1 system of arabidopsis thaliana by nitric oxide. *The Plant Cell*, 22(8):2894–2907, 2010.

Xi Liu, Shian Liu, Yingang Feng, Jian-Zhong Liu, Yuling Chen, Khanh Pham, Haiteng Deng, Kendal D Hirschi, Xinquan Wang, and Ninghui Cheng. Structural insights into the n-terminal giy–yig endonuclease activity of arabidopsis

glutaredoxin atgrxs16 in chloroplasts. *Proceedings of the National Academy of Sciences*, 110(23):9565–9570, 2013.

Verne A Luckow and Max D Summers. Trends in the development of baculovirus expression vectors. *Bio/technology*, 6(1):47–55, 1988.

Bruno Manta, Matías N Möller, Mariana Bonilla, Matías Deambrosi, Karin Grunberg, Massimo Bellanda, Marcelo A Comini, and Gerardo Ferrer-Sueta. Kinetic studies reveal a key role of a redox-active glutaredoxin in the evolution of the thiol-redox metabolism of trypanosomatid parasites. *Journal of Biological Chemistry*, 294(9):3235–3248, 2019.

Jennifer L Martin. Thioredoxin—a fold for all reasons. *Structure*, 3(3):245–250, 1995.

Laura Martins, Johannes Knuesting, Laetitia Bariat, Avilien Dard, Sven A Freibert, Christophe H Marchand, David Young, Nguyen Ho Thuy Dung, Wilhelm Voth, Anne Debures, et al. Redox modification of the iron-sulfur glutaredoxin grxs17 activates holdase activity and protects plants from heat stress. *Plant Physiology*, 184(2):676–692, 2020.

Lefentse N Mashamaite, Johann M Rohwer, and Ché S Pillay. The glutaredoxin mono-and di-thiol mechanisms for deglutathionylation are functionally equivalent: implications for redox systems biology. *Bioscience reports*, 35 (1), 2015.

Lucia Maß, Michael Holtmannspötter, and Sabine Zachgo. Dual-color 3d-dstorm colocalization and quantification of roxy1 and rnapii variants throughout the transcription cycle in root meristem nuclei. *The Plant Journal*, 104 (5):1423–1436, 2020.

Despoina AI Mavridou, Emmanuel Saridakis, Paraskevi Kritsiligkou, Erin C Mozley, Stuart J Ferguson, and Christina Redfield. An extended active-site motif controls the reactivity of the thioredoxin fold. *Journal of Biological Chemistry*, 289(12):8681–8696, 2014.

Nikola Mesecke, Sarah Mittler, Elisabeth Eckers, Johannes M Herrmann, and Marcel Deponte. Two novel monothiol glutaredoxins from saccharomyces cerevisiae provide further insight into iron-sulfur cluster binding, oligomerization, and enzymatic activity of glutaredoxins. *Biochemistry*, 47(5):1452–1463, 2008.

Joris Messens and Jean-François Collet. Pathways of disulfide bond formation in escherichia coli. *The international journal of biochemistry & cell biology*, 38(7):1050–1062, 2006.

Andreas J Meyer and Tobias P Dick. Fluorescent protein-based redox probes. *Antioxidants & redox signaling*, 13(5):621–650, 2010.

Andreas J Meyer, Thorsten Brach, Laurent Marty, Susanne Kreye, Nicolas Rouhier, Jean-Pierre Jacquot, and Rüdiger Hell. Redox-sensitive gfp in arabidopsis thaliana is a quantitative biosensor for the redox potential of the cellular glutathione redox buffer. *The Plant Journal*, 52(5):973–986, 2007.

Yves Meyer, Wafi Siala, Talaat Bashandy, Christophe Riondet, Florence Vignols, and Jean Philippe Reichheld. Glutaredoxins and thioredoxins in plants. *Biochimica et Biophysica Acta (BBA) - Molecular Cell Research*, 1783(4): 589–600, 2008. ISSN 0167-4889. Redox regulation of protein folding.

Ian M Moller, Poul Erik Jensen, and Andreas Hansson. Oxidative modifications to cellular components in plants. *Annual review of plant biology*, 58(1):459–481, 2007.

Anna Moseler, Isabel Aller, Stephan Wagner, Thomas Nietzel, Jonathan Przybyla-Toscano, Ulrich Mühlenhoff, Roland Lill, Carsten Berndt, Nicolas Rouhier, Markus Schwarzländer, et al. The mitochondrial monothiol glutaredoxin s15 is essential for iron-sulfur protein maturation in arabidopsis thaliana. *Proceedings of the National Academy of Sciences*, 112(44): 13735–13740, 2015.

Anna Moseler, Inga Kruse, Andrew E Maclean, Luca Pedroletti, Marina Franceschetti, Stephan Wagner, Regina Wehler, Katrin Fischer-Schrader, Gernot Poschet, Markus Wirtz, et al. The function of glutaredoxin grxs15 is required for lipoyl-dependent dehydrogenases in mitochondria. *Plant physiology*, 186(3):1507–1525, 2021.

Ulrich Mühlenhoff, Sabine Molik, José R Godoy, Marta A Uzarska, Nadine Richter, Andreas Seubert, Yan Zhang, JoAnne Stubbe, Fabien Pierrel, Enrique Herrero, et al. Cytosolic monothiol glutaredoxins function in intracellular iron sensing and trafficking via their bound iron-sulfur cluster. *Cell metabolism*, 12(4):373–385, 2010.

Stefanie J Müller-Schüssele, Finja Bohle, Jacopo Rossi, Paolo Trost, Andreas J Meyer, and Mirko Zaffagnini. Plasticity in plastid redox networks: evolution of glutathione-dependent redox cascades and glutathionylation sites. *BMC plant biology*, 21(1):1–20, 2021.

Jhadeswar Murmu, Michael J Bush, Catherine DeLong, Shutian Li, Mingli Xu, Madiha Khan, Caroline Malcolmson, Pierre R Fobert, Sabine Zachgo, and Shelley R Hepworth. Arabidopsis basic leucine-zipper transcription factors

tga9 and tga10 interact with floral glutaredoxins roxy1 and roxy2 and are redundantly required for anther development. *Plant Physiology*, 154(3):1492–1504, 2010.

Hajime Nakamura, Leonore A Herzenberg, Jie Bai, Shinichi Araya, Norihiko Kondo, Yumiko Nishinaka, Leonard A Herzenberg, and Junji Yodoi. Circulating thioredoxin suppresses lipopolysaccharide-induced neutrophil chemotaxis. *Proceedings of the National Academy of Sciences*, 98(26):15143–15148, 2001.

Ivan Ndamukong, Ayed Al Abdallat, Corinna Thurow, Benjamin Fode, Mark Zander, Ralf Weigel, and Christiane Gatz. Sa-inducible arabidopsis glutaredoxin interacts with tga factors and suppresses ja-responsive pdf1. 2 transcription. *The Plant Journal*, 50(1):128–139, 2007.

Luis ES Netto and Fernando Antunes. The roles of peroxiredoxin and thioredoxin in hydrogen peroxide sensing and in signal transduction. *Molecules and cells*, 39(1):65, 2016.

Motohiko Nishida, Shigeharu Harada, Shuji Noguchi, Yoshinori Satow, Hideshi Inoue, and Kenji Takahashi. Three-dimensional structure of escherichia coli glutathione s-transferase complexed with glutathione sulfonate: catalytic roles of cys10 and his106. *Journal of molecular biology*, 281(1):135–147, 1998.

Graham Noctor, Jean-Philippe Reichheld, and Christine H Foyer. Ros-related redox regulation and signaling in plants. In *Seminars in cell & developmental biology*, volume 80, pages 3–12. Elsevier, 2018.

Jan Oberdiek. *Funktionale Analyse des CC-Typ Glutaredoxin ROXY19 in Arabidopsis thaliana*. PhD thesis, Georg-August-Universität Göttingen, 2018.

Yuri Ohkubo, Mina Tanaka, Ryo Tabata, Mari Ogawa-Ohnishi, and Yoshikatsu Matsubayashi. Shoot-to-root mobile polypeptides involved in systemic regulation of nitrogen acquisition. *Nature plants*, 3(4):1–6, 2017.

Valle Ojeda, Juan Manuel Pérez-Ruiz, and Francisco Javier Cejudo. 2-cys peroxiredoxins participate in the oxidation of chloroplast enzymes in the dark. *Molecular Plant*, 11(11):1377–1388, 2018.

Masaki Okumura, Hiroshi Kadokura, and Kenji Inaba. Structures and functions of protein disulfide isomerase family members involved in proteostasis in the endoplasmic reticulum. *Free Radical Biology and Medicine*, 83:314–322, 2015.

Ryosuke Ota, Yuri Ohkubo, Yasuko Yamashita, Mari Ogawa-Ohnishi, and Yoshikatsu Matsubayashi. Shoot-to-root mobile cepd-like 2 integrates shoot nitrogen status to systemically regulate nitrate uptake in arabidopsis. *Nature communications*, 11(1):1–9, 2020.

Jonathan L Pan and James CA Bardwell. The origami of thioredoxin-like folds. *Protein science*, 15(10):2217–2227, 2006.

Jason S Papadopoulos and Richa Agarwala. Cobalt: constraint-based alignment tool for multiple protein sequences. *Bioinformatics*, 23(9):1073–1079, 2007.

Kurt Patterson, Laura A Walters, Andrew M Cooper, Jocelyn G Olvera, Miguel A Rosas, Allan G Rasmusson, and Matthew A Escobar. Nitrate-regulated glutaredoxins control arabidopsis primary root growth. *Plant Physiology*, 170 (2):989–999, 2016.

Candice E Paulsen and Kate S Carroll. Chemical dissection of an essential redox switch in yeast. *Chemistry & biology*, 16(2):217–225, 2009.

Arden Perkins, Kimberly J Nelson, Derek Parsonage, Leslie B Poole, and P Andrew Karplus. Peroxiredoxins: guardians against oxidative stress and modulators of peroxide signaling. *Trends in biochemical sciences*, 40(8):435–445, 2015.

Antoine Picciocchi, Cyril Saguez, Alain Boussac, Corinne Cassier-Chauvat, and Franck Chauvat. Cgfs-type monothiol glutaredoxins from the cyanobacterium synechocystis pcc6803 and other evolutionary distant model organisms possess a glutathione-ligated [2fe-2s] cluster. *Biochemistry*, 46(51): 15018–15026, 2007.

Leslie B Poole. The basics of thiols and cysteines in redox biology and chemistry. *Free Radical Biology and Medicine*, 80:148–157, 2015.

Jonathan Przybyla-Toscano, Clément Boussardon, Simon R Law, Nicolas Rouhier, and Olivier Keech. Gene atlas of iron-containing proteins in arabidopsis thaliana. *The Plant Journal*, 106(1):258–274, 2021.

Guoping Ren, Daniel Stephan, Zhaohui Xu, Ying Zheng, Danming Tang, Rosemary S Harrison, Mareike Kurz, Russell Jarrott, Stephen R Shouldice, Annie Hiniker, et al. Properties of the thioredoxin fold superfamily are modulated by a single amino acid residue. *Journal of Biological Chemistry*, 284(15): 10150–10159, 2009.

Pascal Rey, Noëlle Becuwe, Sébastien Tourrette, and Nicolas Rouhier. Involvement of arabidopsis glutaredoxin s14 in the maintenance of chlorophyll content. *Plant, Cell & Environment*, 40(10):2319–2332, 2017.

Arne Rietsch, Dominique Belin, Nancy Martin, and Jonathan Beckwith. An in vivo pathway for disulfide bond isomerization in escherichia coli. *Proceedings of the National Academy of Sciences*, 93(23):13048–13053, 1996.

Christophe Riondet, Jean Paul Desouris, Jocelyne Guilleminot Montoya, Yvette Chartier, Yves Meyer, and JEAN-PHILIPPE REICHHELD. A dicotyledon-specific glutaredoxin grxc1 family with dimer-dependent redox regulation is functionally redundant with grxc2. *Plant, Cell & Environment*, 35(2):360–373, 2012.

Marıa Teresa Rodrıguez-Manzaneque, Jordi Tamarit, Gemma Bellı, Joaquim Ros, and Enrique Herrero. Grx5 is a mitochondrial glutaredoxin required for the activity of iron/sulfur enzymes. *Molecular biology of the cell*, 13(4): 1109–1121, 2002.

Thomas Roret, Bo Zhang, Anna Moseler, Tiphaine Dhalleine, Xing-Huang Gao, Jérémy Couturier, Stéphane D Lemaire, Claude Didierjean, Michael K Johnson, and Nicolas Rouhier. Atypical iron-sulfur cluster binding, redox activity and structural properties of chlamydomonas reinhardtii glutaredoxin 2. *Antioxidants*, 10(5):803, 2021.

Nicolas Rouhier, E Gelhaye, and J-P Jacquot. Plant glutaredoxins: still mysterious reducing systems. *Cellular and Molecular Life Sciences CMLS*, 61(11): 1266–1277, 2004.

Nicolas Rouhier, Hideaki Unno, Sibali Bandyopadhyay, Lluis Masip, Sung-Kun Kim, Masakazu Hirasawa, José Manuel Gualberto, Virginie Lattard, Masami Kusunoki, David B Knaff, et al. Functional, structural, and spectroscopic characterization of a glutathione-ligated [2fe–2s] cluster in poplar glutaredoxin c1. *Proceedings of the National Academy of Sciences*, 104(18):7379–7384, 2007.

Nicolas Rouhier, Jérémy Couturier, Michael K Johnson, and Jean-Pierre Jacquot. Glutaredoxins: roles in iron homeostasis. *Trends in biochemical sciences*, 35(1):43–52, 2010.

Meng-Bin Ruan, Yi-Ling Yang, Kai-Mian Li, Xin Guo, Bin Wang, Xiao-Ling Yu, and Ming Peng. Identification and characterization of drought-responsive cc-type glutaredoxins from cassava cultivars reveals their involvement in aba signalling. *BMC plant biology*, 18(1):1–17, 2018.

Meng-Bin Ruan, Xiao-Ling Yu, Xin Guo, Ping-Juan Zhao, and Ming Peng. Role of cassava cc-type glutaredoxin megrxc3 in regulating sensitivity to mannitol-induced osmotic stress dependent on its nuclear activity. *BMC plant biology*, 22(1):1–14, 2022.

Cha San Koh, Claude Didierjean, Nicolas Navrot, Santosh Panjikar, Guillermo Mulliert, Nicolas Rouhier, Jean-Pierre Jacquot, André Aubry, Omar Shawkataly, and Catherine Corbier. Crystal structures of a poplar thioredoxin peroxidase that exhibits the structure of glutathione peroxidases: insights into redox-driven conformational changes. *Journal of molecular biology*, 370 (3):512–529, 2007.

Freya Q Schafer and Garry R Buettner. Redox environment of the cell as viewed through the redox state of the glutathione disulfide/glutathione couple. *Free radical biology and medicine*, 30(11):1191–1212, 2001.

Daniel Schnaubelt, Guillaume Queval, Yingping Dong, PEDRO Diaz-Vivancos, Matome Eugene Makgopa, Gareth Howell, Ambra De Simone, Juan Bai, Matthew A Hannah, and Christine H Foyer. Low glutathione regulates gene expression and the redox potentials of the nucleus and cytosol in a rabidopsis thaliana. *Plant, cell & environment*, 38(2):266–279, 2015.

Ewald Schröder and Chris P Ponting. Evidence that peroxiredoxins are novel members of the thioredoxin fold superfamily. *Protein Science*, 7(11):2465–2468, 1998.

M Schwarzländer, MD Fricker, C Müller, L Marty, T Brach, J Novak, LJ Sweetlove, R Hell, and AJ Meyer. Confocal imaging of glutathione redox potential in living plant cells. *Journal of microscopy*, 231(2):299–316, 2008.

Markus Schwarzländer, Tobias P Dick, Andreas J Meyer, and Bruce Morgan. Dissecting redox biology using fluorescent protein sensors. *Antioxidants & redox signaling*, 24(13):680–712, 2016.

Antonio J Serrato, Juan Fernández-Trijueque, Juan-de-Dios Barajas-López, Ana Chueca, and Mariam Sahrawy. Plastid thioredoxins: a “one-for-all” redox-signaling system in plants. *Frontiers in plant science*, 4:463, 2013.

Heather L Shearer, Yu Ti Cheng, Lipu Wang, Jinman Liu, Patrick Boyle, Charles Després, Yuelin Zhang, Xin Li, and Pierre R Fobert. Arabidopsis clade i tga transcription factors regulate plant defenses in an npr1-independent fashion. *Molecular plant-microbe interactions*, 25(11):1459–1468, 2012.

Jinbo Shen, Pui Kit Suen, Xiangfeng Wang, Youshun Lin, Sze Wan Lo, Enrique Rojo, and Liwen Jiang. An in vivo expression system for the identification of

cargo proteins of vacuolar sorting receptors in a rabidopsis culture cells. *The Plant Journal*, 75(6):1003–1017, 2013.

Patrick Sodano, Tai-he Xia, John H Bushweller, Olof Björnberg, Arne Holmgren, Martin Billeter, and Kurt Wüthrich. Sequence-specific1h nmr assignments and determination of the three-dimensional structure of reduced escherichia coli glutaredoxin. *Journal of molecular biology*, 221(4):1311–1324, 1991.

Elke Ströher, Julia Grassl, Chris Carrie, Ricarda Fenske, James Whelan, and A Harvey Millar. Glutaredoxin s15 is involved in fe-s cluster transfer in mitochondria influencing lipoic acid-dependent enzymes, plant growth, and arsenic tolerance in arabidopsis. *Plant Physiology*, 170(3):1284–1299, 2016.

Tongjun Sun, Lucas Busta, Qian Zhang, Pingtao Ding, Reinhard Jetter, and Yuelin Zhang. Tgacg-binding factor 1 (tga 1) and tga 4 regulate salicylic acid and pipecolic acid biosynthesis by modulating the expression of systemic acquired resistance deficient 1 (sard 1) and calmodulin-binding protein 60g (cbp 60g). *New Phytologist*, 217(1):344–354, 2018.

Tsuyoshi Tachibana, Shoko Okazaki, Asako Murayama, Akira Naganuma, Akio Nomoto, and Shusuke Kuge. A major peroxiredoxin-induced activation of yap1 transcription factor is mediated by reduction-sensitive disulfide bonds and reveals a low level of transcriptional activation. *Journal of Biological Chemistry*, 284(7):4464–4472, 2009.

Jordi Tamarit, Gemma Belli, Elisa Cabiscol, Enrique Herrero, and Joaquim Ros. Biochemical characterization of yeast mitochondrial grx5 monothiol glutaredoxin. *Journal of Biological Chemistry*, 278(28):25745–25751, 2003.

Wilena Telman, Michael Liebthal, and Karl-Josef Dietz. Redox regulation by peroxiredoxins is linked to their thioredoxin-dependent oxidase function. *Photosynthesis research*, 145(1):31–41, 2020.

Geng Tian, Song Xiang, Robert Noiva, William J Lennarz, and Hermann Schindelin. The crystal structure of yeast protein disulfide isomerase suggests cooperativity between its active sites. *Cell*, 124(1):61–73, 2006.

Stefano Toppo, Stefano Vanin, Valentina Bosello, and Silvio CE Tosatto. Evolutionary and structural insights into the multifaceted glutathione peroxidase (gpx) superfamily. *Antioxidants & redox signaling*, 10(9):1501–1514, 2008.

Katrin Treffon. *Functional analysis of the Arabidopsis thaliana glutaredoxin ROXY9*. PhD thesis, Niedersächsische Staats-und Universitätsbibliothek Göttingen, 2019.

Daniel Trnka, Anna D Engelke, Manuela Gellert, Anna Moseler, Md Faruq Hossain, Tobias T Lindenberg, Luca Pedroletti, Benjamin Odermatt, João V de Souza, Agnieszka K Bronowska, et al. Molecular basis for the distinct functions of redox-active and fes-transfering glutaredoxins. *Nature communications*, 11(1):1–12, 2020.

Joachim F Uhrig, Li-Jun Huang, Sina Barghahn, Moritz Willmer, Corinna Thurow, and Christiane Gatz. Cc-type glutaredoxins recruit the transcriptional co-repressor topless to tga-dependent target promoters in arabidopsis thaliana. *Biochimica et Biophysica Acta (BBA)-Gene Regulatory Mechanisms*, 1860(2):218–226, 2017.

Ashwinie A Ukuwela, Ashley I Bush, Anthony G Wedd, and Zhiguang Xiao. Reduction potentials of protein disulfides and catalysis of glutathionylation and deglutathionylation by glutaredoxin enzymes. *Biochemical Journal*, 474 (22):3799–3815, 2017.

Ashwinie A Ukuwela, Ashley I Bush, Anthony G Wedd, and Zhiguang Xiao. Glutaredoxins employ parallel monothiol–dithiol mechanisms to catalyze thiol–disulfide exchanges with protein disulfides. *Chemical science*, 9(5): 1173–1183, 2018.

Pavan Umate. Genome-wide analysis of thioredoxin fold superfamily peroxiredoxins in arabidopsis and rice. *Plant signaling & behavior*, 5(12):1543–1546, 2010.

Chrysanthi Valassakis, Irene Dervisi, Adamantia Agalou, Nikolaos Papandreou, Georgios Kapetsis, Varvara Podia, Kosmas Haralampidis, Vassiliki A Iconomidou, Herman P Spaink, and Andreas Roussis. Novel interactions of selenium binding protein family with the picot containing proteins atgrxs14 and atgrxs16 in arabidopsis thaliana. *Plant Science*, 281:102–112, 2019.

Pankaj Kumar Verma, Shikha Verma, Rudra Deo Tripathi, Nalini Pandey, and Debasis Chakrabarty. Cc-type glutaredoxin, osgrx_c7 plays a crucial role in enhancing protection against salt stress in rice. *Journal of Biotechnology*, 329:192–203, 2021.

Stéphane Vuilleumier. Bacterial glutathione s-transferases: what are they good for? *Journal of bacteriology*, 179(5):1431–1441, 1997.

Andrew Waterhouse, Martino Bertoni, Stefan Bienert, Gabriel Studer, Gerardo Tauriello, Rafal Gumienny, Florian T Heer, Tjaart A P de Beer, Christine Rempfer, Lorenza Bordoli, et al. Swiss-model: homology modelling of protein

structures and complexes. *Nucleic acids research*, 46(W1):W296–W303, 2018.

Andrzej Weichsel, John R Gasdaska, Garth Powis, and William R Montfort. Crystal structures of reduced, oxidized, and mutated human thioredoxins: evidence for a regulatory homodimer. *Structure*, 4(6):735–751, 1996.

Malcolm F White and Mark S Dillingham. Iron–sulphur clusters in nucleic acid processing enzymes. *Current opinion in structural biology*, 22(1):94–100, 2012.

Ricardo A Wolosiuk and Bob B Buchanan. Thioredoxin and glutathione regulate photosynthesis in chloroplasts. *Nature*, 266(5602):565–567, 1977.

Yuliang Wu and Robert M Brosh Jr. Dna helicase and helicase–nuclease enzymes with a conserved iron–sulfur cluster. *Nucleic acids research*, 40(10): 4247–4260, 2012.

Wenchuan Xie, Junfeng Huang, Yang Liu, Jianan Rao, Da Luo, and Miao He. Exploring potential new floral organ morphogenesis genes of arabidopsis thaliana using systems biology approach. *Frontiers in plant science*, 6:829, 2015.

S Xing, A Lauri, and S Zachgo. Redox regulation and flower development: a novel function for glutaredoxins. *Plant Biology*, 8(05):547–555, 2006.

Shuping Xing and Sabine Zachgo. Roxy1 and roxy2, two arabidopsis glutaredoxin genes, are required for anther development. *The Plant Journal*, 53(5): 790–801, 2008.

Shuping Xing, Mario G Rosso, and Sabine Zachgo. Roxy1, a member of the plant glutaredoxin family, is required for petal development in arabidopsis thaliana. 2005.

Hui Xu, Zhen Li, Peng-Fei Jiang, Li Zhao, Chang Qu, Yves Van de Peer, Yan-Jing Liu, and Qing-Yin Zeng. Divergence of active site motifs among different classes of populus glutaredoxins results in substrate switches. *The Plant Journal*, 110(1):129–146, 2022.

RS Yang, F Xu, YM Wang, WS Zhong, L Dong, YN Shi, TJ Tang, HJ Sheng, D Jackson, and F Yang. Glutaredoxins regulate maize inflorescence meristem development via redox control of tga transcriptional activity. *Nature Plants*, 7(12):1589–1601, 2021a.

Yuting Yang, Wanyu Xue, Panpan Chen, Xin Yuan, Xvzhen Li, Tingting Zhang, and Shuxia Chen. Identification and expression analyzes of cc-type glutaredoxin in cucumber (cucumis sativus l.) under abiotic stress. *Scientia Horticulturae*, 289:110417, 2021b.

Han Yu, Jian Yang, Yafei Shi, Jimmonique Donelson, Sean M Thompson, Stuart Sprague, Tony Roshan, Da-Li Wang, Jianzhong Liu, Sunghun Park, et al. Arabidopsis glutaredoxin s17 contributes to vegetative growth, mineral accumulation, and redox balance during iron deficiency. *Frontiers in plant science*, 8:1045, 2017.

Mirko Zaffagnini, Laure Michelet, Vincent Massot, Paolo Trost, and Stéphane D Lemaire. Biochemical characterization of glutaredoxins from chlamydomonas reinhardtii reveals the unique properties of a chloroplastic cgfs-type glutaredoxin. *Journal of Biological Chemistry*, 283(14):8868–8876, 2008.

Mirko Zaffagnini, Mariette Bedhomme, Christophe H Marchand, Jérémy Couturier, Xing-Huang Gao, Nicolas Rouhier, Paolo Trost, and Stéphane D Lemaire. Glutaredoxin s12: unique properties for redox signaling. *Antioxidants & redox signaling*, 16(1):17–32, 2012a.

Mirko Zaffagnini, Mariette Bedhomme, Christophe H Marchand, Samuel Morisse, Paolo Trost, and Stéphane D Lemaire. Redox regulation in photosynthetic organisms: focus on glutathionylation. *Antioxidants & redox signaling*, 16(6):567–586, 2012b.

Mirko Zaffagnini, Simona Fermani, Christophe H Marchand, Alex Costa, Francesca Sparla, Nicolas Rouhier, Peter Geigenberger, Stéphane D Lemaire, and Paolo Trost. Redox homeostasis in photosynthetic organisms: novel and established thiol-based molecular mechanisms. *Antioxidants & Redox Signaling*, 31(3):155–210, 2019.

Mark Zander, Shuxia Chen, Julia Imkampe, Corinna Thurow, and Christiane Gatz. Repression of the arabidopsis thaliana jasmonic acid/ethylene-induced defense pathway by tga-interacting glutaredoxins depends on their c-terminal alwl motif. *Molecular plant*, 5(4):831–840, 2012.

Flavien Zannini, Jérémy Couturier, Olivier Keech, and Nicolas Rouhier. In vitro alkylation methods for assessing the protein redox state. In *Photorespiration*, pages 51–64. Springer, 2017.

Flavien Zannini, Anna Moseler, Raphaël Bchini, Tiphaine Dhalleine, Andreas J Meyer, Nicolas Rouhier, and Jérémy Couturier. The thioredoxin-mediated recycling of arabidopsis thaliana grxs16 relies on a conserved c-terminal

cysteine. *Biochimica et Biophysica Acta (BBA)-General Subjects*, 1863(2): 426–436, 2019.

Andre Zapun, James CA Bardwell, and Thomas E Creighton. The reactive and destabilizing disulfide bond of dsba, a protein required for protein disulfide bond formation in vivo. *Biochemistry*, 32(19):5083–5092, 1993.

Bo Zhang, Sibali Bandyopadhyay, Priyanka Shakamuri, Sunil G Naik, Boi Hanh Huynh, Jérémy Couturier, Nicolas Rouhier, and Michael K Johnson. Monothiol glutaredoxins can bind linear [fe3s4]+ and [fe4s4] 2+ clusters in addition to [fe2s2] 2+ clusters: spectroscopic characterization and functional implications. *Journal of the American Chemical Society*, 135(40):15153–15164, 2013.